UNIVERSITY OF GAZIANTEP

GRADUATE SCHOOL OF

NATURAL & APPLIED SCIENCES

DESIGN, CONSTRUCTION AND CONTROL OF AN ELECTROMAGNETIC GUIDANCE SYSTEM

M.Sc. THESIS

IN

ELECTRICAL AND ELECTRONICS ENGINEERING

BY

SULAF IBRAHIM EZZAT

MAY 2016

Design, Construction and Control of an Electromagnetic Guidance System

M.Sc. Thesis

in

Electrical and Electronics Engineering

University of Gaziantep

Supervisor

Assoc. Prof. Dr. Vedat Mehmet KARSLI

By

Sulaf Ibrahim EZZAT

May 2016

REPUBLIC OF TURKEY

UNIVERSITY OF GAZIANTEP

GRADUATE SCHOOL OF NATURAL & APPLIED SCIENCES

ELECTRICAL AND ELECTRONIC ENGINEERING DEPARTMENT

Name of the thesis: Design, Construction and Control of an Electromagnetic Guidance System

Name of the student: Sulaf Ibrahim EZZAT

Exam date: May 2016

Approval of the Graduate School of Natural and Applied Sciences.

Prof. Dr. Metin BEDİR
Director

I certify that this thesis satisfies all the requirements as a thesis for the degree of Master of Science.

Prof. Dr. Ergun ERÇELEBİ
Head of Department

This is to certify that we have read this thesis and that in our consensus / majority opinion, it is fully adequate, in scope and quality, as a thesis for the degree of Master of Science.

Assoc. Prof. Dr. Vedat Mehmet KARSLI
Supervisor

Examining Committee Members: Signature

Prof. Dr. Safar ALHILAL   ....

Assist Prof. Dr. Tolgay KARA   ....

Assoc. Prof. Dr. Vedat M. KARSLI   ....

I hereby declare that all information in this document has been obtained and presented in accordance with academic rules and ethical conduct. I also declare that, as required by these rules and conduct, I have fully cited and referenced all material and results that are not original to this work.

Sulaf Ibrahim EZZAT

ABSTRACT

DESIGN, CONSTRUCTION AND CONTROL OF AN ELECTROMAGNETIC GUIDANCE SYSTEM

EZZAT, Sulaf Ibrahim
M.Sc. in Electrical and Electronic Engineering
Supervisor: Assoc. Prof. Dr. Vedat Mehmet KARSLI
May 2016, 129 Pages

The guidance system is a key system in high-speed Magnetic Levitation (MAGLEV) train to keep the vehicle on the track during travel when it will tend to run aside and depart from the center of guide-way. Guidance magnets are mainly accomplished by using two types of magnetic forces either attractive or repulsive force.

In this work, a proposed structure for a prototype of an electromagnetic guidance system is designed, studied and controlled. Simulation and analysis of the system model are derived based on two dimensional (2D) Finite Element Analysis (FEA) utilizing FEMM software as a concurrent with the analytical approach to fine-tune the design process. The mathematical modeling of the system is developed to find transfer function and state space models. The system is hardly non-linear and open loop unstable. It was linearized around the operating points using Taylor series expansion. Based on the linear and nonlinear models several controllers of phase-lead, PID controllers and complete state feedback controller based on pole-placement technique are designed respectively to control the system. MATLAB, Simulink is provided for simulation and for plotting the results.

In the experimental setup Arduino mega 2560 is used as a digital controller with the system to implement the Fuzzy PID control algorithm to put the system at the desired position. The performance of the controller is tested to investigate the robustness of the proposed control system against the external disturbance force. Consequently, the steady state error is minimized in a certain set position.

Keywords: Electromagnetic guidance system, FEA analysis using FEMM software, Pole- placement controller, Fuzzy PID controller.

ÖZET

ELEKTROMANYETİK YÖNLENDİRME SİSTEMİNİN TASARIM, KONSTRÜKSİYON VE KONTROLÜ

EZZAT, Sulaf Ibrahim
Yüksek Lisans Tezi,Elektrik ve Elektronik Mühendisliği Bölümü
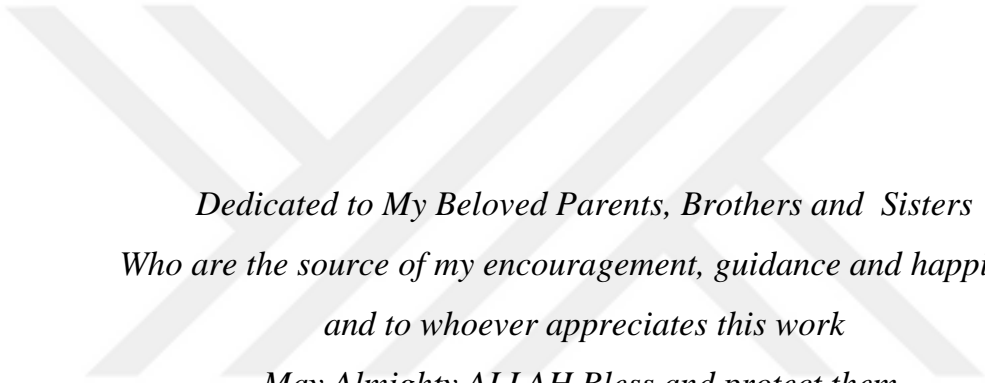Tez Yöneticisi: Doç. Dr. Vedat Mehmet KARSLI
Mayıs 2016, 129 sayfa

Yönlendirme sistemi, yüksek hızlı maglev trenlerinin seyahat esnasında yönlendirme yolundan sapmasını engelleyerek yönlendirme yolunun merkezinde tutan önemli bir sistemdir. Yönlendirme mıknatısları genellikle iki tip manyetik kuvvet vasıtasıyla oluşturulabilir: bunlar ya çeken ya da iten kuvvetlerdir.

Bu çalışmada, elektromanyetik yönlendirme sisteminin prototipi için önerilen yapı tasarlanmış, üzerine çalışılmış ve kontrol edilmiştir. Sistemin analiz ve simülasyonu, 2 boyutlu sonlu öğeli çözümlemeyi temel alan FEMM yazılımıyla (ki bu yazılım aynı zamanda tasarım sürecinin ince ayarı için analitiksel yaklaşımda gereklidir) elde edilmiştir. Sistemin dinamik modeli, transfer fonksiyonu ve durum uzay modelini bulmak için tasarlanmıştır. Sistem nadiren kararsız, açık döngülü ve doğrusal olmayan durumdadır. Sistem, Taylor Seri Açılımı kullanılarak çalışma noktasında doğrusallaştırılmıştır. Sistem kontrolü için çeşitli doğrusal ve doğrusal olamayan modelli çeşitli sistemler olan; evre öndelemesi, PID ve kutup değiştirme tekniğini temel alan durum geri besleme kontrolü kullanılmıştır. MATLAB Simulink sonuçların çizime aktarımında ve simülasyonda kullanılmıştır.

Deneysel aşamada Arduino Mega 2560 bir dijital kontrolör olarak sistemde Fuzzy PID kontrol algoritmasını uygulamak ve sistemi istenilen pozisyonda set etmek için kullanılmıştır. Fuzzy PID kontrolün performansı, öngörülen kontrol sisteminin dış etken kuvvetlere karşı sağlamlılığı araştırılarak başarı ile test edilmiştir. Sonuç olarak, kararlı konum hatası sabit ayar noktasında minimize edilmiştir.

Anahtar Kelimeler: Elektromanyetik kılavuz sistemi, 2D FEMM yazılımı kullanarak FEA analizi, kutup değiştirme denetleyicisi, Fuzzy PID denetleyicisi.

Dedicated to My Beloved Parents, Brothers and Sisters

Who are the source of my encouragement, guidance and happiness

and to whoever appreciates this work

May Almighty ALLAH Bless and protect them.

ACKNOWLEDGEMENTS

TABLE OF CONTENTS

LIST OF FIGURES

LIST OF TABLES

LIST OF SYMBOLS /ABBREVIATIONS

MAGLEV	Magnetic Levitation
EMS	Electromagnetic Suspension
EDS	Electrodynamic Suspension
SCM	Superconducting Magnet
PM	Permanent Magnet
DC	Direct Current
ADC	Analog to Digital Convertor
MOSFET	Metal-Oxide-Semiconductor Field Effect Transistor
IGBT	Insulated-Gate Bipolar Transistor
H∞	Infinity Hysteresis
PD	Proportional Derivative
PID	Proportional Integral Derivative
MATLAB	Matrix Laboratory
GUI	Graphical User Interface
LED	Light Emitting Diode
SISO	Single Input Single Output
MCU	Microcontroller Unit
PWM	Pulse Width Modulation
FEA	Finite Element Analysis
FEMM	Finite Element Method Magnetics
KVL	Kirchhoff Voltage Law
SMC	Sliding Mode Controller
DOF	Degree of Freedom
PLS	Photoelectric Laser Sensor
DSP	Digital Signal Processor
l	Mean length
A	Cross-sectional area
L	Inductance
R	Resistance

$\mathcal{R}$	Reluctance
EMF	Electromotive Force
mmF	Magneto Motive Force
N	Number of turns
Ø	Magnetic flux
B	Magnetic flux density
μ_0	Permeability of air
m	Mass
g	Acceleration of the gravity
a	Acceleration of an object
β	Sensor gain
V	Voltage
F	Force
TF	Transfer Function
KI	Integral gain
KP	Proportional gain
KD	Derivative gain
TI	Integral term
TP	Proportional term
TD	Derivative term
FLC	Fuzzy Logic Controller
FIS	Fuzzy Inference System
NL	Negative Large
NS	Negative Small
Ze	Zero
PS	Positive Small
PL	Positive Large
LCD	Liquid Crystal Display
IDE	Integrated Development Environment

CHAPTER 1

INTRODUCTION

Magnetic levitation (MAGLEV) is an innovative transportation technology, which is contributed to the development and advancement of modern civilization to serve the public in a rapid, reliable and safe manner [1]. The overall structure of the Maglev vehicle consists of independent levitation, propulsion and guidance systems. A high- speed Maglev train utilizes a magnetic field to perform principle for non-contact levitation, guidance and propulsion forces [2].

The main topic of this study is to introduce an electromagnet type guiding system in the maglev system. Because of sideways motion of the train is just as important as the up and down motion of the train that are required to prevent the vehicle from lateral displacement.

The non-contact guidance or steering force refers to the sideward forces that are required to make the vehicle follow the guide-way during travel. The necessary forces are supplied either from attractive or repulsive force [2]. The electromagnetic guided system is commonly used in the field of transport vehicles, conveyor systems, tool machines frictionless bearings and wind tunnel system [3].

The attractive electromagnetic guidance system is described in this thesis. A design procedure for DC electromagnet actuators is presented analytically basis of the system design specifications such as weight of the magnets, air-gap length, lateral force and winding current. Then, two dimensional (2D) Finite Element Analysis (FEA) model is developed using Finite Element Method Magnetics (FEMM) software to verify and fine-tune the design procedure.

The mathematical modeling of the electromagnetic guidance system is derived in both transfer function and state space models, the guidance system is hardly nonlinear and unstable. System linearization is employed using the Taylor series expansion method to linearize the system. For stabilizing the electromagnetic

guidance system which is inherently unstable characteristic, different type of controllers are designed utilizing the root-locus technique. Position control loops are designed using phase-lead and Proportional-Integral-Derivative (PID) controllers to control the system. In addition, complete state feedback controller based on pole-placement technique is designed and applied to control the air-gap displacement of both sides around the equilibrium position. Then the simulation results are presented and compared for different controllers using MATLAB Simulink.

In the experimental setup, the physical structure of the guidance system consists of pair of E-shaped electromagnets are placed on both sides of the rigid guide-way in horizontal direction. Each electromagnet is used as the force actuator which produces the force to attract the rigid ferromagnetic guide-way in lateral ward against other side force. This prototype is considered as a laboratory sample of single-axis electromagnetic guidance system. The photoelectric distance sensor in laser type is installed to detect the position, the magnets work together with the sensor to keep the position between two electromagnets and the guide-way.

To control the system at desired position Fuzzy PID controller is designed, Arduino mega 2560 is programmed for implementing the control algorithm to generate two suitable 8-bit of Pulse Width Modulation (PWM) signals for driving the switching devices for supplying the guiding system and to collect distance information through the channel of Analog to Digital Converter (ADC) which is multiplexed to read the incoming signal. Various circuits are utilized for building the system and protecting the components. The performance of the controller is tested to investigate the robustness of the proposed control system against the external disturbance force which is entered by the user. Consequently, the steady state error is minimized in certain set position. The system is controlled and the experimental results are presented. In the following overview of the chapters is summarized.

1.1 Organization of the Thesis

A brief content of this thesis, which consists of eight chapters and description of each chapter is as follows:

Chapter 1: This chapter provides a general introduction and organization of the thesis.

Chapter 2: This chapter includes the background on the electromagnetic guidance system, types of guidance techniques and literature survey of the electromagnetic guidance system.

Chapter 3: This chapter presents the design procedure of DC single electromagnetic coil using shell type core, that is analytically designed according to the specifications of system design and then the design procedures are validated using finite element analysis model using FEMM software.

Chapter 4: Mathematical modeling of the single-axis electromagnetic guidance system is derived using electrical and mechanical characteristics of the system. Transfer function and state space models are obtained.

Chapter 5: This chapter discusses and synthesis of controller design results using root locus technique. Phase lead compensator, PID and adaptive pole placement controller are designed to control the system at the equilibrium position and comparing between them.

Chapter 6: This chapter provides the detail of the system setup and components with their performance characteristics that are used for composing electromagnetic guidance system with presenting simulation and hardware implementation of magnetic driver unit and the controller scheme.

Chapter 7: It explains the software program that is utilized for programming the microcontroller board (Arduino mega2560) to process the control algorithm and experimental results.

Chapter 8: The last chapter draws conceptual conclusions about the success and limitations of the results of this research and recommendations with suggests in some areas for further work. Also presents all the sources of information which are used for creating this study. These sources are: scientific literature, books, and internet sources.

CHAPTER 2

ELECTROMAGNETIC GUIDANCE SYSTEM OVERVIEW AND LITERATURE SURVEY

2.1 Introduction

This chapter presents guidance system definition, types and literature review of electromagnetic guidance systems. So this chapter describes the importance of the guidance systems to keep the vehicle laterally stable on the track during travel for providing a safe and comfortable ride. Guidance magnets are mainly accomplished by using two types of magnetic forces either attractive or repulsive force.

In the EMS systems, as in the Transrapid system the necessary guidance force is produced from a separate set of levitation and guidance magnets which were attached by the vehicle and interacting with ferromagnetic rails on the sides of the guide-way. Whereas, in the JHSST system the guidance force is generated from integrating set of levitation and guidance coil by locating the levitation magnets to produce both levitation and guidance force simultaneously, the guidance force is produced from laterally offsetting them with respect to the guide-way [4].

In the EDS systems, "null-flux" guidance is produced by cross-coupled conducting coils mounted on each sidewall of the guide-way. When the vehicle is running centrally, each pair of coils has zero net flux linkage from the on-board superconducting magnets and no current is induced. However, a lateral displacement will produce a net flux linkage and circulating current will induce between these two coils which produces the guiding force [4]. The details for each type will be given in the following sections.

2.2 MAGLEV Guidance System Overview

The MAGLEV train is a non-contact system that requires a guiding force for the prevention of lateral displacement, to keep the vehicles on the track during travel when it will tend to run aside and depart from the center of guide-way [5].

Because of the propulsion and levitation magnets do not provide enough guidance force to maintain the dynamic position of the vehicle against the lateral disturbances [6] or any other force that affects the vehicle such as centrifugal force when going round a curve. Guidance magnets and sensors are located on both sides along the entire length of the vehicle to keep the train centered at all points during the ride and turns as shown in Figure 2.1. Additionally the guidance magnets allow the train to pitch, tilt and roll during turns [7].

The guidance force is accomplished electromechanically as in the case of levitation either by magnetic attraction force or magnetic repulsive force [5, 7]. They can be accomplished by various different methods utilizing electromagnets, permanent magnets and superconducting magnets (SCM). Each of these concepts has its own advantages and disadvantages; each will be briefly discussed in the following sections [8]. The guidance function is mainly accomplished by using two types of magnetic force namely:

➢ Magnetic attraction force
➢ Magnetic repulsive force
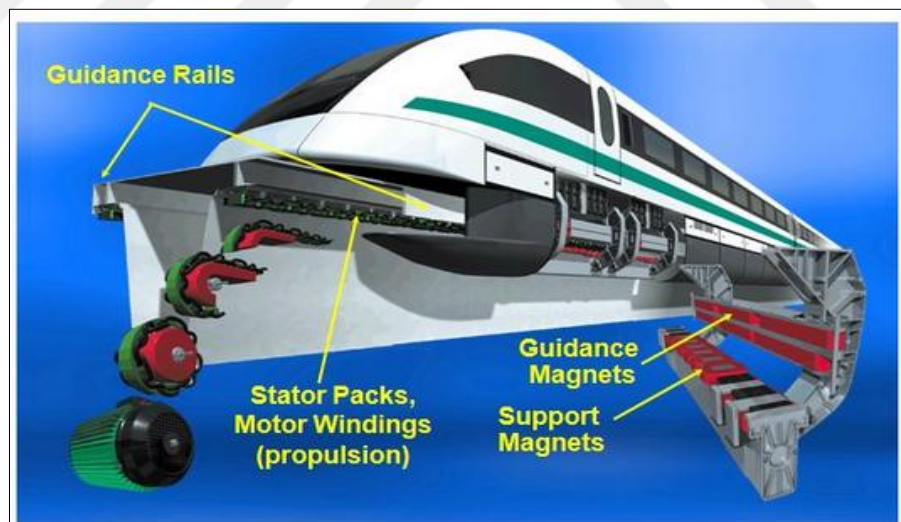
Figure 2.1 Transrapid maglev guidance coils [2].

2.2.1 Using Magnetic Attraction Force

Guidance is achieved by utilizing the force of attraction between the electromagnets on-board the vehicle and a ferromagnetic rail placed on the underside of an elevated guide-way, which generally operates with a small air-gap at around 10 mm [8].
There are two types of EMs technologies:

1) The guidance and levitation integrated type such as Japanese (HSST) and Korean (UTM).

2) The levitation and guidance separated type such as German Transrapid.

An integrated suspension and guidance type EMS, as indicated in Figure 2.2 has been used by the Japanese HSST and South Korean UTM. When the vehicle displaces laterally the guidance force is created in the way to reduce the reluctance and increase the inductance [5, 8]. This type is suitable for low cost and low- speed application because the number of electromagnets and controllers is reduced. The rate of consuming electric power in an integrated type is smaller than the separated type. Further interference between the guidance and levitation magnets makes it difficult to control the levitation and guidance system [5].
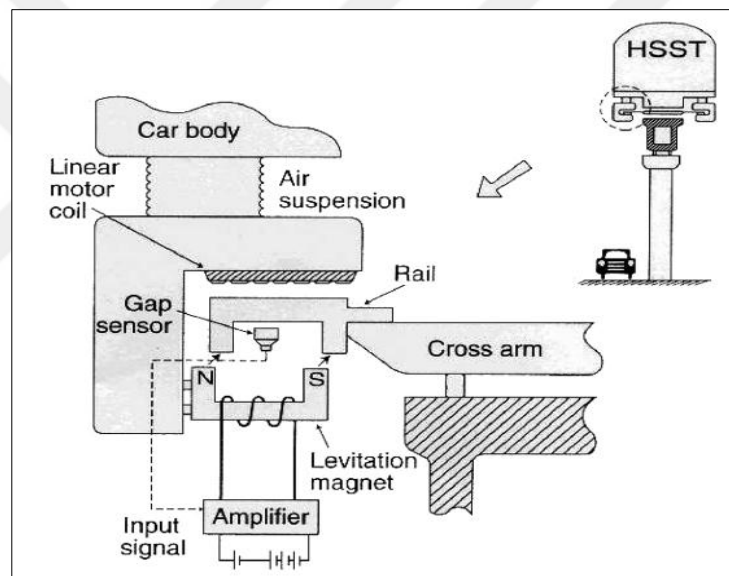
Figure 2.2 Japanese type with integrated levitation and guidance electromagnets [5]

In the type of the German Transrapid, the guidance and suspension magnets are separated from each other. Guidance electromagnets are attached on the side wall of the vehicle and reaction rails are placed on both sides of the guide-way. The guidance force is created due to interaction between the electromagnets and the iron-rail as shown in Figure 2.3. This type is suitable for high-speed operation because guidance and levitation magnets don't interfere with each other, but the number of controllers increases [5, 8].
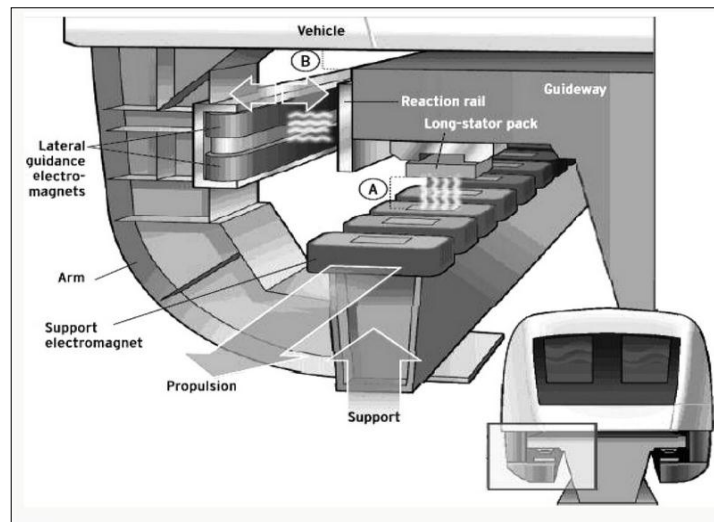
Figure 2.3 Transrapid type with separated levitation and guidance electromagnets [5]

2.2.2 Using Magnetic Repulsive Force

MAGLEV uses repulsive force for the guidance and suspension, which has been developed by Central Japan Railways. The MLX01 high-speed system operates at a suspension height about 11cm above the guide-way, the vehicle is guiding about 1 to 10 cm from the track using a vertical null-flux structure that provides both lift and guidance force for the vehicle [8]. This type is so stable magnetically to control the air-gap and highly suitable for high-speed operation and long distance. The guide-way has two coil arrangements as shown in Figures 2.4 a, b: [9]

1. Horizontal ground coils for levitation with sidewall coils for propulsion and guidance.
2. Figure-eight-shaped coils for levitation and guidance in combination with double-layer propulsion coils [9].
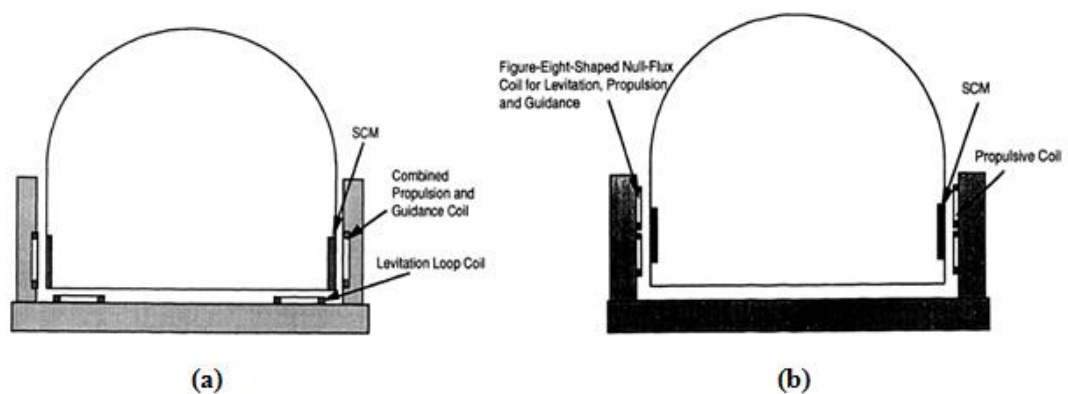
Figure 2.4 a- MLU001 test vehicle with a U-shaped guide-way configuration b- Combined sidewall levitation, propulsion, and guidance maglev [9].

7

a) **Horizontal Ground Coils for Levitation with Sidewall Coils for Propulsion and Guidance**

The first version of the MLU001 test vehicle was tested primarily during the 1980s as indicated in Figure 2.4a. The system used a U-shaped guide-way configuration, in which the levitation forces were generated by the interaction between the levitation loop coils arranged horizontally on the guide-way and the vertically oriented SCM aboard the vehicle. The propulsion and guidance forces were generated by the interaction of these same SCMs with coils which are mounted vertically on both side walls (left and right sides) of the guide-way [9]. As shown in Figure 2.5, when the train runs in the center of the guide-way the induced electromotive force (EMF) cancels out each other. Otherwise, once a train runs nearer to side wall of the guide-way, an electric current is flowing through the coils the EMF induced by the difference of distance which produce the guidance force [5, 7]. The coils were excited by a three-phase external power source and cross connected to form a combined null-flux guidance and propulsion system [9].
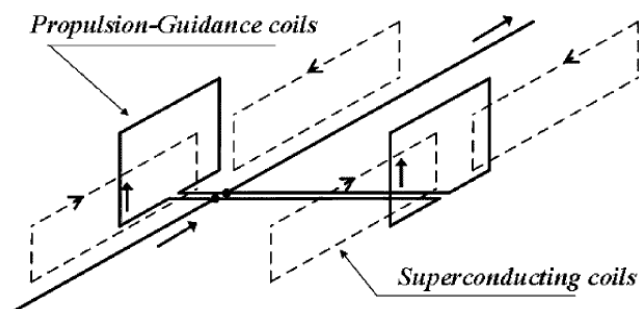
Figure 2.5 Sketch of connecting guidance and propulsion coils

b) **Figure-Eight-Shaped Null-flux Coils for Levitation and Guidance in Combination with Double-Layer Propulsive Coils**

The Japanese type of EDS MAGLEV system invented by Fujiwara et al. It uses a concept of combined propulsion and null-flux suspension. The system consists of two arrays of figure-eight-shaped null-flux coils which are mounted on the side walls of the guide-way as shown in Figure 2.6 [9].

The propulsion coils are oval in shape and electro-magnetically coupled with each other because of double-layered attachment to minimize the magnetic fluctuating

8

force for the on-board superconducting coils and to reduce harmonics and provides better propulsion performance. Additionally, from both sidewalls the propulsion coils are electro-magnetically coupled with the combined levitation-guidance system [10].

(a)   (b)
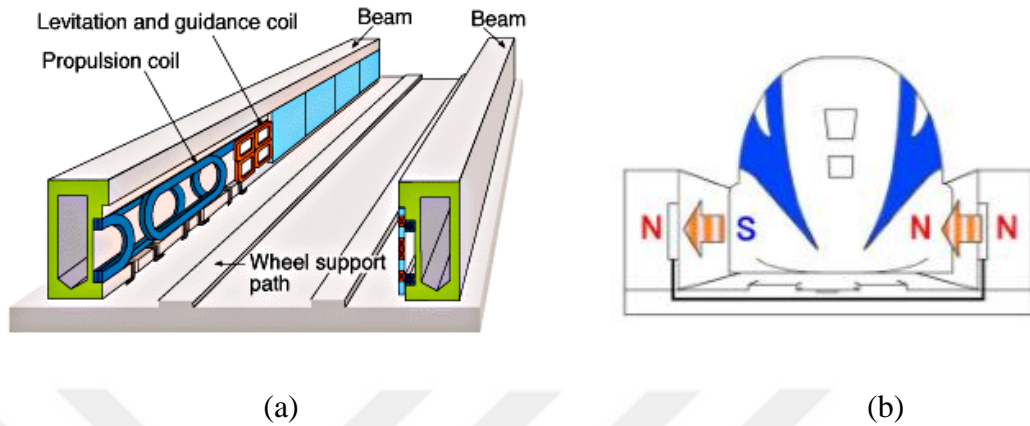
Figure 2.6 a) Coil attachment in the Japanese MLX01 maglev using null flux structure. b) Guidance system in the Japanese MLX01 [8]

Sidewall guidance and levitation coils consist of two coils of lower and upper twisted coil like figure- eight- shaped on both sidewalls, which are connected with a null flux cable in order to the vehicle follow the guide-way during the ride and turns as shown in Figure 2.7 [10,11].
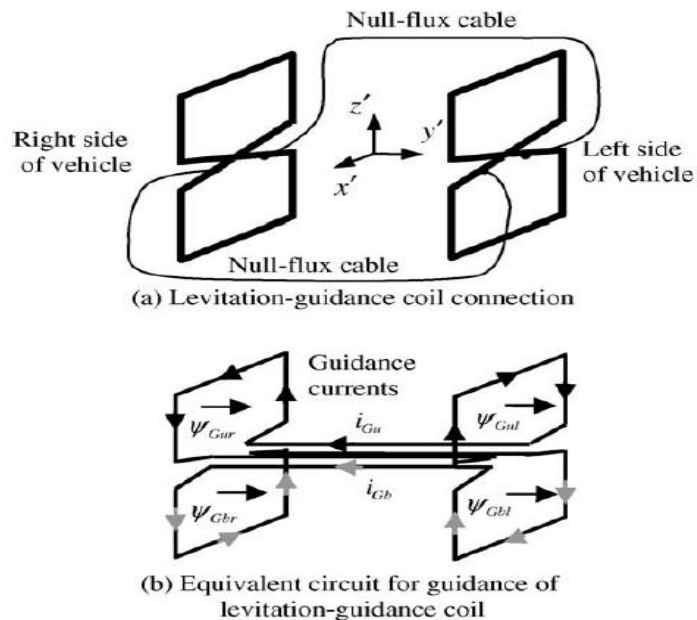
Figure 2.7 Sketch of connecting null–flux coils of levitation-guidance used in Japanese MLX [11]

9

During running once the vehicle displaces laterally or in other words, when one side of the train near the sidewall of the guide-way, the super conducting magnets on the train induces a repulsive force from the levitation coils on the side closer to the vehicle, otherwise from the farther side the coils produce an attractive force, circulating currents between these two coils are induced and this produces the guiding force to locate the train in the center of the guide-way. Thus, both the null-flux levitation and the null-flux guidance forces are generated by the interaction between two rows of SCMs aboard the vehicle and two rows of null-flux coils on the guide-way [9].

Figure 2.8 is a sketch of composing and combining figure-eight-shaped coils on the sidewall of the guide-way with superconducting coils on board the vehicle for performing three functions of propulsion, levitation, and guidance. Two rows of figures-eight-shaped coils on opposite sides are cross-connected to make a null-flux circuit of levitation and guidance system and in the same row the coils are connected in series to form three-phase propulsion windings. Thus, the three functions of propulsion, levitation, and guidance are expected to be achieved with one set of figure-eight-shaped guide-way coils. The lateral displacement generates the voltage difference between the figure-eight-shaped coils on the two sides and produces the null-flux guidance force. The coils on each side wall are connected in a three-phase configuration and energized by a power supply [12, 13].
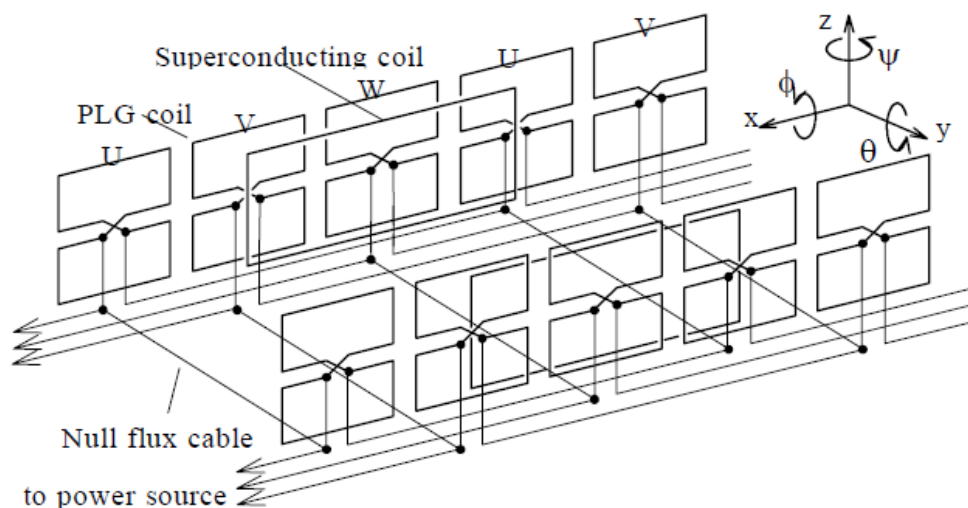
Figure 2.8 A Sketch of combined and composition coils of levitation, propulsion and guidance system [12, 13]

2.3 Literature Review of an Electromagnetic Guidance System

This section reviews literature relevant to the electromagnetic guidance system. Previous work in electromagnetic guidance system spans many fields; some well-known fields include MAGLEV transportation, wind tunnel levitation, magnetic bearings, and linear elevator. Here, however, the thesis will only investigate the MAGLEV guidance techniques in the field of transportation application, including high- speed MAGLEV and linear elevator which have been a tremendous amount of development [14].

David L. Trumper (1997) proposed the system which consists of dual–actuator electromagnets E-shaped core of pairwise opposition with the suspended element constrained to allow motion only in the direction of control. The state equations for the dual actuator system were derived. Two types of controllers were designed and tuned in the hardware to achieve essentially identical step responses at the centered position. The linear controller used a bias current for each electromagnets to linearize the system around an operating point and this can be done by comprising a unity dc gain lead term in the feedback path to stabilize the loop and a lag term in the forward path to provide good steady-state performance, the nonlinear controller was used based on feedback linearization. Thereafter the performances of these two controllers were compared which was shown that feedback linearization had better performance, but it required more accurate plant models [15].

Mei-Yung Chen, Li-Chen F, Ming-Jyh Wang (1999) designed a prototype of a single-axis MAGLEV guiding system with high precision positioning. Complete analytical model with full Degree of Freedom (DOF) was derived without taking the degree for large-range actuation. The system controller was digitally created via a microcontroller and an adaptive controller was applied, which was treated with unknown parameters to accomplish both guidance and positioning and to regulate the system degree. Experimental results were shown that the effectiveness and system's feasibility have been demonstrated clearly, satisfactory performance including stiffness and resolution have been carried out, alignment imperfections were eliminated completely and tracking for positioning-axis was achieved [16].

By Byeong- Seok Lee (2000) in his thesis investigated and studied on the attractive electromagnetic guidance system for 6 m long prototype system of Linear Switched

Reluctance Machine (LSRM) that was needed for providing a safe and comfortable ride. The prototype of guidance system consists of four DC electromagnets, two guide rails and four gap sensors for independent control. The guidance magnets were installed on the lateral surface perpendicular to the levitation surface of the vehicle and the guide-way. A design procedure for DC electromagnets was presented analytically basis on the specifications of system design such as the weight of the vehicle, air-gap position, lateral force, and current winding. Afterwards FEA was utilized to verify the design of the DC electromagnet. The mathematical model of the electromagnetic guiding system was achieved. PID, PD and PI controllers were designed using the analog control circuit to control the air-gap position and force/current of the electromagnets for stable operation of the system. Experimental result was proved the validity of the controller design and showed the feasibility of the LSRM guidance systems [6].

D'arrigo Aldo, Rufer Alfred (2000) presented a simple magnetic model for the study of the levitation and guidance forces in the Swiss Metro project, which were produced between the electromagnet coupled with an iron rail with neglecting the leakage fluxes and magnetic potential losses in the iron parts. So it dealt with the study of the guidance force in the case of a vertical position control and showed that the guidance force can be stronger than in an open loop study. Three different shapes of the rail were proposed to get levitation and guidance force with the same electromagnet, including of flat wide rail, flat narrow rail and C-shaped rail. The results were proved that the guidance force does not appear in the case of a flat wide rail otherwise, for the flat narrow rail the guidance force was obtained is about twice and more than twice for the C-shaped rail coupling. In a C-shaped rail the guidance force was more than twice due to the symmetry of the two air-gaps [17].

Cassat Alain, Jufer Marcel, Espanet Christophe (2006) in this paper concentrated on the determination of the passive guidance forces of the active magnetic way based on 3D FEM analysis to guide the vehicle. A unique aspect of MAGLEV was presented which was the combination of the propulsion with the levitation in the Swiss-metro project to minimize the heat due to the iron and copper losses in the levitation and guidance inductors and decrease the number of the reference surfaces by specifying the air-gap 20 mm for the propulsion, levitation and the guidance. Two cases were considered for determining static guidance force includes passenger comfort and

vehicle at stalls according to the International Standard [ISO 2631], which was dealing with random and shock vibration and harmonic vibration that had a great impact in both vertical and horizontal directions. In the former case the guidance force can be calculated by admitting a maximum admissible acceleration with the mass of vehicle, otherwise the other limit case was defined when the vehicle stalls at no speed, in a curve the guidance force can be calculated by taking the angle of maximum plane inclination curve with the mass of the vehicle [18].

Hao Aming, Liu Hengkun, She longhua, Chang Wensen (2007) proposed the structure and modeled of an electromagnetic guidance system in MAGLEV high-speed train. A new controlling method (double ring controller) was researched to stabilize the system and controlling the attractive force between electromagnets and guide-way to guide the vehicle at the center of the guide-way. The double ring controller was a combination between (inner ring) force feedback and (out the ring) gap feedback controller to improve the dynamic stiffness and to resist any kind of disturbances that impact the guidance system. The force feedback was used to meet the rapid change of disturbance through control the current in the magnet coils and to improve the responding speed of the magnet by installing the current sensor and accelerometer to measure the acceleration directly. Whereas, the gap feedback was used to meet the gap change and can be measured directly from the sensor. MATLAB platform was applied to simulate the double ring controller for meeting the quick change of gap and force factor. The result indicated that this controlling strategy was very effective to ensure dynamic stiffness of guidance system and to enhance the ability of the system for anti-disturbance [19].

Qing Hu, Lisheng Ou and Hao Liu (2010) implemented the nonlinear fuzzy PID controller based on feedback linearization to adopt the magnetic guiding system in linear elevator. Fuzzy PID was used to control the air-gap position in permanent magnet linear synchronous motor PMLSM that changed frequently, to minimize noise in all stages of operation and to control the vibration level. MATLAB was used for system modeling, presenting and analyzing the results that the fuzzy PID controller was achieved high performance with robustness and stabilization [20].

Shinya Hasegawa, Takayoshi Narita and Yasuo Oshinoya (2010) made a study on the impact of horizontal magnetic attractive force to the stationary levitated ultra-thin

steel plate (A plate made of zinc-coated material steel SS400, length 800mm, width 600mm, thickness 0.3mm). At two edges of the steel plate four electromagnets were installed with four laser displacement sensors to measure the horizontal displacement of the plate. The velocities of the plate were detected by differentiating signals from the displacement sensors in the computer. Digital optimal time controller was designed using Digital Signal Processor (DSP) with Simulink for controlling horizontal positioning system and for converting the values of analog data to digital in the sampling interval then fed to the four electromagnets through four power amplifiers. The result was shown that the application of a magnetic field in the horizontal direction was confirmed to suppress deflection in the levitated flexible steel plate and improves the stability of levitated ultra-thin steel plates [21].

Jeng-Dao Lee and Zhi-Bin Wang (2011) employed the strategy of electromagnetic attractive force in the electromagnetic guiding system to retain the moving platform along the central line. The novel of electromagnetic guiding device was composed of two electromagnets EI-type, gap sensor was used to detect the lateral displacement, a moving platform, linear guide-way and auxiliary wheels were adopted in the guiding device to maintain the motion only along the x-axis direction and to reduce the friction as much as possible. Two current controller and voltage controller were typically utilized to control the electromagnetic force and to reduce the current errors. Current controller includes of a pulse width modulation controller and a buck converter for driving the electromagnets and operated in the continuous conduction mode (CCM). A gap controller with bipolar switching device was used to control the gaps between the moving platform and the magnets. So this paper proposed the numerical simulations of the Cascade SMC Control (CSMC) and Cascade sliding-mode-based genetic algorithm control (CSGAC) which were implemented via MATLAB software. The system with proposed approach had good tracking response and so robust under different step commands and load variations [22].

Mingliang Hao, Qing Hu and Hao Liu (2011) applied an adaptive sliding mode controller (SMC) based on the feedback linearization for the MAGLEV guiding actuator in ropeless elevator. The controllers were simulated in MATLAB platform to control the air-gap altitude of guiding actuator in order to improve elevator performance. The result was shown that the system with SMC has rapid response, non-overshoot and good performance with robustness [23].

Qing Hu, Dongmei Yu, He Wang (2012) described and designed the topological structure of an electromagnetic guidance system in linear elevator. The system includes of eight similar electromagnetic devices which were fixed on the outside the car. According to the balance relation of the electromagnetic guiding force the mathematical model of single electromagnetic guiding U-actuator was established with the rail in X- axis. H∝ control technique was utilized for controlling the guide rail and providing zero-touch between the car and guide rail with considering the impact of disturbances force, parametric variations and uncertainty of the electromagnetic guiding actuator for linear elevator. H∝ control technique was applied to the system based on the principles of selecting three proper weighted functions included of sensitivity weighted function for disturbance, fill sensitivity weighted function for making output recur input, and linear weighted of the controlled station. MATLAB Simulink was used to realize the simulation and the result was shown that the control system had ability to anti disturbance, more accurate and robust stability [24].

Hasan Alipour, Bana Sharifian, Mohammad Bagher, Hadi Afsharirad (2012) proposed three different applicable controllers for double side ropeless elevator guiding systems to provide suitable and smooth motion. The proposed controllers were PID, sliding mode, and new parallel controller based on PID sliding mode controllers. PID controlled the transient part of the system, then the controller was switched to SMC after the rise time of the system response. So in this paper a new application of SMC was introduced, namely equivalent control effect and switching control effect. The system certainties can be controlled by equivalent control effect which can be attained from deriving sliding surface. On the other hand, switching control effect can be controlled the uncertainties of the system which was added to the input signal to the system. The simulation result was realized by MATLAB to illustrate the effect of three controllers, parallel PID sliding mode controller had better performance, short transient time with minimum overshoot and more strong robustness compared with the other controllers [25].

Qing Hu, Dongmei Yu and Mingliang Hao (2012) proposed and described different type of controllers for the single electromagnetic guiding system in the linear elevator to ensure robustness and fast tracking of the system. The proposed controllers were Radial Basis Function (RBF) neural network based on adaptive

sliding mode control method with parallel proportional and differential controller (PD). The guiding system consists of two electromagnets actuators were placed on two sides of the guide-way. At equilibrium position lower and upper positions were equal between the electromagnets and the guide groove. The neural network (RBFNN) was used to replace the switching items of the conventional sliding mode control, to compensate the uncertain parameters and to eliminate vibration of the system. So PD controller was designed as one of parallel control part to adjust RBF network parameters in a small range, to improve the convergence process of neural network and to increase system stability. The controllers were simulated in MATLAB platform and the result showed that the system with proposed controllers was more robustness and had good tracking performance [26].

Han-Wook Cho, Ju-Seong Yu, Chang-Hyun Kim , Ki-JungKim, (2013) proposed a model of dynamic performance evaluation strategy for a 5-degree of freedom magnetic levitation and guidance device. The levitation part was composed of two magnets from left and right side that the capacity was 150 kg, as well as the guidance part was composed of four magnets at each corner that the guidance capacity was 1kg. To obtain an electromechanical interaction between the guidance and levitation magnets, the control systems were modeled and simulated by using the dynamic force equations in the time domain analysis which obtained from the equivalent magnetic circuit model. The PID controller were designed for the levitation and guidance system to regulate the measured air-gaps constantly, which were simulated in MATLAB Simulink and applied on the experimental setup based on DSP control computer. Additionally, digital input filters, discrete sampling times and time delays for calculation of analog to digital converter were considered in the simulations [27].

Chang-Hyun Kim, Jin-Woo Park, Changsun Ahn, Doh Young Park (2013) described and designed the discrete- time PD controller with combing second derivative term of error to the controller for levitating and guiding the magnets in a passive magnetic levitation tray. The area of moving tray was (1m $\times$ 1m) area and weights 100kg which was completely contactless and it can be guided and lifted by external guidance and levitation electromagnets. The length of the system was 3.4 m, the guidance magnets were installed on the both sides of the side frame which constrain the lateral motion of the tray using attractive force. Inductive gap sensors were installed along with electromagnets to measure the air-gap length between the tray

and electromagnets. The second derivative term in the PD controller was used to reduce vibration between the electromagnet support frame and the tray. The passive tray was controlled completely to follow its reference trajectory within 100 um, the stability and performance of the systems were tested and evaluated through experiment [28].

Summary

In this chapter MAGLEV guidance system definition and types are presented, which are mainly achieved by two different principles either by magnetic repulsive or attractive force. In EMS maglev uses attractive force for guiding the train. The guidance forces are produced either by a separate set of levitation and guidance electromagnets or by an integrated set of levitation and guidance electromagnets. In EDS maglev uses repulsive force for prevention of lateral displacement by setting and connecting the propulsion coils or levitation coils from both sides of the guide-way. Once a train is shifted and moved from the center of the rail circulating currents between these coils are induced and this produces the guiding force to keep the train in the center of the guide-way.

In the type of repulsive force superconductivity magnets or permanent magnets are used as a source of energy, whereas in the type of attractive force electromagnets are used as a source of energy.

So in this chapter several literature reviews are addressed relevant to the electromagnetic guidance systems in the field of transportation application. Different type of controllers PD, PID, fuzzy PID, SMC and H∝ have been applied for controlling and stabilizing the guidance system at a desired position based on linear and nonlinear model of the system.

CHAPTER 3

DESIGN PROCEDURE FOR A DC SINGLE ELECTROMAGNETIC COIL HAVING SHELL TYPE CORE

3.1 Introduction

In this chapter, a design procedure for the prototype of an electromagnetic guiding system is described which is analytically modeled and computationally analyzed. In electromagnetic attraction type the shape of the electromagnet core and placement of winding on the core plays a significant role in producing force of attraction and distribution of flux [29].

In this study E-shaped core has been studied to select a proper suitable core for the developed circuit, because shell type core gives better flux distribution when the winding is to be placed in the center leg as explained below. Firstly, a design procedure for a DC electromagnet is presented utilizing analytical solutions and secondly two-dimensional of FEA is used using FEMM software as a concurrent with the above approach to fine-tune the final design process.

In analytical solution the method is purely based on numerical approaches depending on the system design specifications such as the weight of the magnets, air-gap position, current winding and lateral force. The core of the electromagnet is specified basis of the magnet dimensions, wire gauge sizing are derived for an assumed current density in terms of circular mils per ampere, the length and weight of the coil winding are determined and the number of turns is assumed for determining amount of current which is required to pass through the coil to guide the electromagnets in the horizontal direction.

Then the proposed model is analyzed computationally with 2D FEA using FEMM to find out the magnetic parameters such as coil inductance, flux pattern, flux linkage, air-gap flux density and attractive force. Then, the obtained data from FEMM simulation are compared with the analytical calculation.

3.2 Magnetic Core Shape

For construction of magnetic cores there are two types of construction, core type and shell type which are shown in Figures 3.1 and 3.2. E-shell core type requires one coil where the core surrounds the coil and the magnetic fields are around the outside of the coil. As well as in the U- core type construction the coils are outside of the core and a toroid is a good example for this type [30].
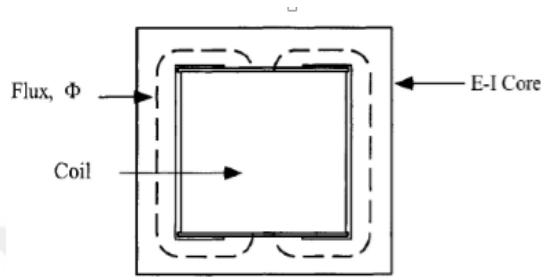
Figure 3.1 E- Shell type construction   **Figure 3.2** U-core type construction
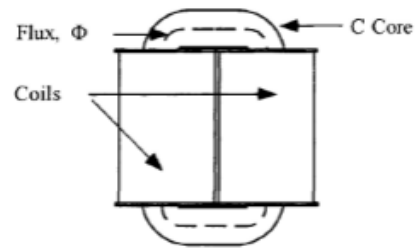
The magnet configuration is chosen on the basis of the required pole face area and the necessary window area to house the excitation coils. There are several types of rail geometries and magnets such as electromagnet with I, U and E shaped rail and various winding arrangements with flat and U-profile rails. The eddy current is generated in the magnetic core which is varied according to the structures of electromagnet and guide-way, this eddy current reduces the attraction force [3, 31].

The shell type core used more for power transformers, autotransformers, and inductors because of E-shaped electromagnet with laminated core structure is a better option which gives less eddy current losses compared to U- shaped core geometry [32].

3.3 Magnetic of E-Shaped Actuator

In this study E-shaped linear actuator is proposed for the horizontal movement system. The silicon iron sheets are arranged in shapes like E, It has a 3-legged structure and each leg can be used for winding but usually the center leg is used [32].

Laminations were chosen over a solid core configuration for two reasons. First and foremost, a laminated core exhibits significantly less eddy currents than a solid core magnet, this eliminates the time delay between a change in the control current and

change in the force. Second, laminations are designed for using in transformers are readily available in materials which exhibit low magnetic hysteresis and high magnetic saturation values [33].

Silicon iron core lamination is selected which is composed of 0.03% Carbon, 0.15% Manganese, 4.25% Silicon and Iron (Fe) material with relative permeability µr 9000, thin (0.25 – 0.50 mm) and insulated to prevent eddy current losses. In AC and DC circuits silicon iron has high permeability, high electrical resistivity, and minimum hysteresis loss [31, 33].

At the center of the core, the coil former (bobbin) is needed for winding the coil systematically that can be made from paper or plastic. A schematic showing the overall structure of laminations and the coil bobbin are given in Figures 3.3, 3.4.
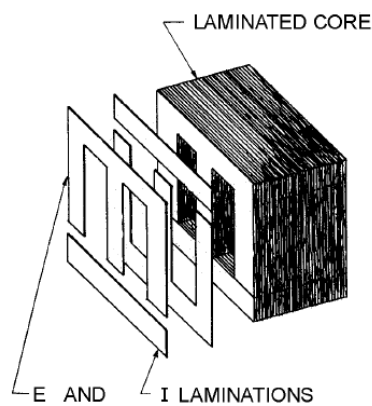
Figure 3.3 Lamination core structure   **Figure 3.4** Coil former (Bobbin)
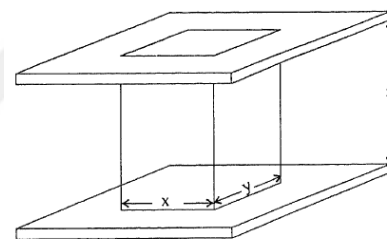
3.3.1 Magnetic Equivalent Circuit

The configuration of physical arrangement EI core is depicted in Figure 3.5, which consists of two U cores and a ferrous plate. It has a joint flux in the center leg and twin flux paths in the other legs of the E core. The center pole length must be greater than two times with the other poles in order not to saturate E core [32].

The magnetic equivalent circuit can be depicted as Figure 3.6, it forms two flux loops Ø1, Ø2 in the E-shaped electromagnet, magnetic flux passes through the air-gap between the poles of the electromagnet and ferrous plate in each loop and this generates a force of attraction to guide a ferrous plate at a nominal operating air-gap of 10 mm and the parameters are given in Table 3.1 [35].
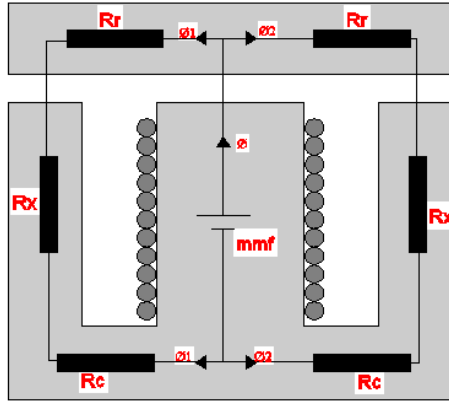
Figure 3.5 Magnetic circuit of EI Core
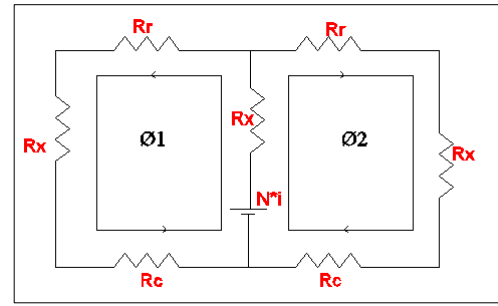
Figure 3.6 Magnetic equivalent circuit of one EI type electromagnet

Table 3.1 Parameters of EI core magnetic circuit

Symbol	Parameters	Unit
mmF	Magneto motive force	At
$\emptyset$	Total magnetic flux	Wb
$\emptyset1$, $\emptyset2$	Parallel magnetic flux	Wb
N	Turn number of a coil	turn
Rx	Reluctances of the air-gap length	H^{-1}
Rr	Reluctances of the rail body	H^{-1}
Rc	Reluctances of the magnetic core	H^{-1}

3.3.2 Dimension of Silicon Iron Shell Type Core and Guide- Rail

The overall dimensions of the iron core laminations are 192 mm (length), 128 mm (height) and 70mm (thickness) with the mass is 12.4 kg. The main dimensions of the core lamination are sketched in Figure 3.7. Table 3.2 lists the electromagnet dimension indices along with the relevant values for the experimental electromagnet.
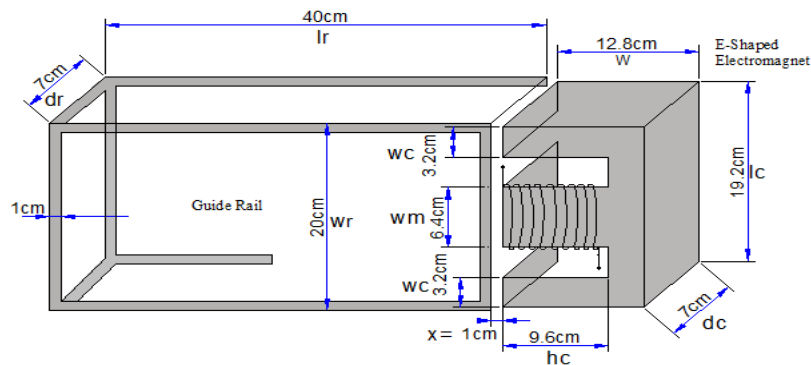
Figure 3.7 Dimension of E-shaped actuator and the ferromagnetic plate

Table 3.2 Experimental electromagnet indices and value

Index	Value	Dimension
Ferromagnetic guide-rail		
Ar	0.014 m^2	Cross section area of ferromagnetic plate
Mr	20 kg	Mass of ferromagnetic plate
lr	40 cm	Length of ferromagnetic plate
wr	20 cm	Width of ferromagnetic plate
hr	9 cm	Height of the ferromagnetic plate
dr	1 cm	Thickness of ferromagnetic plate
Dimension of shell type core		
Magnet type		3 pole shell type (E-shaped)
Mc	12.4 kg	Mass of the electromagnet
w	12.8 cm	Width of the magnetic core
lc	19.2 cm	Length of the electromagnet
dc	7 cm	Thickness of the electromagnet core
hc	9.6 cm	Height of the pole pieces
wc	3.2 cm	Width of the pole pieces
wm	6.4 cm	Width between the electromagnets pole pieces
x	1 cm	Lateral air-gap length

3.4 Design Procedure

In this section the design procedure of the prototype guidance system is presented based on an analytical approach and FEA, which is used for simplicity of the design procedure and overall high reliability of the system. The prototype of the electromagnetic guiding system consists of two symmetrical actuators, thereafter the analysis and design of one electromagnet is sufficient for the analysis of the system.

3.4.1 Analytical Approach

The capability of the magnet to attract a ferromagnetic guide-way from a given air-gap position is the attractive force. Strength of magnetic force will vary with different shape of the magnet. The maximum force can be expressed by [36]:

$$F = \frac{B^2 \cdot A}{2\mu_0} \tag{3.1}$$

where, F is the electromagnetic attractive force in Newton,

B is the magnetic flux in tesla,

A is the cross sectional area of the pole face in square meters and

μ_0 is the free space (air) permeability, $\mu_0 = 4\pi \times 10^{-7} \; HM^{-1}$

In this design a center pole of E- shaped core is used for winding that is made from silicon iron pole with the dimensions; 640 mm width, height 70 mm and 960 mm pitch. The cross-sectional area can be found in (3.2).

Area of center pole limb is:

$$A = X \cdot Y \quad m^2 \tag{3.2}$$

$$A = 0.064 \times 0.07$$

$$A = 0.00448 \; m^2$$

When the magnet energizes, it will tend to attract the ferromagnetic guide-way around its pole, in such a case study the maximum mass of the ferromagnetic guide-way to be attracted is (10 Kg) and the gravitational force is (9.81 m/ s²), we already know,

$$F_g = m \cdot g \tag{3.3}$$

$$F_g = (10 \; kg) \times (9.81 \; m/s^2)$$

$$F_g = 98.1 \; N$$

Substituting in (3.1)

$$F = \frac{B^2 \cdot A}{2\mu_0}$$

$$98.1 = (B^2 \times 0.00448)/(2 \times 4\pi \times 10^{-7})$$

$$B = 0.23 \quad wb/m^2$$

From (3.1), the flux density B for a given core geometry can be calculated, if the value of B is more than 1.6T, a larger core must be used. When the B field needed is known, the mmF force can be computed from the product of the number of turns in the winding and the current [36, 37].

The total flux density in the core is the same flux density in the air-gap; hence it can be obtained from (3.4)

$$\emptyset = B \cdot A \tag{3.4}$$

$\emptyset = 0.23 \times 0.00448, \quad \emptyset = 0.00103 \text{ Wb}$

The magnetizing field (H) in the air-gap is given by:

$$H_g = B/\mu_0 \tag{3.5}$$

$$H_g = 0.23/(4 \times 3.14 \times 10^{-7})$$

$$H_g = 183,121 \quad At/m$$

$$H_c = B/\mu_0 \cdot \mu_r$$

$$H_c = \frac{0.23}{9000 \times 4 \times 3.14 \times 10^{-7}}$$

$$H_c = 20.3 \quad At/m$$

$$H = 183,141 \quad At/m$$

Applying the Ampere's circuital law and suppose the leakage flux is negligible. L_g is the air-gap length specified as 10 mm, the magneto-motive force mmF is the product of the number of turns of the wire and the current that will flow the electromagnet which is given in (3.6) [36].

$$NI = H_c \cdot L_c + H_g \cdot L_g \tag{3.6}$$

$$NI = (20.3 \times 0.608) + (183121 \times 10 \times 10^{-3})$$

$$mmF = 1834 \quad AT$$

To obtain the defined excitation it is necessary to choose either the current (i) or number of turns N. In practice this decision will be affected by the current (or voltage) capability of the magnet power amplifier, although apart from a scaling effect the overall dynamics are largely unaffected by this decision. If one of the variable is chosen the other variable can be computed, thus if the number of turns is chosen to be 553, then the electromagnet current can be obtained by [36]:

$$i = \frac{mmF}{N} \tag{3.7}$$

$$i = \frac{1859}{553} \qquad N = 553 \ turns$$

$$i = 3.3 \ A$$

Finally the attractive force which is produced between E-shaped magnet and a ferromagnetic guide-way is described by:

$$F = \frac{\mu_0 N^2 A}{2} \left[\frac{i(t)}{x(t)} \right]^2 \tag{3.8}$$

where, $N = 553\ turns$, $A = 0.00448\ m^2$, $i = 3.3\ A\ and\ x = 0.01\ m$

$F = 93.6\ \ Newtons$

3.4.1.1 Wire Selection

For a given current density the choice of the wire gauges is conveniently selected in terms of circular mils per ampere. A circular mil usually abbreviated as (Cir mil), it is the area of a circle which is diameter is 1 mil (0.001 inch). To determine the circular mils for any wire, the required current and current density need to be known before selecting and computing the wire gauge [36].

$Cirmils\ =\ current\ \cdot\ working\ current\ density$ \hspace{1cm} (3.9)

The standard working current density (j) is: (700, 1000, 1500, 2000….. etc).

In such a case the working current density is assumed to 1000, and then the circular mils can be obtained from (3.9).

$Cirmils\ =\ 3.3 \times 1000 = 3300$

According to the standard Annealed copper wire, solid standard wire gauge (B&S) in English units can be extracted from the following:

For gauge number 16 the cir mil is 4095.88
For gauge number 17 the cir mil is 3135.91
For gauge number 18 the cir mil is 2303.93

The diameters of 3 different wire gauges are:
Diameter of 16 SWG is 0.06 inch
Diameter of 17 SWG is 0.056 inch
Diameter of 18 SWG is 0.048 inch

According to the SWG and considering of 3 different types of wire gauge as mentioned in the above the gauge 17 is selected for this design because it gives the approximate values to compute/selected values. The diameter of wire gauge 17 is 0.056 inch which is equivalent to 1.4mm.

3.4.1.2 Determining the Number of the Layers

To determine the number of the layers that is needed to be winding on the former of the electromagnet. The following parameters are known; the diameter of the former is 100 mm, the former length is 96 mm and the diameter of the wire to be winding is 1.4 mm [36]. In the first layer the maximum number of winding is:

$$\frac{96\ mm}{1.4\ mm} = 68.5\ turns$$

Chosen a stacking factor of 0.9, the maximum number of turns is:

$$68.5 \times 0.9 = 62 \quad turns$$

If each layer is to have this maximum number of turns, then, the total number of layers required to give the total number of turns is:

$$Total\ no.of\ layers = \frac{total\ number\ of\ turns}{total\ no.of\ turns\ on\ the\ first\ layer} \tag{3.10}$$

Total number of layers = 553/62= 8.9 layers ≈ 9 layers

3.4.1.3 Determining the Length of the Wire Used

The perimeter of each subsequent layer is increased by 2d at rewinding the wire, where, d is the diameter of the wire (1.4 mm).

Hence, according to form of an arithmetic progressive (AP).

The perimeter (length) of first layer is:

$$\pi \times D \times 62 = \pi \times 100mm \times 62\ turns = 314mm \times 62\ turns$$

First layer: the wire length of one turn is 314 mm

Second layer: the wire length of one turn is:

$$(314\ mm + 2d) = 314\ mm + 2 \times (1.4\ mm)$$

Third layer: the wire length of one turn is = perimeter of second layer + 2d

Fourth layer: the length of one turn is = perimeter of third layer + 2d

Fifth layer: the length of one turn is = perimeter of fourth layer + 2d ……etc

The formed of AP has the following parameters:

First term (a) = 314 mm, common difference $d = 2d = 2.8\ mm$, number of terms $n = 10$

Using the sum of arithmetic progressive the wire length can be computed:

$$Sum = \frac{n}{2}\ (2\ a + (n - 1) \cdot d) \tag{3.11}$$

$$Sum = \frac{9}{2}\left((2 \times 314) + (9 - 1) \times 1.4\right)$$

$$Sum = 2876.4\ mm$$

Hence the required total wire length is the sum multiply by the total number of turns. The total length is ($2876.4 \times 62 = 178336\ mm$) or 178 m, which is the same as 194.6 yards or 584 feet.

Total length of the wire = 178 m

3.4.1.4 Wire Resistance

From the table of resistance the resistance of the wire is calculated, the resistance of 17 gauge is 10.9 Ω per km and 35.6 Ω per 1000 ft. [36].

Since the length of the wire is 584 feet and the wire resistance is:

$$\left(10.9 \times \frac{178}{1000}\right) = 1.94\ \Omega.$$

So the resistance of the wire can be found from,

$$R = \rho \frac{L}{A} \tag{3.12}$$

where, ρ is the resistivity of conductor copper (1.68×10^{-8}) Ω. m, diameter of wire is 1.4 mm, A is cross sectional area of the wire

$$A = \left(\frac{1.4 \times 10^{-3}}{2}\right) \times 3.14$$

$$A = 1.54 \times 10^{-6}\ m^2$$

$$l = 178\ m$$

$$R = 1.94\ \Omega$$

3.4.1.5 Determining the Weight of the Wire

Normally the wire is sold per kilogram, from the table of standard wire gage the gage of (17) has a weight of 0.0142 kg per meter and 0.00952 Ib/ft. As mentioned above, the length of the wire used is 178 m, thus the weight of wire is computed as follows:

$$\left(0.0142 \frac{kg}{m}\right) \times 178\ m = 2.52\ kg$$

The electromagnet was designed and constructed according to the above procedure and the parameters are shown in the table below.

Table 3.3 Parameters of two actuators of the guidance system

Parameters	Values
Mass of each electromagnet	12.4 kg
No of turns of the coil	553 turns
No of magnets	2
Resistivity of core (estimated value)	98 n Ωm
Gauge of enamel copper wire	17 gauge
Resistance of the coil 1	2.05 ohms
Resistance of the coil 2	2.04 ohms
Coil inductance 1	0.142 H
Coil inductance 2	0.152 H

3.4.1.6 Circuit Theory Inductance

The coil inductance of the wire is calculated as follows:

$$L(x) = \frac{N\text{Ø}}{I} \quad \text{or,} \tag{3.13}$$

$$L(x) = \frac{\mu_0 \cdot A_c \cdot N^2}{x}$$

$$L(x) = \frac{553 \times 0.00103}{3.3} = 0.17 \ H$$

The coil inductance depends on the total reluctance which varies according to the plate positions (x) and winding current (i). The inductance profile is affected because the BH curve of the core material is nonlinear. Magnetic permeability is $\mu = \mu_0 \mu_r$ and the coefficient depends on the B/H ratio. So as the coil current and position increases, the value of inductance is reduced. The coil inductance reaches its maximum value (L_a) at the position ($x = 0$), its minimum value (L_u) at positions ($x = 2$ cm). This situation is taken into consideration in the FEA. So the coil inductance is verified experimentally and it was measured with an LCR meter for each plate position as shown in Figure 3.8 [32]. In order to avoid any significant error, the coil inductance must be computed based upon the effective gap area rather than the actual center-pole area [38].
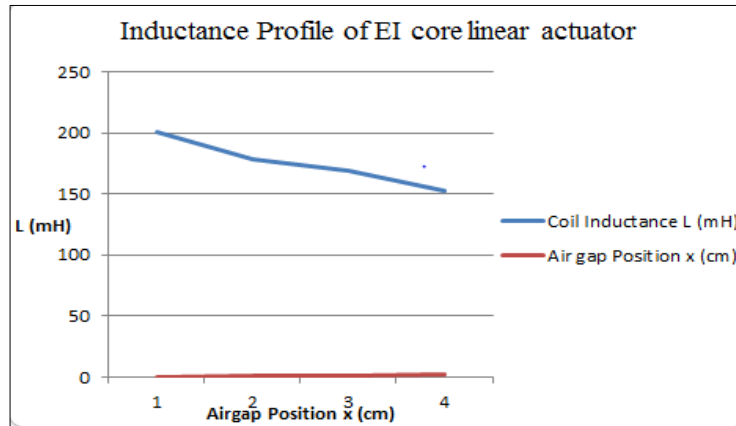
Figure 3.8 Inductance profile of EI core linear actuator

3.4.2 FEA Approach and FEMM Software for the Proposed System

Two-dimensional FEA simulation has been accomplished to illustrate the proposed structure of electromagnetic phenomenon [39] and to verify the design parameters of DC electromagnets with the analytical method. FEA is a numerical technique for detecting approximate solutions to the partial differential equations that arise in many scientific and engineering applications. In general, it provides more accurate results than the magnetic analytical method with the equivalent circuit method because it considers a large number of flux paths compared to the magnetic equivalent circuit method [6]. FEMM software has been used for this purpose.

FEMM is a suite of programs for solving low frequency electromagnetic problems on 2D planar and 3D axisymmetric domains. The program addresses currently linear and nonlinear time harmonic magnetic problems, magneto static linear and nonlinear problems, linear electrostatic problems and steady-state heat flow problems [40]. Based on the Maxwell's equations the electromagnetic field equations are expressed in terms of the magnetic field (H), electric field intensity, flux density (B) and the current density (J) [41].

3.4.2.1 Simulation using FEMM

Analyzing the proposed system in FEMM simulation consists of three steps are:

A- Pre-processing stage

In the pre-processing step, according to the actual units of length the model of the magnetizing system is designed. Material properties for each component are assigned

29

that are used in the magnetizing system. At this stage also the current windings in the coil, the number of turns, and direction must be defined. Afterwards, the defined model is meshed into small pieces (elements) of simple shapes connected at specified points (nodes). FEMM generates a uniform mesh for the whole geometry through using an automatic mesh generator to enhance the accuracy of the solution and to refine the mesh in the area of interest. Finally, the boundary condition is defined to minimize the model size and assist the solution as a shown in Figure 3.9 [42].
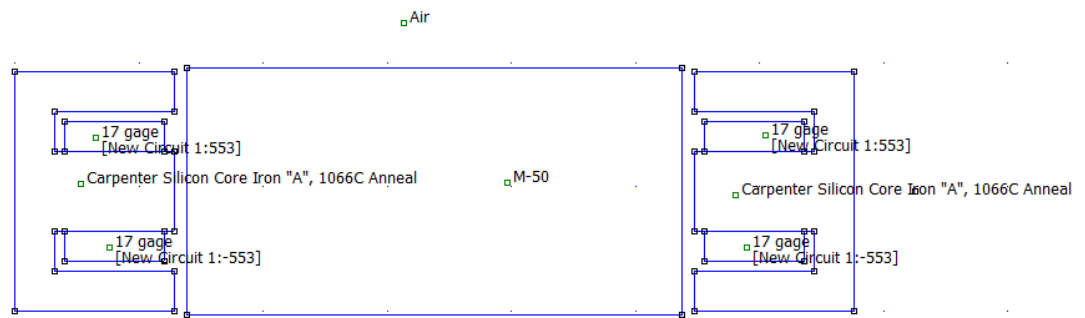
Figure 3.9 Design of problem in pre-processing stage

B- Solving Stage

To describe the problem, the solver starts to solve automatically after taking a set of data file and solves according to the relevant Maxwell's equations to obtain values for the desired field throughout the solution domain [41, 42]. Figure 3.10 shows the formulated field equations in the pre-processing step. It has to be observed that in each triangle the value of potential is approximated from the linear interpolation of its values at its three vertices [43].
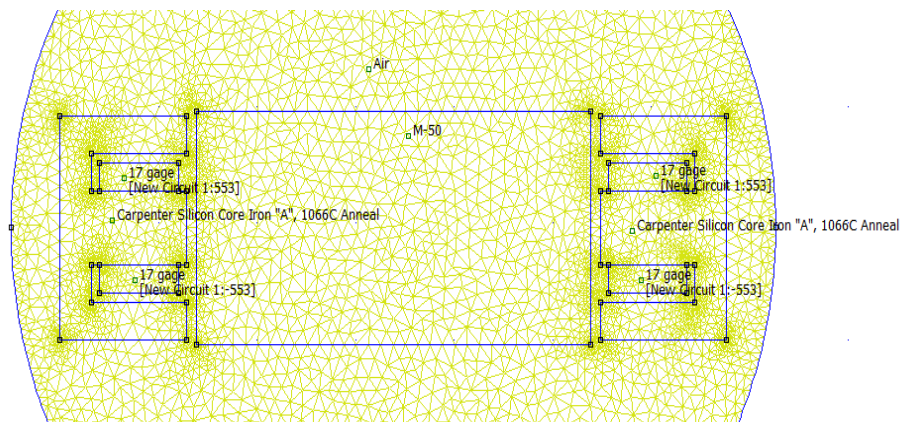
Figure 3.10 Finite element distributions in solving stage after meshed

30

C- Post-Processing Stage

The evaluation can be done at this stage; the solver output is processed to determine the required parameters [42, 43]. This stage has three modes to view the solutions; point mode, block mode and contour mode. In the point values mode various points can be selected in the solution region, in block mode a sub domain can be defined in the solution region otherwise in contour mode arbitrary contours can be defined in the solution region [44]. Field solutions can be displayed in the form of contour and density plots. Figures 3.11, 3.12 present symmetrical simulations of flux pattern, magnetic flux density, and field strength of two silicon iron E-shaped inductors with 1cm air-gap length.
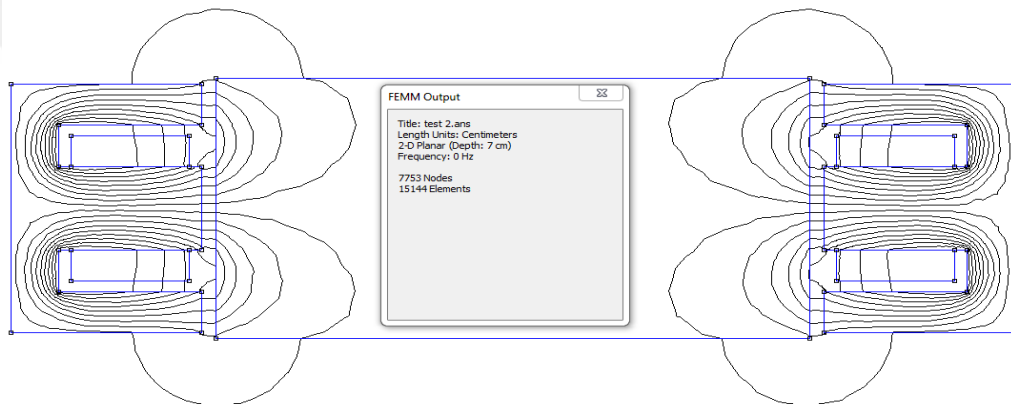
Figure 3.11 Simulation of magnetic flux density in post-processing stage
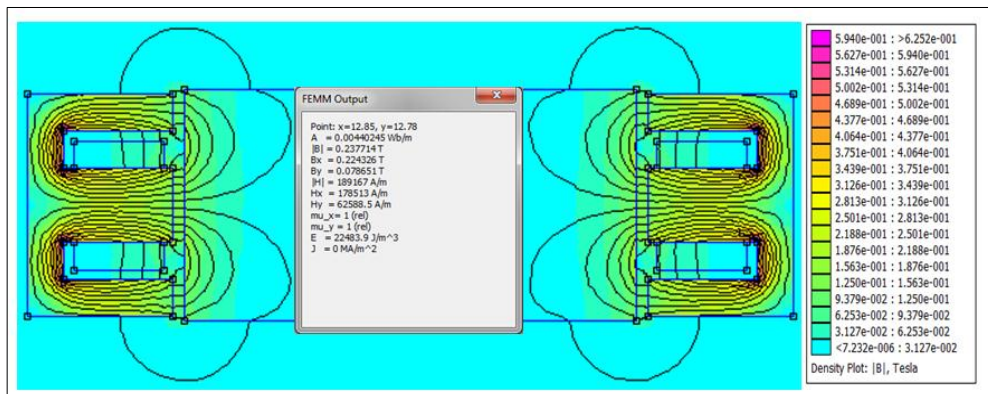
Figure 3.12 Magnetic field of silicon iron E- shaped actuator

3.4.2.2 Finite Element Electromagnetic DC Force

The attractive DC electromagnetic force can be computed based on two methods; the "Weighted Stress Tensor" block integral and through the "Maxwell Stress Tensor"

line integral. The Weighted Stress Tensor is the recommended method that can be used to determine the force. It is easier to select the block regions upon which the force is to be computed as shown in Figures 3.13 and 3.14.
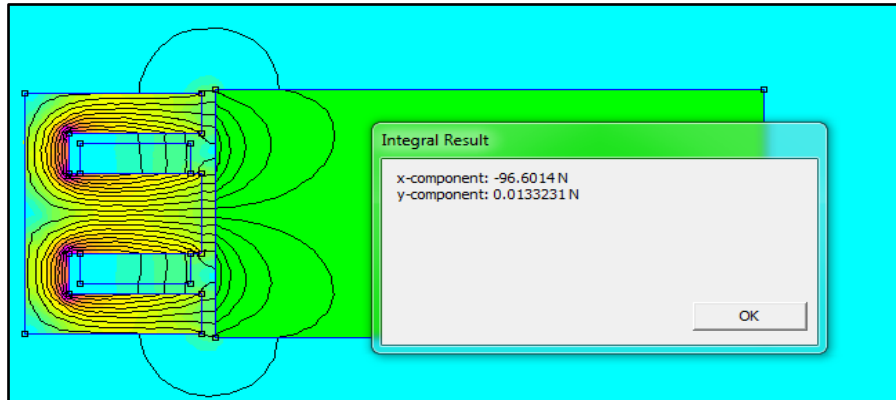
Figure 3.13 Block integral force on I-section with 1cm air-gap length
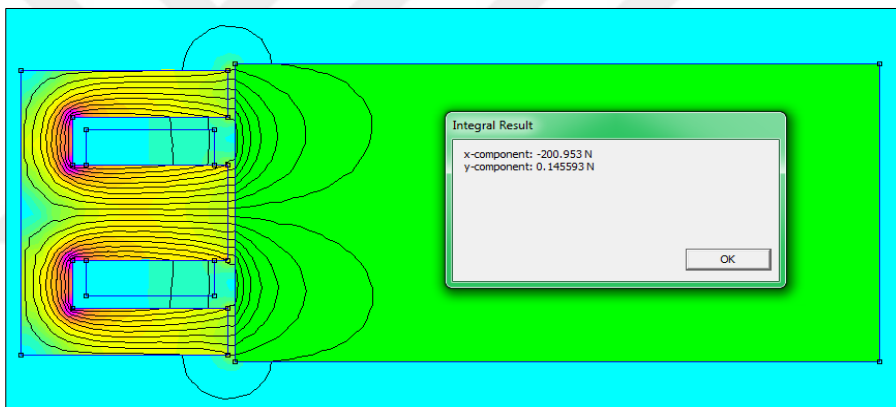
Figure 3.14 Block integral force on I-section with 0.5 cm air-gap length

Figures 3.15 and 3.16 show the effect of two inductors on the ferromagnetic plate at different air-gap position under similar operating conditions (number of turns and exciting current). It has been noticed that the resultant of the lateral guidance force is zero when the ferromagnetic plate is placed centrally with the two electromagnets, in other words the air-gap length between two electromagnets and rail is 1cm as depicted in Figure 3.15. The shifting of two electromagnets has been done in both directions, which is 1.5 cm from one side and 0.5 cm in other side with respect to the center position 1 cm, the value of guidance force has been changed as shown in Figure 3.16.

It can be noticed that in Figure 3.15 and Figure 3.16 with the decrease of air-gap position the developed attractive force between electromagnets and the ferromagnetic plate has been increased. Otherwise in actual situation the force between the electromagnet and ferromagnetic plate will vary inversely proportion to the square of the air-gap.
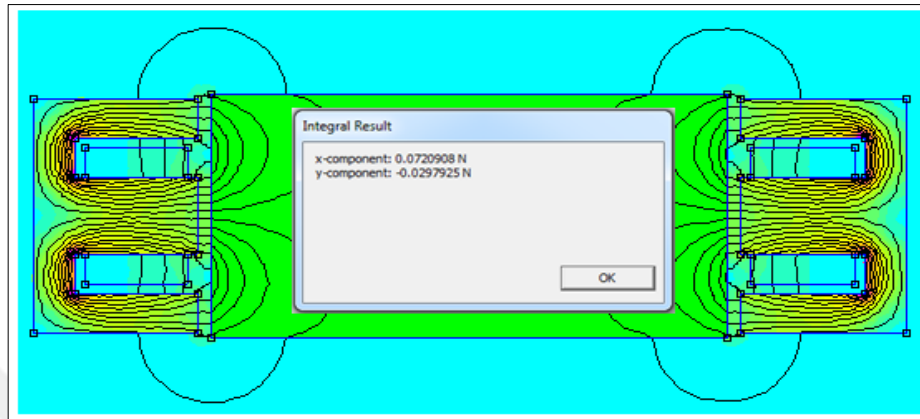
Figure 3.15 Block integral force of the system structure for 1cm air-gap length
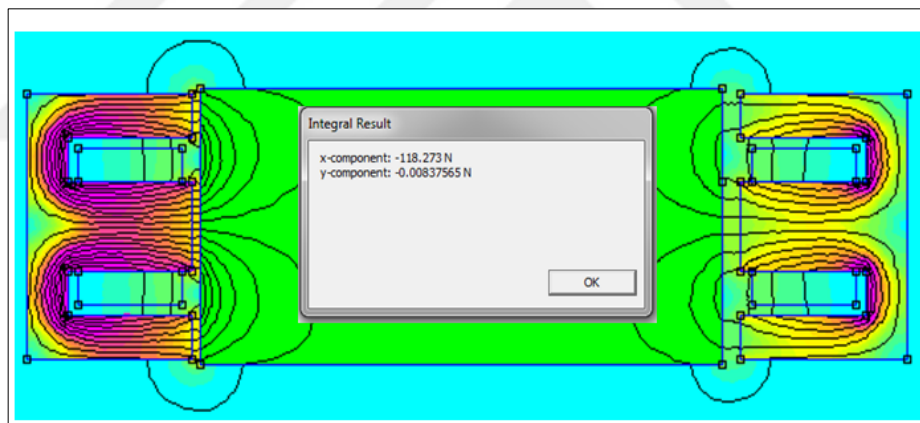
Figure 3.16 Block integral force of the system structure for (0.5 and 1.5) cm air-gap length

3.4.2.3 Finite Element Inductance

For the purposes of calculating the coil inductance (L) in the finite element solution, at the center of the middle pole core the inductor is placed, a current of 3.3A and the number of turns are applied to the coil. After analyzing the model, the coil inductance can be derived from the circuit properties button, the value of "Flux/Current" can be interpreted directly as self-inductance ($L = 0.17$ H). The Figures below show the circuit properties dialog for coil inductance value with different air-gap length.

33
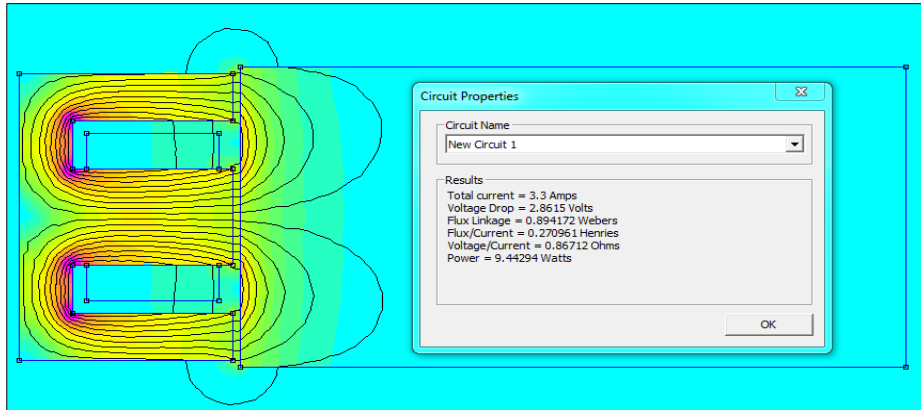
Figure 3.17 Circuit properties for 0.5 cm air-gap length
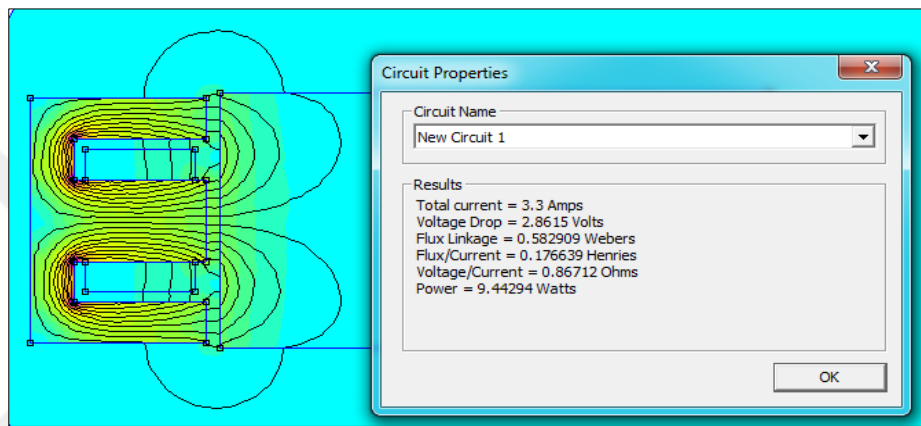
Figure 3.18 Circuit properties for 1cm air-gap length

In FEA analysis, BH characteristic of the core material is taken into consideration and the BH curve is given in Figure 3.19.
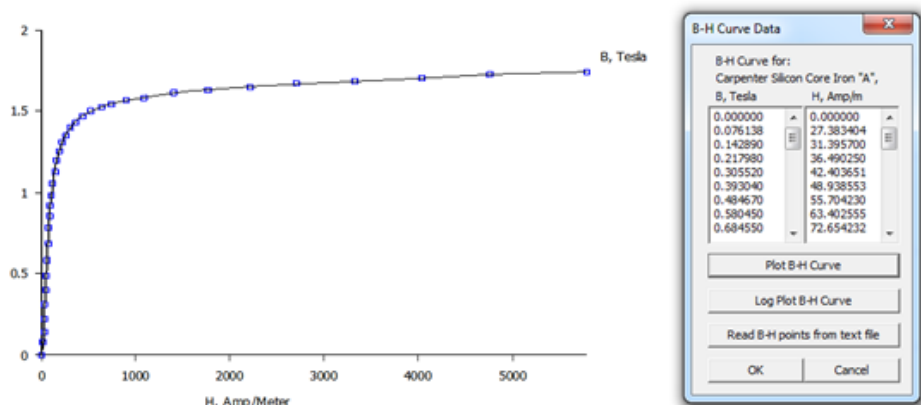
Figure 3.19 BH curve of the core material

Table 3.3 shows comparing magnetic parameters from FEA and analytical approach. The attractive force and coil inductance are obtained by setting the DC excitation

34

current circuit to 3.3 A with N=553 turns of 17 SWG copper coil (1.4 mm diameter). It can be seen that the parameter values from the analytical and finite element results are very close with each other. On the other hand, the value of coil resistance has a rate of error; this error is attributable to the coil properties in terms of resistivity, length and cross sectional area of the wire gauge.

Table 3.4 Comparing magnetic parameters

Magnetic Parameters at excitation current (3.3A)	Analytical method	FEA method
Coil inductance (H)	0.17	0.17
Flux density B (T)	0.23	0.2347
Coil resistance (Ω)	1.94	1.73
Magnetic field H (AT/m)	183141	186372
Attractive force of one coil (N)	93.6	96.6

3.4.2.4 Simulation Results and Discussion

In this analysis, different simulations have been carried out for the two inductors in terms of flux pattern, magnetic field and plot of the flux density vector. Figures 3.20 and 3.21 show the plot of flux density, flux pattern and density plot respectively for 2- coils that the air-gap is 0.5 cm from left side and 1.5 cm length from right side, with coil-current of 3.3A and no. of turns 553. Figures 3.22 and 3.23 represent the characteristic of vector plot of flux density, flux pattern and field density plot for 2 inductors respectively, with symmetrical air-gap length of both sides of the ferromagnetic plate at the same number of turns and coil-current.
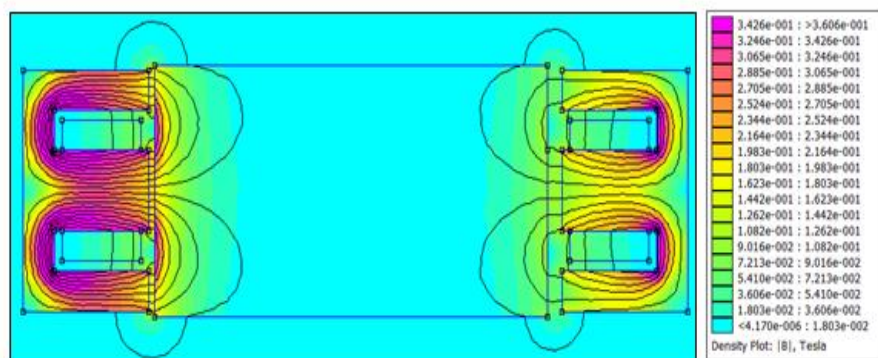
Figure 3.20 Flux pattern and flux density of 2 inductors plot for x=0.5 and 1.5 cm
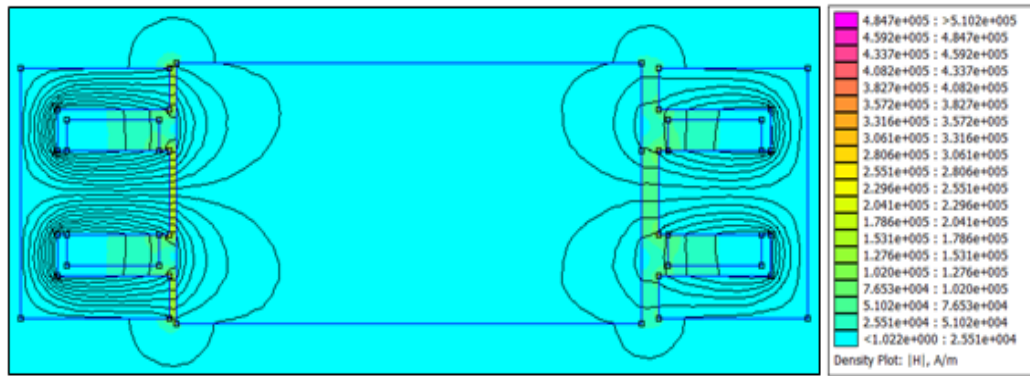
Figure 3.21 Density plot of 2 inductors for x=0.5 cm and 1.5 cm
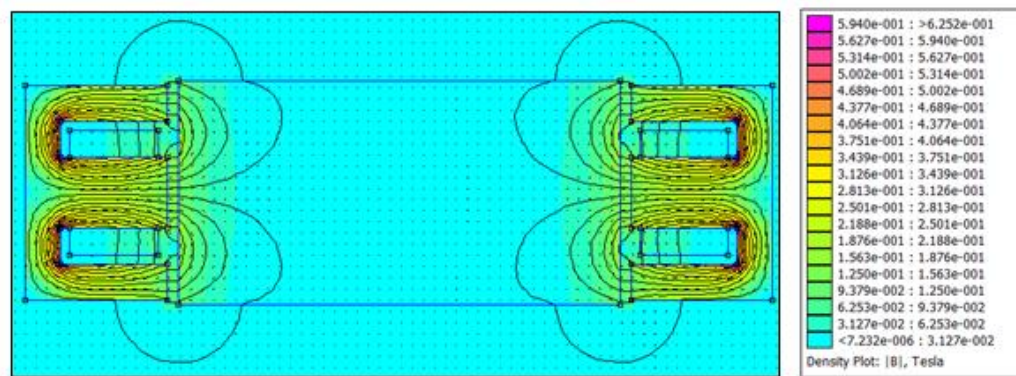
Figure 3.22 Flux pattern and flux density of 2 inductors for symmetrical air-gap length 1cm
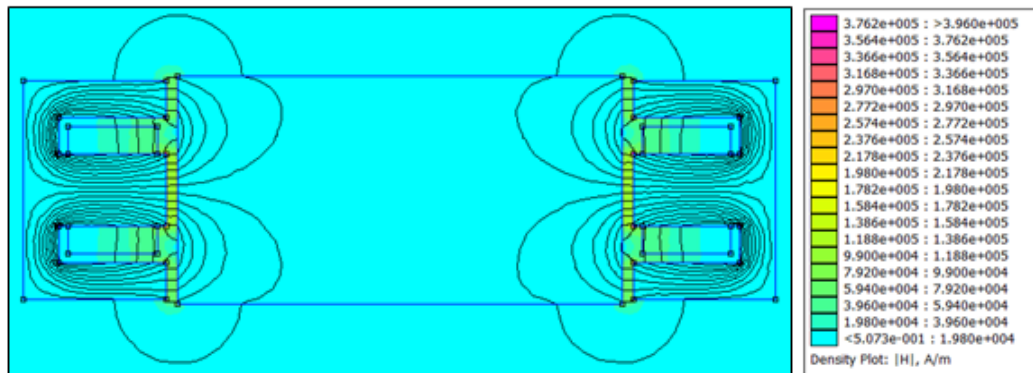
Figure 3.23 Density plot of 2 inductors for symmetrical air-gap length 1cm

From the analysis above, it has been observed that with the increase of air-gap the generated flux, flux linkage, flux density, and attractive forces between electromagnets and plate are decreased and leakage flux is increased and vice-versa.

Summary

The design procedures of the prototype guidance system have been built based on the given dimension which is designed analytically and computed numerically. 2D FEA

is used as a tool for solution of magneto static problems and to verify the overall design process. FEMM solution requires three steps; pre- processing stage starts with the creation of a geometrical model of the system according to the actual units of length, then specifying the material properties of each component that are used in the magnetizing system.

Afterwards the defined model is meshed into a uniform mesh for the whole geometry using an automatic mesh generator to enhance the accuracy of the solution and to refine the mesh in the area of interest. Finally, the boundary condition is set properly to minimize the model size and assist the solution. After analyzing the model in the post processing stage, the influence of the air-gap thickness on the coil inductance, magnetic flux and attractive force are investigated.

CHAPTER 4

SYSTEM STRUCTURE AND MATHEMATICAL REPRESENTATION OF AN ELECTROMAGNETIC GUIDANCE SYSTEM

4.1 Introduction

Although the actual overall lateral guidance system is composed of several electromagnets modules along the side wall of the vehicle, each module has motion freedom. The system can be simplified into two electromagnetic circuits on each side of the vehicle which are controlled by a specific current.

In this chapter the mathematical model and theoretical background of an electromagnetic guidance system is discussed using the basic concept, the models for the force actuator, the plant, the sensor for considering distance dependent dynamic and both electrical and mechanical characteristics of the system. Electrical formula comes from the Kirchhoff Voltage Law (KVL) of the electrical circuit of the system. Dynamic equation of horizontal direction is the net force of the system, which can be represented the difference of an electromagnetic force between the right and left side. Electromagnetic force formula represents that the current passing though the coil which produces an electromagnetic force, relation of current and electromagnetic force is second order polynomial, so the system is nonlinear. The system must be linearized to be able to control it at the nominal operating points using linear control theory, for the purpose of linearizing the system characteristics Taylor Series Expansion technique is used to abbreviate the high order.

Based on the linear model, the transfer function can be obtained by transforming time domain into Laplace domain. A transfer function (TF) is the ratio of the output of the system to the input of the system, in the Laplace domain considering system initial conditions and equilibrium points to be zero. The system must be linear and time-invariant to get transfer function. TF is a criterion to comment on stability, performance, response and characteristics of the system [45].

4.2 System Structure

The physical structure of the guidance system as depicted below in Figure 4.1 consists of a pair of electromagnets placed on both sides of the rigid ferromagnetic plate (guide-way) in the horizontal direction. Each electromagnet is used as the force actuator; it produces the force to attract the rigid ferromagnetic guide-way in lateral ward against other side force. Both electromagnets are same in the structure and parameters, each of the E-shaped magnets is a single-pole coil, single-pole area (A). At the balance position the static current (i_0) passes through the magnets on both sides where the air-gap positions are same (x_0). Once the magnets move away from this balance position the gap is changing by Δx, the current will get larger by Δi on this side where gap gets larger, as well as the current will decrease on the other side where gap gets smaller by Δx, (taking the left direction as positive direction) [19]. The difference between these two forces keeps the position between two electromagnets and the guide-way in the horizontal direction.

There are also some disturbances such as wind, fluctuation in the line voltage. The effect of disturbance is supposed to be negligible compared to other two forces that are acting on the plate. The target is to balance these two forces at a certain position known as the desired position or steady-state position [46].
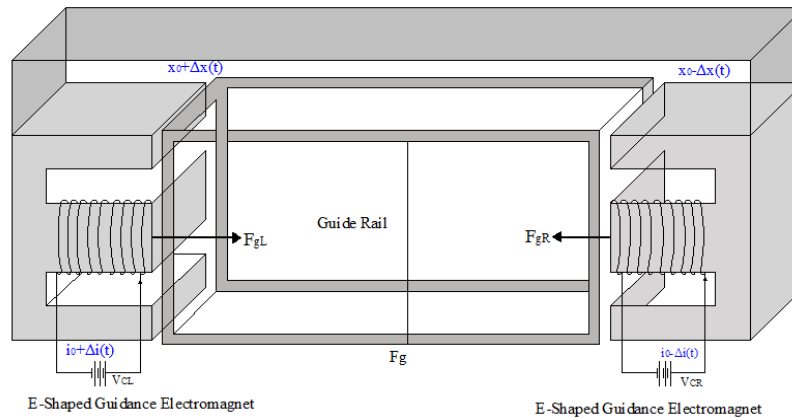
Figure 4.1 System structure of single point guidance system in X- axis direction

4.2.1 Force Actuator Model of Single E-shaped Electromagnet

The dual electromagnets act as an actuator which provides the basic guidance force. For analyzing the electromagnetic guidance force acting of single actuator is considered. Magnetic flux is generated when the electric current is passed through a

wire wrapped around a core. Assuming an air-gap flux is uniform and magnetic flux which are produced by the electromagnets pass through the linear guide-way with ignoring leakage flux and eddy current losses [3, 47]. The coil inductance can be expressed as: [3]

$$L(x) = \frac{N}{i(t)} \cdot \emptyset \tag{4.1}$$

$$L(x) = \frac{N \cdot}{i(t)} \frac{Ni(t)}{R} \quad , \quad L(x) = \frac{N^2}{R} \tag{4.2}$$

where, N is the No. of the coil turns, $i(t)$ is the instantaneous current through the coil, $\emptyset$ is the total flux in the magnetic circuit and R is the total reluctance of the entire magnetic circuit [3, 47].

So, the instantaneous coil inductance can be expressed in (4.3) with reference to the Figure 3.6, the reluctance of magnetic core can be ignored, hence only the reluctance of the air-gap is considered in the magnetic equivalent circuit, the total length of the air-gap is equal to $x(t)$.

$$L(x) = \frac{\mu_0 \cdot N^2 \cdot A_c}{x(t)} \tag{4.3}$$

where, μ_0 is the permeability of free space, $x(t)$ is the air-gap length between ferromagnetic plate and magnet pole [3].

At any equilibrium position (x_0) the normalize inductance of the magnet coil is given by (4.4) [3].

$$L_0(x) = \frac{\mu_0 \cdot N^2 \cdot A}{x_0} \tag{4.4}$$

At operating point the value of coil inductance is not constant varies approximately with lateral position. When the electromagnet is closer to the plate, total inductance increases otherwise it is far away from the plate, total inductance decreases. Thus, under the effect of the rigid plate the total inductance value can be approximated in (4.5) [48].

$$L(x) = L_c + \frac{L_0 \cdot x_0}{x} \tag{4.5}$$

where, the inductance $L(x)$ has its largest value when the magnet is next to the ferromagnetic plate and decreases to a constant value. L_c is the self-inductance of the coil in the absence of the ferromagnetic plate, L_0 is the additional value

contributed by the ferromagnetic plate (inductance at reference position x_0), x_0 defined reference position and x is the position of ferromagnetic plate from x_0 [48].

To determine the value of self-inductance, AC voltage and ampere method is applied to the coil at power frequency, the coil impedance is measured at different voltage levels and then the average value is taken for the calculation of coil inductance [49]. The attraction force between the electromagnet coil and the ferromagnetic plate is given in (4.6) at any particular point of the time.

$$F(i,x) = -\frac{d}{dx} \cdot \left[\frac{1}{2} L(x) \cdot i(t)^2\right] \tag{4.6}$$

In the above expression the negative sign indicates the direction of the generated force. The attractive force attempts to decrease the air-gap length with the incremental change of current coil. Now putting the inductance value from (4.3) and substituted into (4.6), the equation of attraction force becomes: [47].

$$F(i,x) = \frac{\mu_0 \cdot N^2 \cdot A}{2} \left[\frac{i(t)}{x(t)}\right]^2 \tag{4.7}$$

At the equilibrium points (i_0, x_0) the equation will be,

$$F(i_0, x_0) = \frac{\mu_0 \cdot N^2 \cdot A}{2} \left[\frac{i_0}{x_0}\right]^2 \tag{4.8}$$

A magnetic force for single electromagnetic coil can be written in a simple form as:

$$F(i,x) = K \left[\frac{i(t)}{x(t)}\right]^2 \tag{4.9}$$

where, $K = \frac{\mu_0 \cdot N^2 \cdot A}{2}$

Second Derivation to obtain Electromagnetic Force of a Single Electromagnet E-Shaped:

To obtain the electromagnetic force, the reluctance of the core must be defined using cross-sectional area of the core and air-gaps. Magneto motive force can be determined using current passing though the coil and number of turns. The electromotive force mmF (A.t) is:

$$mmF = N.i \tag{4.10}$$

Magnetic flux $\emptyset$ is the ratio of magnetomotive force to the total reluctance which produced through the coil as given in (4.11)

$$\emptyset = \frac{MMF}{R_{total}} \qquad\qquad (4.11)$$

Reference to the Figure 3.6 the reluctance is the function of magnetic parameter and geometrical core, the total reluctance of the electromagnet circuit consists of the reluctance of magnet core R_c, the reluctance of ferromagnetic guide-way R_{fo} and the reluctance of air-gap R_g. The E-shaped magnetic circuit consists of two identical U shaped core halves; all reluctances are in parallel, so the total reluctance is denoted by the following equation [50].

$$\frac{1}{R_{Total}} = \frac{1}{R_c + R_{fo} + 2R_g} + \frac{1}{R_c + R_{fo} + 2R_g} \qquad\qquad (4.12)$$

The reluctance of the magnetic circuit can be defined using the mean length of the magnetic circuit, permeability of the core material, cross-sectional area of the core and air-gap length. According to the dimensions as given in Figure 4.2 the mean length of the magnetic circuit obtained as follows:

$$l_{core} = 0.608 \qquad\qquad (m) \qquad\qquad\qquad (4.13.\,a)$$

$$l_{air} = x \qquad\qquad\qquad (cm) \qquad\qquad\qquad (4.13.\,b)$$

$$l_{ferrous\,plate} = 0.47 \qquad (m) \qquad\qquad\qquad (4.13.\,c)$$

and cross-sectional area can be found as an equation.

$$A_{core} = 0.00448 \qquad\qquad (m^2) \qquad\qquad\qquad (4.14.\,a)$$

$$A_{air} = 0.00448 \qquad\qquad (m^2) \qquad\qquad\qquad (4.14.\,b)$$

$$A_{ferrous\,plate} = 0.014 \qquad\qquad (m^2) \qquad\qquad\qquad (4.14.\,c)$$

To derive phase reluctance of the actuator, air-gap, ferromagnetic guide-way and leakage reluctances can be calculated respectively via equations [50].

The reluctance of the magnetic circuit can be written as:

$$R_{core} = \frac{l_{core}}{\mu r_{core} \cdot \mu_0 \cdot A_{core}} \qquad (A.t/Wb) \qquad\qquad (4.15)$$

$$R_{air} = \frac{l_{air}}{\mu_0 \cdot A_{air}} \qquad (A.t/Wb) \qquad\qquad (4.16)$$

$$R_r = \frac{l_r}{\mu r_r \cdot \mu_0 \cdot A_r} \qquad (A.t/Wb) \qquad\qquad (4.17)$$

$$R_l = \frac{l_l}{\mu_r \cdot \mu_0 \cdot A_l} \qquad (A.t/Wb) \qquad\qquad (4.18)$$
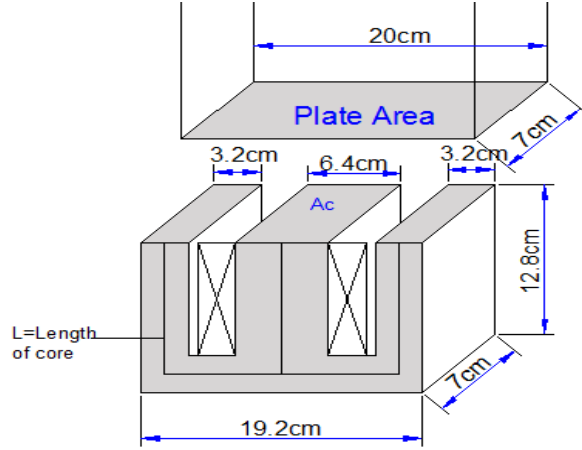
Figure 4.2 Dimension and structure of E type electromagnetic core

In the magnetic equivalent circuit only the reluctance of the air-gap is considered, due to the high permeability of silicon iron, the reluctance of cores can be ignored, hence ,

$$\frac{1}{R_{Total}} = \frac{1}{2R_g} + \frac{1}{2R_g} \tag{4.19}$$

$$R_{Total} = \frac{x}{\mu_0 \cdot A} \tag{4.20}$$

In addition, the magnetic flux term in (4.11) may be expanded using (4.20) and yields,

$$\emptyset = \frac{NI}{R_{Total}} = \frac{\mu_0 \cdot A \cdot N \cdot I}{x} \qquad \text{(Wb)} \tag{4.21}$$

In the air-gap, magnetic flux density is a ratio of magnetic flux in the air cross-sectional area of the passing magnetic flux and denoted by:

$$B = \frac{\emptyset}{A_{air}} = \frac{\mu_0 \cdot N \cdot I}{x} \qquad \text{(Wb/m}^2\text{)} \tag{4.22}$$

The electromagnetic force is determined:

$$F_{mag} = \frac{B^2 \cdot A_{air}}{2 \cdot \mu_0} \tag{4.23}$$

Since, the electromagnetic force equation that is generated in a single acting actuator can be written in terms of; air-gap $x(t)$ is the distance between the pole-face of the magnet and ferromagnetic plate, $i(t)$ is the instantaneous current passing though the coil, N is the No. of turns of the coil, A is the cross sectional area of the magnetic flux in the air-gap, and μ_0 is the air permeability.

$$F_{mag} = \frac{\mu_0 \cdot A_{air} \cdot N^2 \cdot i^2}{2 \cdot x^2} \tag{4.24}$$

4.3 Electrical Formula

The electrical circuit of the system as depicted in Figure 4.3. The relation between the time varying voltage $v(t)$ across an inductor (L) and the time varying current $i(t)$ passing through it, which is derived from the differential equation using KVL. The electromagnetic coil is adequately modeled by a series of resistor and an inductor. Voltage drop on the resistor is $R \cdot i(t)$ and an inductor $L\frac{di}{dt}$ which can be described the relevant dynamics of the 1st order system [49].
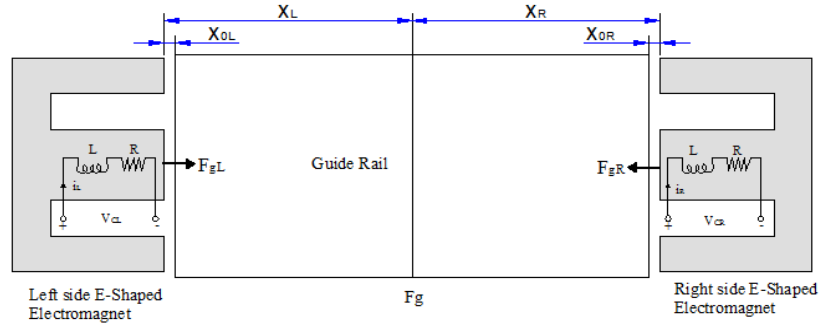
Figure 4.3 Electrical circuit of the guidance system

$$v(t) = R \cdot i(t) + L(x)\frac{di(t)}{dt} \tag{4.25}$$

where, R is an electrical resistance of the circuit, $i(t)$ is the current circuit, $v(t)$ is the applied input voltage to the circuit and $L(x)$ is the coil inductance.

By substituting $L(x)$ from (4.3) into (4.25) and the derivative yields:

$$v(t) = R \cdot i(t) + \frac{\mu_0 \cdot N^2 \cdot A}{x(t)} \cdot \frac{di(t)}{dt} \tag{4.26}$$

Basis of the (4.26) the voltages on both sides of the electromagnets coil are:

$$v_{CR}(t) = R \cdot i_R(t) + \frac{\mu_0 \cdot N^2 \cdot A}{x(t)} \cdot \frac{di_R(t)}{dt} \tag{4.27.a}$$

$$v_{CL}(t) = R \cdot i_L(t) + \frac{\mu_0 \cdot N^2 \cdot A}{x(t)} \cdot \frac{di_L(t)}{dt} \tag{4.27.b}$$

Then (4.26) can be attained by reorganizing the equation in terms of current perturbation.

$$\frac{di}{dt} = \frac{1}{L(x)}[v(t) - R \cdot i(t)]$$

$$\frac{di}{dt} = \frac{v(t)}{L(x)} - \frac{R \cdot i(t)}{L(x)} \tag{4.28}$$

44

4.4 Dynamics Formula (Plant model)

Dynamic formula can be obtained using Newton's second law of motion of the system. Suppose the air-gap length between guidance magnets and guide-way is $x_L(t)$ and $x_R(t)$ from left and right sides respectively, voltages on left and right sides of the magnets are $v_L(t)$ and $v_R(t)$, currents are $i_L(t)$ and $i_R(t)$, the electromagnetic force of the left and right sides are $F_L(t)$ and $F_R(t)$ (taking the direction of the left side as positive direction) [19].

Guidance system normally works as differential mode. At the balance position x_0 the static current i_0 go through the magnets, both magnets of right and left sides have the same gap change, but different in direction $\Delta x = \Delta x_L(t) = -\Delta x_R(t)$ [19].

So, the air-gap length $x(t)$ and the coil current $i(t)$ are represented in terms of two parts a steady state values of x_0 and i_0 and much smaller components of the displacement $\Delta x(t)$ and the current $\Delta i(t)$ which provides the attractive force for balancing any variation around the equilibrium points $(i_0, \ x_0)$ as [27].

$$x_L(t) = x_{0L} + \Delta x(t), \qquad i_L(t) = i_{0L} + \Delta i(t) \tag{4.29}$$

$$x_R(t) = x_{0R} - \Delta x(t), \qquad i_R(t) = i_{0R} - \Delta i(t) \tag{4.30}$$

Then the dynamic equation in the lateral direction of the guidance systems is described in (4.31). It is the net force that affects the system which can be represented the difference of electromagnetic force from the right and left sides with the disturbance force, however the effect of disturbance force has not been taken into account.

$$F_{net} = m\Delta x''(t) = F_{gR}(i_R, x_R) - F_{gL}(i_L, x_L) + F_d(t) \tag{4.31}$$

$$F_{gR}(i_R, x_R) = \frac{\mu_0 \cdot N^2 \cdot A}{2} \left[\frac{i_{0R} - \Delta i(t)}{x_{0R} - \Delta x(t)} \right]^2 \tag{4.32}$$

$$F_{gL}(i_L, x_L) = \frac{\mu_0 \cdot N^2 \cdot A}{2} \left[\frac{i_{0L} + \Delta i(t)}{x_{0L} + \Delta x(t)} \right]^2 \tag{4.33}$$

$$m\Delta x''(t) = \frac{\mu_0 \cdot N^2 \cdot A}{2} \left[\frac{i_{0R} - \Delta i(t)}{x_{0R} - \Delta x(t)} \right]^2 - \frac{\mu_0 \cdot N^2 \cdot A}{2} \left[\frac{i_{0L} + \Delta i(t)}{x_{0L} + \Delta x(t)} \right]^2 + F_d(t) \tag{4.34}$$

$$m\Delta x''(t) = \frac{\mu_0 \cdot N^2 \cdot A}{2} \left[\left[\frac{i_{0R} - \Delta i(t)}{x_{0R} - \Delta x(t)} \right]^2 - \left[\frac{i_{0L} + \Delta i(t)}{x_{0L} + \Delta x(t)} \right]^2 \right] + F_d(t) \tag{4.35}$$

4.5 Position Sensor

In the electromagnetic attraction type of guiding system as said earlier have actuators to produce the sideward forces with the ferromagnetic guide-way that are required to make the vehicle follow the guide-way. For proper functioning and to provide stable support, actuators need accurate information to guide the guide-way for doing this sensor is required. The output of the sensor varies with the position of the electromagnets [29].

4.5.1 Sensor Formula (Sensor Model)

Feedback signal comes from distance sensor. The position sensor should be tested and calibrated according to the degree of sensing or blocking, this calibration is achieved by incrementing a light or rays shield according to type of sensors used that corresponds to the rail's size in the x- direction [46]. For such system photoelectric laser type sensor is used to detect the lateral displacement, to determine the gain of the sensor the output voltage data are taken under different air-gaps experimentally as a displacement from the electromagnet coil to the side of the ferromagnetic plate. Output is normally estimated as a linear function (see Figure 6.18), a simple function must be estimated to reduce the processing duration. So the linear region can be expressed in (4.36) by the relation between the output voltage of the distance sensor and air-gap position [45, 46]. The relationship is given by:

$$V_x = \beta . x \qquad \text{(v)} \tag{4.36}$$

where, β is the gain of the sensor its unit is V/m which is found as (62), x is the lateral distance in m and V_x is the voltage across the sensor in volt [46].

4.6 Derivation of State Equation of the System

From the differential equation of motion in (4.35) and (4.28) the state equation of the guidance system can be obtained. The state vectors can be defined as:

$$x(t) = (x(t) \quad x'(t) \quad i(t)^T) \quad \in R^n , \; n = 3$$

where, $x(t)$ is the horizontal gap or position, $x'(t)$ is lateral velocity of electromagnetic coil and $i(t)$ is the coil current. Finally the equations of state-variable can be obtained by subject to initial condition as illustrated in below. The state variables are:

$$x_1(t) = x(t), \qquad\qquad x_2(t) = x'(t) = \frac{d_x}{dt}, \qquad\qquad x_3(t) = i(t)$$

$$x_1'(t) = \frac{dx}{dt} = x_2(t) \qquad\qquad x_2'(t) = \frac{dx''}{dt} \qquad\qquad x_3'(t) = \frac{di(t)}{dt}$$

$$x_1'(t) = x_2(t) \tag{4.37}$$

$$x'_2(t) = \frac{\mu_0 \cdot N^2 \cdot A}{2m}\left[\left[\frac{i_{0R} - \Delta i(t)}{x_{0R} - \Delta x(t)}\right]^2 - \left[\frac{i_{0L} + \Delta i(t)}{x_{0L} + \Delta x(t)}\right]^2\right] \tag{4.38}$$

$$\frac{di}{dt} = \frac{v(t)}{L(x)} - \frac{R \cdot i(t)}{L(x)}$$

$$x_3'(t) = \frac{v(t)}{L(x)} - \frac{R \cdot x_3}{L(x)} \tag{4.39}$$

4.7 Linearization of the Non - Linear System

As can be seen in the model, the system is non-linear due to the inherent nonlinearities of the electromagnetic circuit. The magnetic force formula is second order polynomial and not linear equation. The system cannot be stabilized using linear control techniques thus, the system should be linearized either through a Taylor Series Expansion or nonlinear transformation technique. For small perturbations around nominal operating points (i_0, x_0) Taylor series expansion is used, in the series expansion high order terms will be neglected to get linear equation, thus the linearized model of the system can be determined around stable operating points [51]. The General form of the Taylor Series Expansion is seen in (4.40):

$$f = f_0 + \frac{1}{1!} \cdot \frac{df}{dx} \cdot x + \frac{1}{2!} \cdot \frac{d^2 f}{dx^2} \cdot x^2 + \frac{1}{3!} \cdot \frac{d^3 f}{dx^3} \cdot + \cdots \tag{4.40}$$

Constant and the first order term is used for magnetic force formula in the control algorithm.

$$F_{mag} = f_0 + \frac{1}{1!} \cdot \frac{df}{d(x,i)} \cdot (x, i) \qquad (N) \tag{4.41}$$

The magnetic force is related to air-gap distance and current. Last equation of the magnetic force is put in series and is differentiated by using partial differential operation with air-gap distance and current.

$$F_{mag} = f_0 + \frac{1}{1!} \cdot \frac{dF\,mag}{di} \cdot i + \frac{1}{1!} \cdot \frac{dF\,mag}{dx} \cdot x \tag{4.42}$$

$$f(x, i) = f(x_0, i_0) + \left(\frac{\partial(f(x_0, i_0))}{\partial(x_0)} \cdot x(t) + \frac{\partial(f(x_0, i_0))}{\partial(i_0)} \cdot i(t)\right) \tag{4.43}$$

47

$$m\Delta x''(t) = F_{gR}(i_R, x_R) - F_{gL}(i_L, x_L)$$

$$m\Delta x''(t) = \frac{\mu_0 \cdot N^2 \cdot A}{2}\left[\left[\frac{i_{0R} - \Delta i(t)}{x_{0R} - \Delta x(t)}\right]^2 - \left[\frac{i_{0L} + \Delta i(t)}{x_{0L} + \Delta x(t)}\right]^2\right] \tag{4.44}$$

Let $K = \frac{\mu_0 \cdot N^2 \cdot A}{2}$, yields:

$$m\Delta x''(t) = K \cdot \left[\left[\frac{i_{0R} - \Delta i(t)}{x_{0R} - \Delta x(t)}\right]^2 - \left[\frac{i_{0L} + \Delta i(t)}{x_{0L} + \Delta x(t)}\right]^2\right] \tag{4.45}$$

$$f(x,i) = K_1\left[\frac{i_{0R}^2}{x_{0R}^2} + \frac{d}{dx_{0R}}\left[\frac{(i_{0R} - \Delta i(t))^2}{(x_{0R} - \Delta x(t))^2}\right] \cdot x(t) + \frac{d}{di_{0R}}\left[\frac{(i_{0R} - \Delta i(t))^2}{(x_{0R} - \Delta x(t))^2}\right] \cdot i(t)\right] -$$
$$K_2\left[\frac{i_{0L}^2}{x_{0L}^2} + \frac{d}{dx_{0L}}\left[\frac{(i_{0L} + \Delta i(t))^2}{(x_{0L} + \Delta x(t))^2}\right] \cdot x(t) + \frac{d}{di_{0L}}\left[\frac{(i_{0L} + \Delta i(t))^2}{(x_{0L} + \Delta x(t))^2}\right] \cdot i(t)\right] \tag{4.46}$$

By substituting (4.46) into (4.45) yields:

$$m\Delta x''(t) = K_1\left[\frac{i_{0R}^2}{x_{0R}^2} + 2\left[\frac{(i_{0R} - \Delta i(t))^2}{(x_{0R} - \Delta x(t))^3}\right] \cdot x(t) - 2\left[\frac{i_{0R} - \Delta i(t)}{(x_{0R} - \Delta x(t))^2}\right] \cdot i(t)\right] - K_2\left[\frac{i_{0L}^2}{x_{0L}^2} - \right.$$
$$2\left[\frac{(i_{0L} + \Delta i(t))^2}{(x_{0L} + \Delta x(t))^3}\right] \cdot x(t) + 2\left[\frac{i_{0L} + \Delta i(t)}{(x_{0L} + \Delta x(t))^2}\right] \cdot i(t)\right] \tag{4.47}$$

At equilibrium position $i_{0R} = i_{0L} = i_0$, $x_{0R} = x_{0L} = x_0$ and $K_1 = K_2 = K = \frac{\mu_0 . N^2 . A}{2}$ hence,

$$m\Delta x''(t) = K\left[2\left[\frac{(i_{0R} - \Delta i(t))^2}{(x_{0R} - \Delta x(t))^3}\right] + 2\left[\frac{(i_{0L} + \Delta i(t))^2}{(x_{0L} + \Delta x(t))^3}\right]\right] \cdot x(t) - K\left[2\left[\frac{i_{0R} - \Delta i(t)}{(x_{0R} - \Delta x(t))^2}\right] + \right.$$
$$2\left[\frac{i_{0L} + \Delta i(t)}{(x_{0L} + \Delta x(t))^2}\right]\right] \cdot i(t) \tag{4.48}$$

The state equations now contain two control inputs, i_R and i_L , assuming these are driven by current loops. However, because each actuator is capable of generating force in only one direction the currents i_R and i_L will be coordinated such that the system can still be considered as a single input [15]. The linearized model of the dynamic equation around stable operating points can be simplified into (4.49)

$$\Delta x''(t) = \frac{4k}{m}\left[\left\{\frac{i_0^2}{x_0^3}\right\}\right] \cdot x(t) - \frac{4k}{m}\left[\left\{\frac{i_0}{x_0^2}\right\}\right] \cdot i(t) \tag{4.49}$$

4.8 System Model

1- State - Space Model

The state space model of the system can equally be formulated by using the electrical and the force equations. Choosing the state vectors as (x_1, x_2, x_3), where $x_1(t)$ is the horizontal gap or position, $x_2(t)$ is lateral velocity of electromagnetic coil, $x_3(t) = i(t)$ is the coil current and $u(t)$ or $v(t)$ is the applied voltage. Once the

current is changed near the static current i_0, the above model can be linearized and the state space model of guidance system can be got as in below matrix.

$$\begin{bmatrix} x_1' \\ x_2' \\ x_3' \end{bmatrix} = \begin{bmatrix} 0 & 1 & 0 \\ 4\dfrac{K}{m}\left(\dfrac{i_0^2}{x_0^3}\right) & 0 & -4\dfrac{K}{m}\left(\dfrac{i_0}{x_0^2}\right) \\ 0 & 0 & -\dfrac{R}{L} \end{bmatrix} \begin{bmatrix} x_1 \\ x_2 \\ x_3 \end{bmatrix} + \begin{bmatrix} 0 \\ 0 \\ \dfrac{1}{L} \end{bmatrix} . \left(\Delta vc(t)\right)$$

$$y = \begin{bmatrix} \beta & 0 & 0 \end{bmatrix} \begin{bmatrix} x_1 \\ x_2 \\ x_3 \end{bmatrix} \tag{4.50}$$

where, $K = \dfrac{\mu_0 \cdot N^2 \cdot A}{2}$, $L = \dfrac{\mu_0 . N^2 . A}{x_0}$

The parameters of the system are the constants of the electromagnet, the resistance and inductance of the magnetic coil, the gain of the sensor, the steady-state current and the equilibrium position [46].

The coil resistance (R) and inductance (L_1) are measured in ohms and inductance meter respectively. For balancing the position of the system from both sides, selecting the operating point plays a significant role in the design and development of the system. The operating air-gap position between the pole-face of the magnets and the ferromagnetic guide-way cannot be made arbitrarily too large or too small. In the higher operating gap zone, very high current is required which becomes a major constraint in the design of the actuator, controller and power switching. In the lower gap zone the large magnitude of coil-inductance leads to a high ratio of (L/R), which consequently makes it more difficult to achieve faster control of the coil-current and electromagnetic force. Considering all these points, the operating air-gap has been selected as 10 mm for the present system [52]. After a series of experiments, the parameters are obtained and given in Table (4.1).

Then substituting these data into the linearized state space model to get the final state- space model of the system.

$$\begin{bmatrix} x_1' \\ x_2' \\ x_3' \end{bmatrix} = \begin{bmatrix} 0 & 1 & 0 \\ 1405 & 0 & -4 \\ 0 & 0 & -13 \end{bmatrix} \begin{bmatrix} x_1 \\ x_2 \\ x_3 \end{bmatrix} + \begin{bmatrix} 0 \\ 0 \\ 6.32 \end{bmatrix} . \left(\Delta vc(t)\right)$$

$$y = \begin{bmatrix} 62 & 0 & 0 \end{bmatrix} \begin{bmatrix} x_1 \\ x_2 \\ x_3 \end{bmatrix} \tag{4.51}$$

Table 4.1 Parameters of the guidance system

Parameters	Values
Mass of the magnet core and coil	$M_c = 12.4\ kg$
Total mass (including magnets and frame)	$M = 30\ kg$
Mass of ferromagnetic plate	20 kg
Maximum air-gap	20 mm
Equilibrium distance	$x_0 =$ 10 mm
Equilibrium current	$i_0 = 3.5$ A
Number of turns per electromagnet	SWG #17, 553 Turns/magnet
Coil resistance	$R = 2.04\ \Omega$
Coil inductance without the plate	$L_c = 0.15$ H
Coil inductance with the plate	$L_0 = 0.17$ H
Coil inductance $L(x) = L_c + \frac{L_0 \cdot x_0}{x}$	$L(x) = 0.158$ H
Sensor gain	β=62 V/m
DC applied voltage	24 V
Force constant	$K = \frac{\mu_0 \cdot N^2 \cdot A}{2}$=0.00086

2- Transfer Function model

From the transfer function model the stability of the system can be checked to be sure that the system is stable or not. Transfer function is the ratio of output (lateral air-gap position) $X(s)$ to the input current through the magnet $I(s)$ in the Laplace domain. The three equations that described the system are given by (4.26), (4.36) and (4.49).

Taking the Laplace transform of these three equations [46]. Current and voltage relation is expressed as:

$$V(s) = RI(s) + sL_1 I(s) \tag{4.52}$$

$$I(s) = \frac{V(s)}{R+L_1} \tag{4.53}$$

$$\frac{I(s)}{V(s)} = \frac{1}{R+sL} \tag{4.54}$$

Equation of the sensor (4.36) is expressed in the Laplace domain as:

$$V_x(s) = \beta \cdot X(s) \tag{4.55}$$

The net force is a function of distance and current derived in (4.49) can be expressed in the Laplace domain as:

$$m\Delta x''(t) = 4K\left[\left\{\frac{i_0{}^2}{x_0{}^3}\right\}\right] \cdot x(t) - 4K\left[\left\{\frac{i_0}{x_0{}^2}\right\}\right] \cdot i(t)$$

$$ms^2X(s) = \left[4k\frac{(i_0)^2}{(x_0)^3}\right] \cdot X(s) - \left[4k\frac{i_0}{(x_0)^2}\right] \cdot I(s) \tag{4.56}$$

$$\left(ms^2 - 4k\frac{(i_0)^2}{(x_0)^3}\right)X(s) = -\left[4k\frac{i_0}{(x_0)^2}\right] \cdot I(s) \tag{4.57}$$

Solving the above equations of (4.54), (4.55) and (4.57) to get the final transfer function in the S- domain.

$$\left(ms^2 - 4k\frac{(i_0)^2}{(x_0)^3}\right) \cdot \frac{V_x(s)}{\beta} = -\left[4k\frac{i_0}{(x_0)^2}\right] \cdot \frac{V(s)}{R+L_1} \tag{4.58}$$

Finally, transfer function is a ratio of sensor output voltage that is air-gap distance information to the input voltage of the magnet. The output voltage across the sensor is directly proportional to the position of ferromagnetic plate with the electromagnet and the input voltage to the magnet is proportional to its current at constant reactance. So, it is represented in terms of constants and parameters of the system [46].

$$G(s) = \frac{V_x(s)}{V(s)} \tag{4.59}$$

$$G(s) = \frac{-\beta\left(4K\frac{i_0}{(x_0)^2}\right)}{(R + sL_1)\left(ms^2 - 4K\frac{(i_0)^2}{(x_0)^3}\right)}$$

$$G(s) = -\frac{\frac{4K\beta}{mL_1}\frac{i_0}{(x_0)^2}}{\left(s+\frac{R}{L_1}\right)\left(s^2-\frac{4K}{m}\frac{(i_0)^2}{(x_0)^3}\right)} \tag{4.60}$$

Hence (4.60) gives the whole transfer function of the overall open-loop system, and it can be obtained numerically by replacing parameters with numerical values in Table 3.1.

$$G(s) = \frac{-1567.36}{S^3+13S^2-1405\,S-18265} \tag{4.61}$$

From the transfer function of the system knows that the system has no zero and three poles. One of the poles is in the unstable region of the complex plane. Thus, the

system is open-loop unstable. So, the transfer function of the system can be obtained by transforming the state space model directly using the following MATLAB code.

```
M-file: % To define the transfer function  model of the system
A = [0 1 0; 1405 0 4; 0 0 − 13];
B = [0; 0; 6.32];
C = [62 0 0];
D = [0];
sys = ss(A, B, C, D);
[num, den] = ss2tf (A, B, C, D);
sys = tf(num, den)
The result is: num = 0  0  0  1567.3
den = 1.0e + 04 ∗ [0.0001  0.0013 − 0.1405 − 1.8265]
            1567.3
    -----------------------------
   s^3 + 13 s^2 - 1405 s - 18265
```

The transfer function of uncontrolled system is given in (4.61), the numerator of the transfer function is constant and the denominator is a third order polynomial.

The poles of the system are:

S_1= -37.48, S_2= -13, S_3 = 37.48

4.9 Root-Locus Approach to System Design

The root locus design is used to obtain the response of the closed - loop system from the location of open-loop roots in locus plot. The location of roots (poles and zero) of the characteristic equation of the closed loop system is varied from zero to infinity as a specific parameter (gain K) [53].

For system design the root-locus approach is very powerful when the system's specifications are given in terms of time-domain quantities, such as the undamped natural frequency (ω_n) and damping ratio (zeta) of the desired dominant closed-loop poles, settling time, rise time and maximum overshoot [53]. An advantage of the root-locus method is that it can be possible to obtain information on the transient response as well as on the frequency response from the pole-zero configuration of the system in the S- domain.

The system root locus is drawn using the MATLAB command as shown in Figures 4.4 a,b. From the location of open loop zeros and poles the situation of the system can be noticed which is stable or unstable. The system itself is unstable because it has one pole in the right-half plane of the root loci and two poles are in the stable region of the root loci (left-half plane), so the system is a third order polynomial because it has three poles and has no zero.
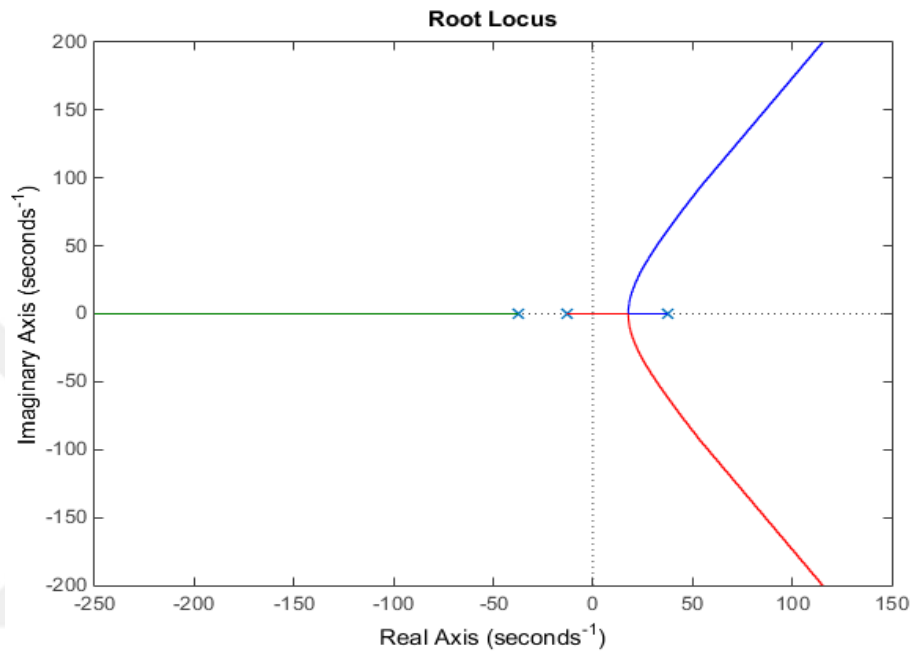
(a)
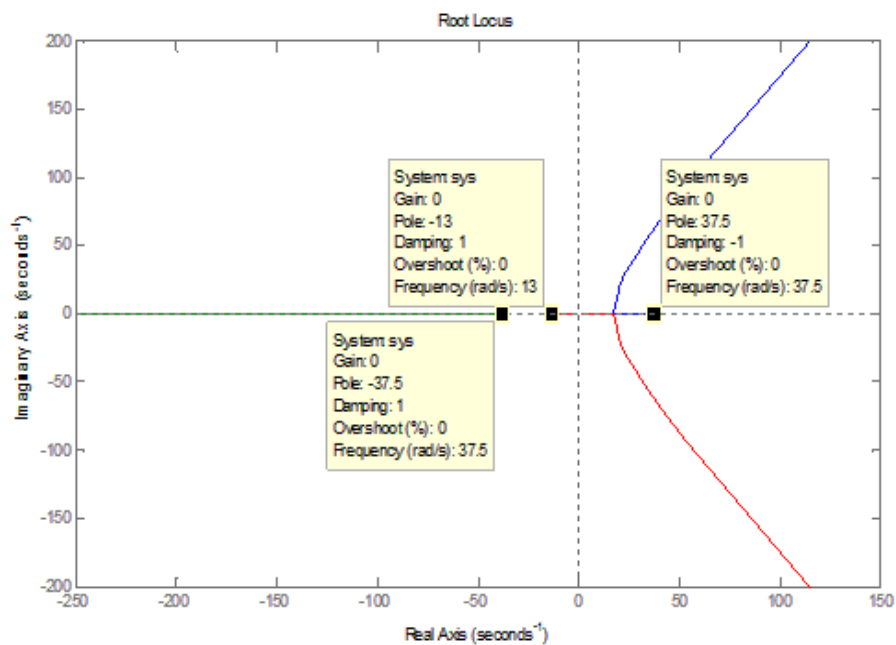
(b)

Figure 4.4 Continuous root locus of uncompensated system

To achieve the system stability the pole must be transferred to the stable region or cancelled. Uncontrolled system step response and impulse response are drawn using step and impulse command, respectively as seen in Figures 4.5 and 4.6. Step response and impulse response curves go to infinity without a controller. It shows that the system is unstable and the electromagnets cannot be set to its desired reference point. The controller must be designed to stable the plant with desired performance criteria.
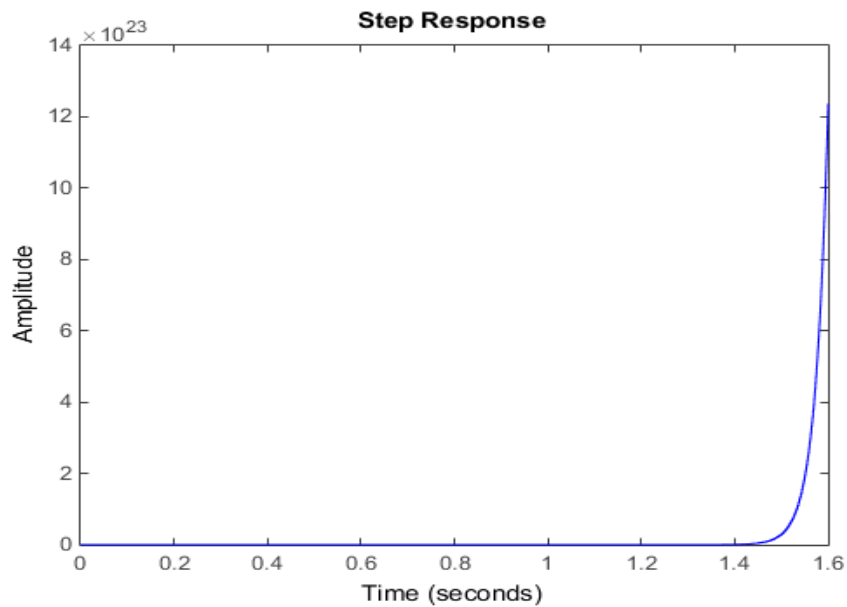
Figure 4.5 Step response of the uncompensated system
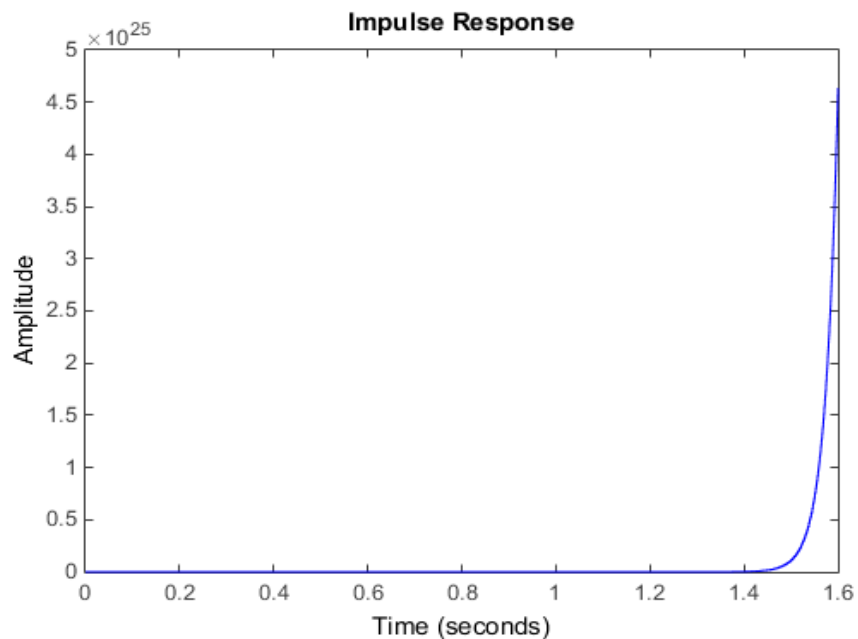
Figure 4.6 Impulse response of the uncompensated system

Summary

Mathematical modeling is one of the fundamental concepts that need to be taken in the system to represent the state space model or transfer function of the plant, which are needed for the control design. State space model of the system is obtained using relation of the electrical, dynamical, electromagnetic and sensor formulas.

Normally, the electromagnetic force formula is second order polynomial, the system cannot be controlled using the linear control theory and this formula is linearized using Taylor series expansion method. Finally, all formula is transformed from time domain to Laplace domain using Laplace transform to obtain the transfer function of the system. The transfer function is the ratio of the lateral air-gap position $X(s)$ to the current through the magnet $I(s)$, however, it can be expressed in terms of output voltage across the sensor and applied input voltage of the magnet.

From the state space and transfer function models of the system, the root locus and step response are obtained. As can be seen that such system is unstable, thus a suitable control law will be designed to compensate the plant instability and improve performance within the linear operating range.

CHAPTER 5

CONTROLLER DESIGN

5.1 Introduction

The controller is the core of the system not only influence the stability of the system, but also impacts the dynamic performance of the system, determines the stiffness, carrying and damping characteristics of the system. The two key performance measurements of the system are the overshoot and the time response [54].

From the transfer function of the system was presented in the last chapter knows that the system is hardly non-linear and open loop unstable. It was linearized around the reference points using Taylor series expansion in order to approximate the behavior of the system for a small range around the operating points. In this section different suitable controller from the classical and adaptive controller are introduced and proposed theoretically to control the system, which are applied to the linear and nonlinear systems to transfer the pole from the right- half plane of the root locus to the stable region. Phase-lead, pole placement and PID controllers are designed for stable operation the system and to satisfy the performance criteria, then performances of the designed controllers are compared with each other. MATLAB scripts are provided for simulating the system and for plotting the root loci.

5.2 Controller Design

Figure 5.1 depicts the overall block diagram of the complete closed loop system, which consists of the plant (two actuators) and a sensor model with a closed loop control system. Here G(s) is the gain or transfer function of the plant, Gc(s) is the compensator gain, which compares the measured value to their desired value and adjusts the input variables to the system, V(s) is the sensor output voltage, H(s) is the gain of the sensor (V/m) to gather information from the plant, E(s) is the error signal, U(s) is the compensator output, R(s) and Y(s) are the desired and actual positions of the system respectively [51].
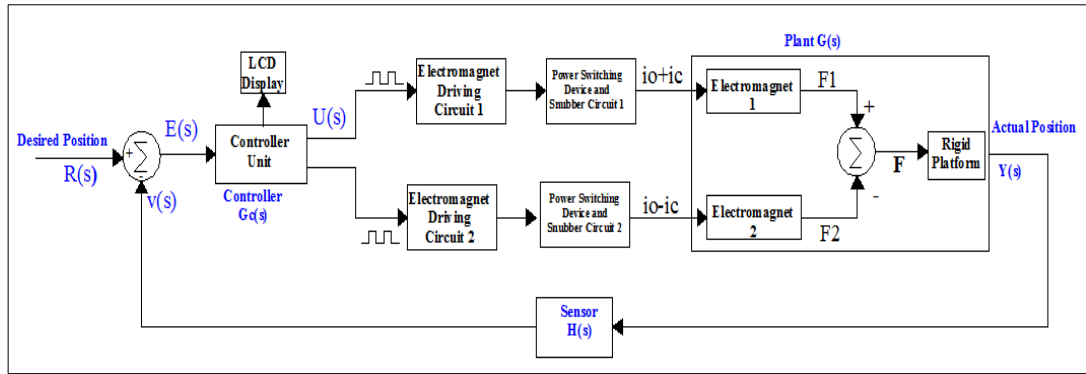
Figure 5.1 Block diagram of the closed loop scheme of an electromagnet type guidance system [22]

The aim of the control system is producing a control signal from the error signal which is the difference between the reference input and the actual position, and from this control signal control the positions between the electromagnets and the rigid body to reach the reference input in a stable manner [55]. Designed system should exhibit as small errors as possible in responding to the input signal. The damping of the system should be reasonable. The undesirable disturbance should be well attenuated [45].

A phase lead and PID from the classic controller and pole placement from advanced controller are chosen to stabilize the system using root locus analysis to perform specific tasks, so that the root locus goes through the desired closed loop poles and the step response of the closed-loop system meets less settling time Ts which is less than 1s with small percent overshoot.

5.3 Performance Criteria

The first step in designing the control system is to collect the required specifications and translate them into a design point in the complex plane representing the desired closed-loop poles based on the transient-response and/or frequency-response requirements, so that the closed loop system needs to satisfy the requirements.

Performance specifications for the root locus method are usually given in terms of natural frequency (ω_n) and damping factor (δ) and the performance parameters must be defined for wanted performance. Damping ratio ξ is selected as 0.7 (a value between 0.4 and 0.8 is preferred) and natural frequency (ω_n) of the system is selected as 25 rad/sec [53].

Assuming that the desired poles in the complex plane are:

$$S_{d1,2} = -\delta\omega_n \pm j\omega_n \sqrt{(1-\delta^2)} \tag{5.1}$$

$$S_{d1,2} = -17.5 \pm j17.85$$

5.4 Classical Linear Controller Design

An acceptable controller should be able to control the displacement between two electromagnets and the ferromagnetic plate in the horizontal direction. From the transfer function of the system knows that the system has three open loop poles P_1, P_2 and P3, the third pole P3 formed by the coil resistance and inductance remains unchanged in spite of any change in the weight. This implies that pole P3 can be counteracted by using the virtual pole assignment or the pole cancellation method [56].

Based on the linearized dynamic equation of the system in (4.49), the transfer function of the plant $G_p(s)$ from incremental current to an incremental position which can be found in (5.3) [52]. In other word the system can be controlled by current controlling rather than the voltage controlling. Therefore, current signal is chosen as a control input that the order of the system is reduced from 3 to 2, which makes it easier to control [25, 56].

$$\Delta x''(t) = \frac{4k}{m}\left[\left\{\frac{i_0{}^2}{x_0{}^3}\right\}\right] \cdot x(t) - \frac{4k}{m}\left[\left\{\frac{i_0}{x_0{}^2}\right\}\right] \cdot i(t)$$

$$G_p(s) = \frac{\Delta Z(s)}{\Delta I(s)} \tag{5.2}$$

$$G_p(s) = \frac{-\left(4K\frac{i_0}{(x_0)^2}\right)}{\left(ms^2 - 4K\frac{(i_0)^2}{(x_0)^3}\right)} \tag{5.3}$$

$$G_p(s) = \frac{4}{(s^2 - 1405)} = \frac{4}{(S-37.48)(S+37.48)}$$

The plant $G_p(s)$ from above equation is a second order polynomial, it has one stable pole at $S_1 = -37.48$ and an unstable pole at $S_2 = 37.48$. The open-loop system is unstable and feedback control is required. The closed loop system has been stabilized with phase lead compensation technique as explained in the following section.

5.4.1. Design of Phase Lead Compensator

The uncompensated root locus in Figure 4.4 showed that the system is unstable and cannot be stabilized by just changing the system gain. It can be seen that, one of the poles will always be in the right hand side of the S-plane irrespective the value of the system gain. To pull the root locus into the left hand plane, there is need to add a compensator's zero in the left –hand plane between the first left hand pole and the origin. The first left hand pole is (-37.48), so compensator's zero should be placed between this location and the origin. Then the required necessary pole is placed deeper than the deepest pole of the system to pull the pole into the left hand of the complex plane and to minimize the impact of the compensator pole on the root locus [57].

The structure of the phase lead compensator is defined as in (5.4) that adding a pole and a zero to the transfer function.

$$G_c(s) = K_c \cdot \alpha \frac{Ts+1}{\alpha Ts+1} = K_c \frac{s+\frac{1}{T}}{s+\frac{1}{\alpha T}}, \qquad 0 < \alpha < 1 \qquad (5.4)$$

$$G_c = K_c \cdot \frac{s+z}{s+p}$$

where, K_c is the controller gain, z is the zero and p is the pole of the controller.

The parameters of phase-lead controller are found using Root Locus Design, Graphical User Interface (GUI) that is opened for use by Prof. Dr. Hadi Saadat. The GUI work with MATLAB and the overview is seen in Figures 5.2 and 5.3 ensure the system is stable while giving acceptable performance.

$$\text{Compensator } G_c(s) = \frac{626.6\, s+1.92\, e^{04}}{s+48.61} \qquad (5.5)$$

$$\text{Compensated open loop system} = \frac{2506\, s+7.681\, e^{04}}{s^3+48.61\, s^2-1405s-6.83\, e^{04}} \qquad (5.6)$$

$$\text{Compensated closed loop system} = \frac{2506\, s+7.681\, e^{04}}{s^3+48.61\, s^2+1101\, s +8508} \qquad (5.7)$$

$K_c = 626.5991$

$Z_0 = 30.6462$

$P_0 = 48.6150$
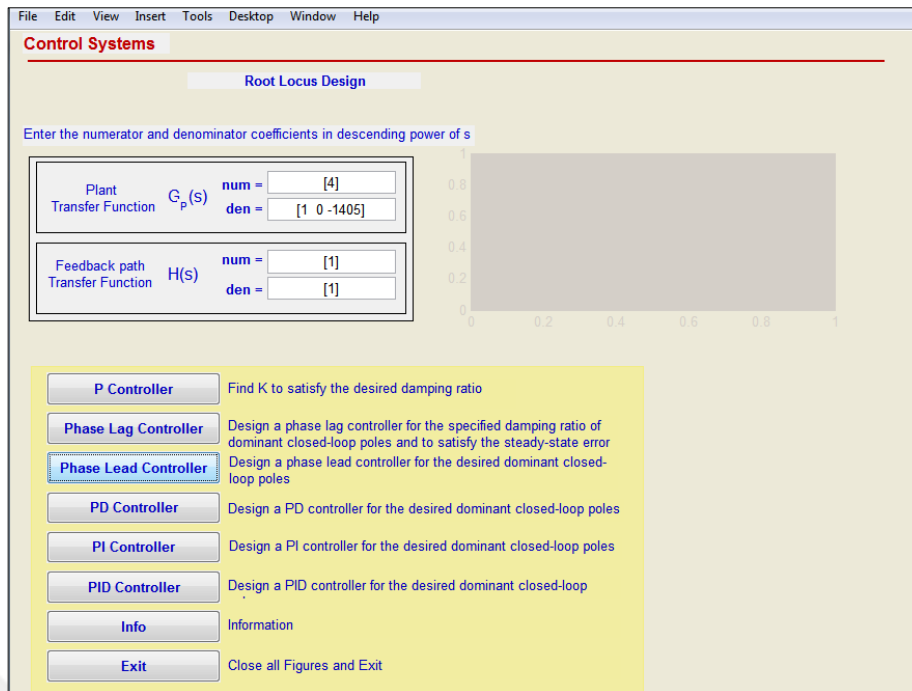
Figure 5.2 Root locus design GUI
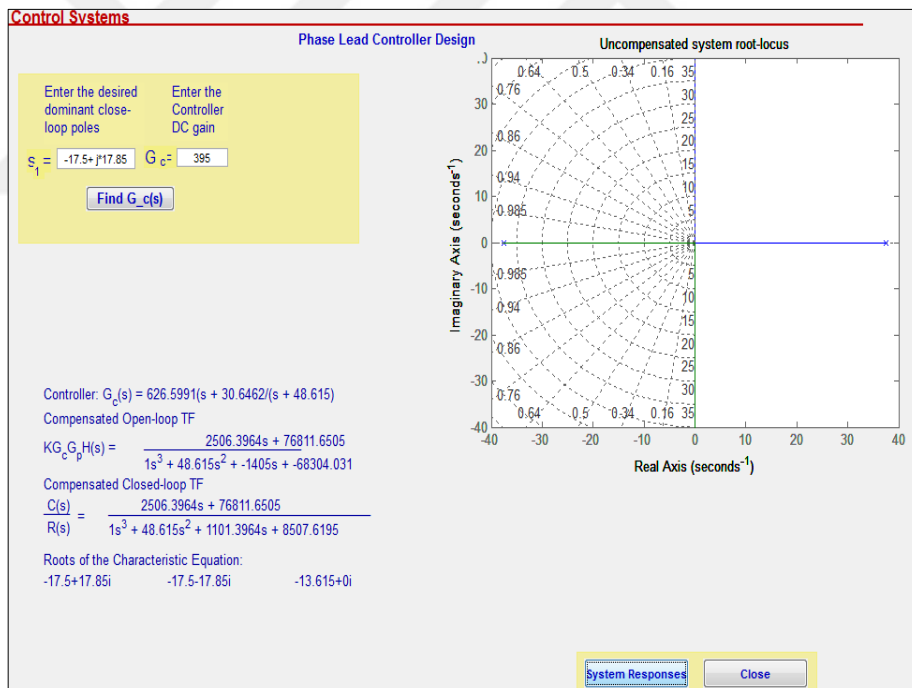
Figure 5.3 Phase-lead controller design GUI

After specifying the damping ratio zeta (ζ) and undamped natural frequency ω_n, the value of K_c was obtained 626.5991 which is satisfied the specification. From the root locus of the system as can be seen in Figure 5.4, all three closed-loop poles can be found on the left half side of the complex plane thus the system with the phase-lead controller becomes stable.

60
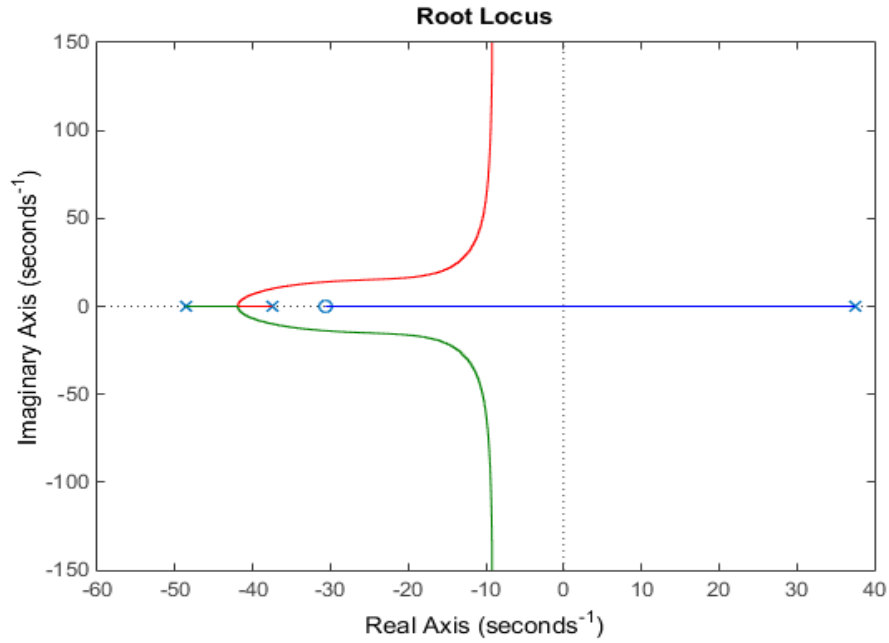
Figure 5.4 Root locus of open loop system
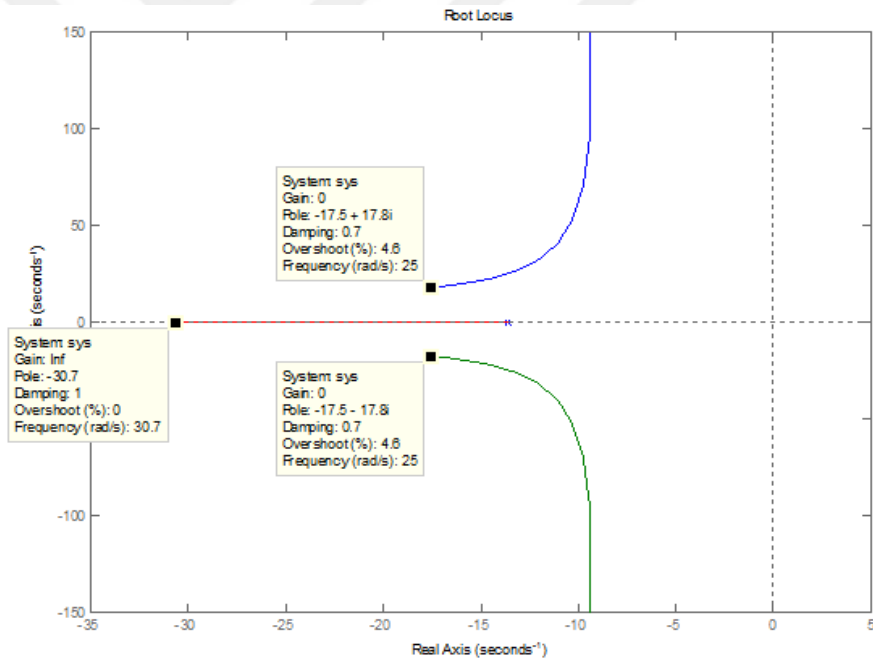
Figure 5.5 Root locus of controlled closed loop system with phase-lead controller

Figure 5.6 illustrates the system step response with parameters. The selected point gives a stable closed loop poles, with less rise time of 0.145 sec, settling time 0.269 sec is good for the system and with no overshoot. The step response graph shows that the controller suppresses the unexpected disturbance and the reference input need to be scaled down in order to catch up with step response. The phase-lead controller has a good response in terms of trajectory tracking and no overshoot.
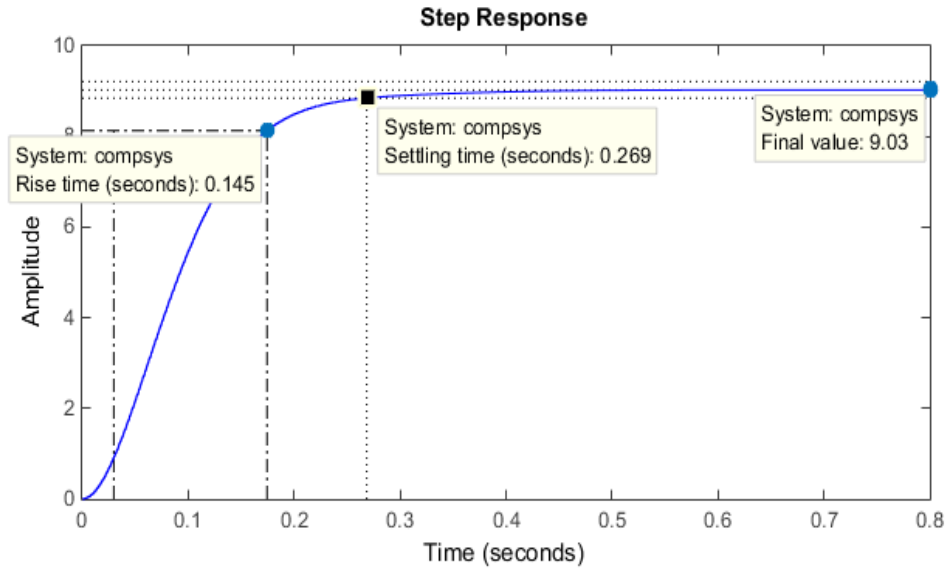
Figure 5.6 System step response with phase-lead controller

The speed of the system response can be measured by the settling time and delay time, which is increased due to increasing of undamped natural frequency w_n. In general, as the damping ratio increases the maximum overshoot decreases. However, with increasing the damping ratio the delay time increases which causes the response of the system sluggish [56].

5.5 Basic Properties of State-Space Model

Before starting with the design of controller gain matrix it needs to check the controllability and observability of the system to be sure it is completely state controllable or not.

a) Controllability

The controllability is related to the system dynamics particularly to the state variables $x(t)$, the condition for complete state controllability where the control vector u is r dimensional. The system in the form of the state space model is given by, [53]

$$x' = Ax + Bu, \qquad x \in R^n, u \in R^r \tag{5.8}$$

It is completely state controllable if only the vectors $B, AB, \dots \dots A^{n-1}B$, are linearly independent, or the $M \in R^{n*nr}$ matrix $M = [B \ AB \dots \dots A^{n-1}B]$ is of rank n. The $M \in R^{n*nr}$ matrix is commonly called the controllability matrix.

$$M = [B \ AB \dots \dots A^2 B] \tag{5.9}$$

$$M = (1.0e + 03) \times \begin{bmatrix} 0 & 0 & -0.0253 \\ 0 & -0.0253 & 0.3286 \\ 0.0063 & -0.0822 & 1.0681 \end{bmatrix}$$

Determinate $(M) = $ -4.0390e+03

Rank $(M) = 3$, so M has full rank and the system is completely state controllable.

b) Output Controllability

In the practical design of a control system, it is desirable to define complete output controllability rather than the complete state controllability of the system. The condition for the complete output controllability is described as follows, which is related to the system matrix A, the input matrix B and the system output $y(t)$ namely C and D matrixes [53].

$$M_O = [CB \quad CAB \dots . CA^{n-1}B \quad D]$$

$$M_O = [CB \quad CAB \dots . CA^2B \quad D] \tag{5.10}$$

$$M_O = [0 \quad 0 \quad -1567 \quad 0]$$

Rank $(M_0) = 1$, since the system is complete output controllable.

c) Complete Observability

The concept of observability is very important in practice, the difficulty encountered with state feedback control is that some of the state variables are not accessible for direct measurement, with the result that becomes necessary to estimate the immeasurable state variables in order to construct the control signals [53].

$$x' = Ax, \qquad x \in R^n, A \in R^{n*n}$$

$$y = Cx, \qquad x \in R^m, C \in R^{m*n}$$

$$N = [C^T \quad A^T C^T \dots \dots (A^T)^{n-2}C^T \quad (A^T)^{n-1}C^T] \tag{5.11}$$

L =transpose (C); P = transpose (A);

$$N = [L \quad P \cdot L \quad P^2 L] \tag{5.12}$$

$$N = \begin{bmatrix} 62 & 0 & 87110 \\ 0 & 62 & 0 \\ 0 & 0 & -248 \end{bmatrix}$$

Determinate $(N) = $ -953312

Rank $(N) = 3$, since the system is a complete state observable

The above determinations illustrate that the rank of the system matrix is fully controllable and observable and equivalent to the dimension of the state variables. Therefore, the guidance system is controllable and simultaneously observable experimentally, thus the controller can be designed to make the system stable.

5.6 Complete State Feedback Controller using the Pole - Placement Technique

The pole - placement approach is a method which is used in feedback control system to put the system's closed-loop poles into their desired locations $s=\sigma \pm j\omega$ in the complex plane. The pole-placement method is slightly similar to the root-locus method in that the closed-loop poles will be placed at desired locations. The basic difference is that in the root-locus design needs only output signal and only the dominant closed loop poles are placed in the desired locations, whereas in the pole-placement design all the state variables need and all closed-loop poles will be forced to lie at specific desired locations [53].

The system given in the form of the state space model is:

$$x' = Ax + Bu \tag{5.13}$$

$$y = Cx + Du$$

where, $x \in R^n$ is the state vector , system matrix A, input matrix B, $u \in R^r$ denotes the control input signal, $y \in R^m$ is the output vector, output matrix C, and the input output distribution matrix D have appropriate dimensions.

The pole-placement method typically comprises three steps:

(1) Assumption 1: Suppose that the system is completely state controllable. Thus, controllability matrix $M = [B \ \ AB \ ... \ ... \ A^2 B]$ has to be full rank.

(2) Assumption 2: Suppose that all the state variables are available and measurable for a full-state feedback control law. In other word observability matrix $N = [C \ AC \ \ A^{n-1}C]^T$ has to be full rank.

(3) With the constant reference input the state feedback control law can be designed for the desired closed loop poles; $\mu_1, \ \mu_2, \ \mu_3 \ ... \mu_n$.

The complete state feedback control law is:

$$u = -K \cdot x + k_1 \cdot r, \qquad K \in R^{r*n} \tag{5.14}$$

The complete state feedback in (5.13) is designed to minimize the following performance index [53].

$$J = \sum_{i=0}^{n} (\mu_i - S_{i)}^2 \to 0, \qquad i = 1,2, \dots . n \tag{5.15}$$

where, S_i is the eigenvalues of the characteristic matrix and μ_i is the desired eigenvalues of the closed loop system.

$$|\lambda I - A| = (\lambda - S_1)(\lambda - S_2) \dots . (\lambda - S_{n-1})(\lambda - S_n) \tag{5.16}$$

After substituting the control law from (5.14) into (5.13), the dynamic of closed loop system with full state feedback control is given in below:

$$x' = (A - B \cdot K)x + B \cdot K_1 \cdot r \tag{5.17}$$

Then the characteristic polynomial of the feedback dynamic is:

$$|\lambda I - (A - BK)| = |\lambda I - (AA)| = (\lambda - \mu_1)(\lambda - \mu_2) \dots . (\lambda - \mu_{n-1})(\lambda - \mu_n) \tag{5.18}$$

To determine feedback control gain matrix K the following methods can be used for pole placement design:

a) Use controllable canonical state space form or transformation matrix T for Multi Input Multi Output MIMO systems. Use *place* commands in the MATLAB control toolbox.

b) Use direct substitute method for low order ($n \leq 3$) system.

c) Use Ackermann's formula for Single Input Single Output (SISO) systems. Use *Acker* commands in the MATLAB control toolbox

To design a control system based on pole-placement approach, the locations of desired closed-loop poles have to be selected. The most frequently used approach is to choose such poles based on experience on the root-locus design. A pair of dominant closed-loop poles are selected near the *jω*-axis in the left hand side in the complex plane and the other pole has to be selected far from the dominant closed-loop poles in the negative real part of the complex plane to reduce the other poles effect on the system response [53].

If the dominant closed-loop poles are selected far from the *jω* axis the system response becomes very fast and the system signals become very large, so that the system became nonlinear and it should be avoided. Another approach for selecting

the desired closed-loop poles is quadratic optimal control approach which is made balance between the acceptable response and the amount of required control energy [53].

5.6.1 Controller Design for the Electromagnetic Guidance System Based on Pole-Placement Technique

Here a linearized system model is considered for deriving the feedback gains of three state variables corresponding to the air-gap, velocity and current being related to the force and complete state feedback is designed. As mentioned in chapter 4 that the guidance system is unstable. For stabilizing the system and putting the closed-loop poles at desired location in the $s=\sigma \pm j\omega$ complex plane, based on state feedback (i.e design a controller to drive all system states from any initial conditions to the origin), stabilizing and keeping the positions to its desired position is the control problem. The linearized state space model of the system is:

$$\begin{bmatrix} x_1' \\ x_2' \\ x_3' \end{bmatrix} = \begin{bmatrix} 0 & 1 & 0 \\ 1405 & 0 & -4 \\ 0 & 0 & -13 \end{bmatrix} \begin{bmatrix} x_1 \\ x_2 \\ x_3 \end{bmatrix} + \begin{bmatrix} 0 \\ 0 \\ 6.32 \end{bmatrix} . \left(\Delta vc(t) \right)$$

$$y = \begin{bmatrix} 62 & 0 & 0 \end{bmatrix} \begin{bmatrix} x_1 \\ x_2 \\ x_3 \end{bmatrix}$$

Figure 5.7 depicts the block diagram of the complete sate feedback control law with reference input signal (r) that can be described in:

$$u = -K \cdot x + k_1 \cdot r,$$

$$u = -[K_1 \ K_2 \ K_3] \begin{bmatrix} x_1 \\ x_2 \\ x_3 \end{bmatrix} + k_1 \cdot r \qquad (5.19)$$
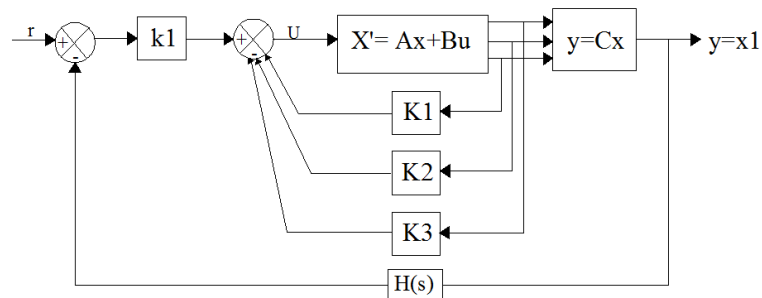
Figure 5.7 Full state feedback control of guidance system

The following steps are required for designing the controller:

First to satisfy the first Assumption A1 and second Assumption A2, the rank of controllability matrix $M = [B\ AB\ A^2 B]$ and observability matrix $N = [C\ CA\ CA^2\ ]^T$ must be examined, the rank of matrix M and matrix N are three, Therefore the system described in (5.8) is completely state controllable, and all state variables are observable. So the pole placement technique is possible.

The second step to design a controller based on pole-placement is to define a desired closed loop poles, the following desired poles are selected to achieve a specific reasonable speed and damping in the response of the designed system and the Ackermann's formula is used. The desired closed loop poles $\mu_1, \mu_2 = -10 \pm J10$ and $\mu_3 = -50$ are chosen. The written MATLAB program using the M-file is:

M-file:

% To determine sate feedback gain matrix K for the system by Ackermann's formula

$A = [0\ 1\ 0;\ 1405\ 0 - 4;\ 0\ 0\ - 13]$;

$B = [0; 0;\ 6.32]$;

$J = [-10 + J \times 10 \quad -10 - J \times 10 \quad -50]$;   % Desired closed loop poles.

$K = acker\ (A, B, J)$;

The controller gains are;

$K = 1.0e + 03\ \times [-4.2860 \quad -0.1030 \quad 0.0090]$

$K = [K_1\ K_2\ K_3]\ = - [\text{-4286}\ \ \text{-103}\ \ 9]$

and the controller dynamic is:

$$u = -[-4286\ \ -103\ \ 9] \begin{bmatrix} x_1 \\ x_2 \\ x_3 \end{bmatrix} + k_1 \cdot r$$

5.6.2 MATLAB Simulation and Results

The MATLAB Simulink model is shown in Figures 5.8 and 5.9 including the state space model of the system and the feedback gain controller obtained from the previous section. The reference value or the set point for the system is set to about 0.01m, this means that the air-gap position between two electromagnets and the plate is to be maintained at 0.01m.
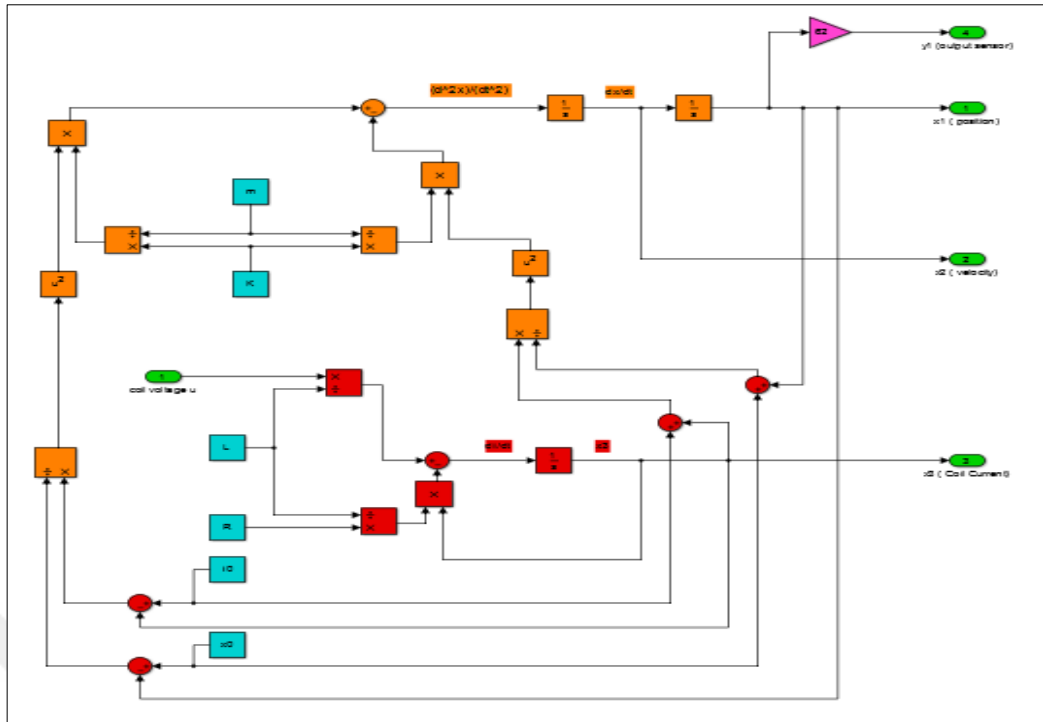
Figure 5.8 State space model of the nonlinear system
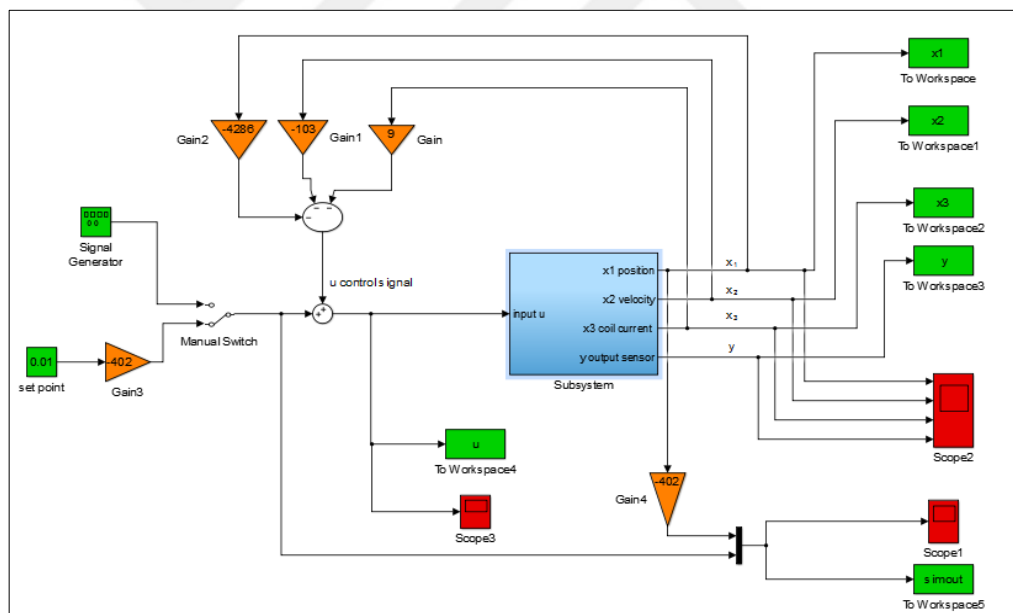
Figure 5.9 Pole placement controller for the electromagnetic guidance system

The performances of closed loop system are depicted in Figure 5.10 on both sides of the prototype. The initial air-gap positions of the DC electromagnets are different from each other, where the initial conditions for the right side are $[x_{1R}(0),\ x_{2R}(0),\ x_{3R}(0)] = [0.015,\ 0,\ 5]$ and for the left side are $[x_{1L}(0),\ x_{2L}(0),\ x_{3L}(0)] = [0.005,\ 0,\ 1.8]$. Figures 5.10 (a) shows the system output position (x_{1R}) in the right side that is started from $x_{1R}(0) = 0.015$ m, and it approaches to 0.01 m which is the

desired position when (t) goes to infinity with the settling time approximately 0.5 sec, otherwise from the left side which is started from 0.005 m and it reaches to 0.01 m. (b) shows the lateral velocity (x_{2R}) in the right side where the maximum value is 0.032 then it will go to zero, whereas the lateral velocity (x_{2L}) in the left side where the maximum value is 0.031 m/sec then they will go to zero. (c) shows a coil current of both sides that are started from 5 A and 1.8 A from the right and left side respectively and they are reached to 3.5 A. And (d) shows the control signals of both sides which are started from 15.5 volt from right side and 1 volt from the left side and they are approached to 7.2 volt when time approaches to infinity. Then all states go to their desired state when (t) goes to infinity. Hence the closed loop system is asymptotically stable.

(a)

(b)

(c)

(d)
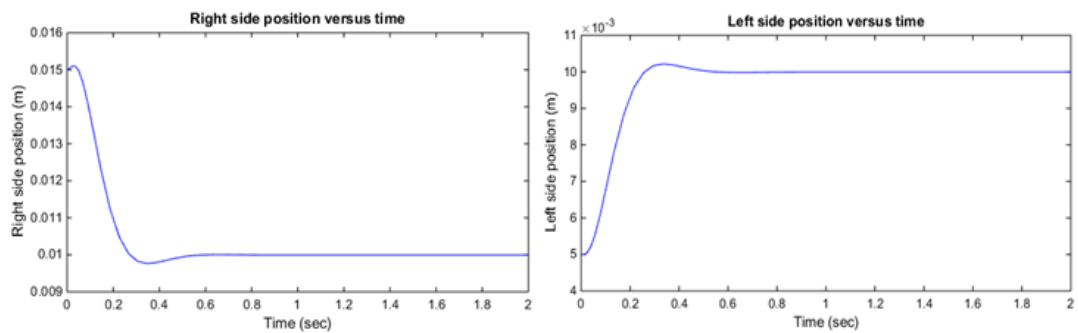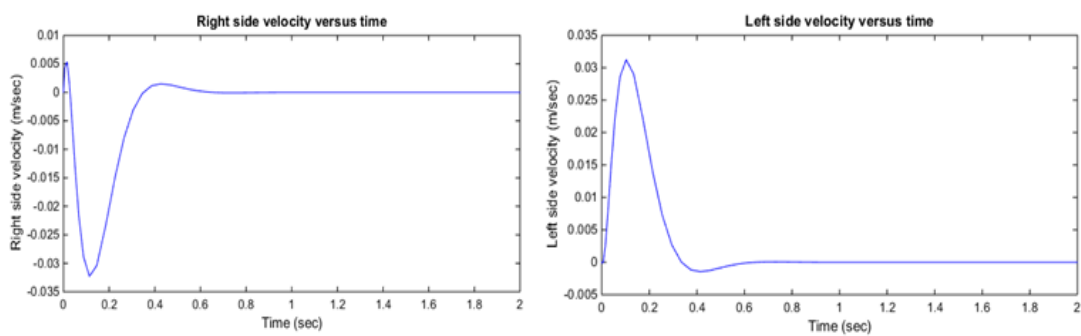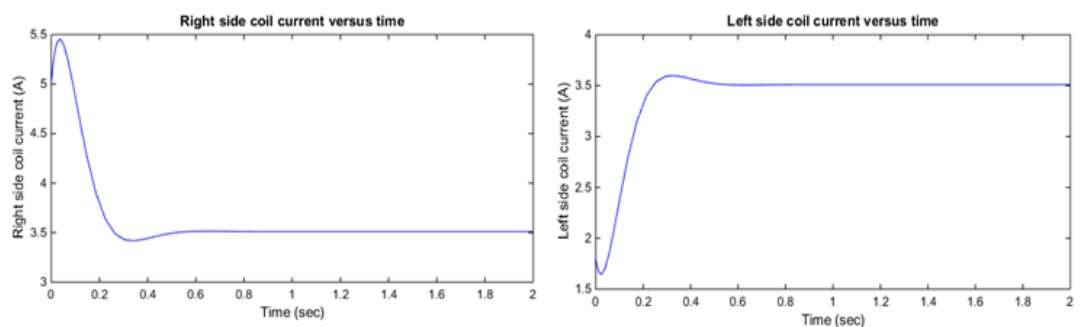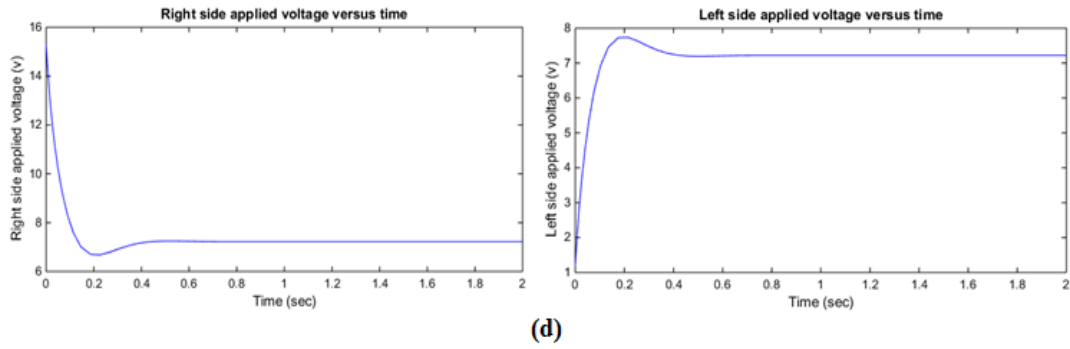
Figure 5.10 (a) Closed loop lateral position, (b) velocity, (c) coil current and (d) applied control signals from both sides of the system

The closed –loop step response of the controlled system as shown in Figure 5.11, where the position goes to its desired position (0.01m) with settling time of 0.4 sec and maximum overshoot approximately % 1.1, it means that the designed controller satisfies the rise time, settling time and the peak overshoot from the desired performance specifications.
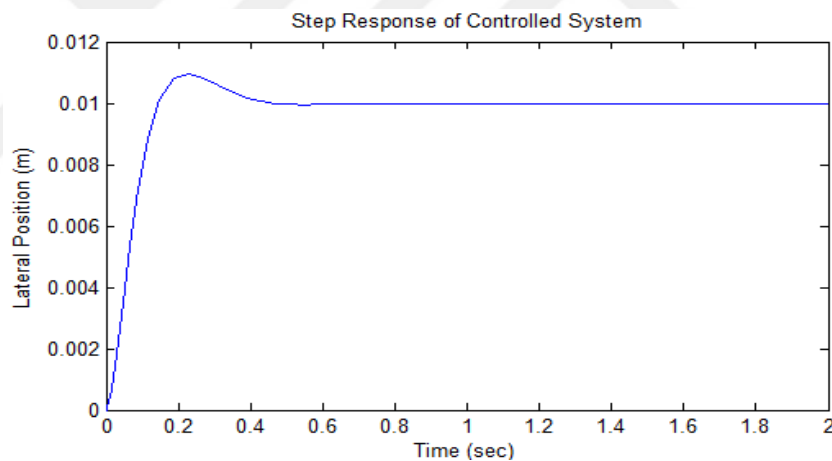
Figure 5.11 Step response of the guidance system

So the performance of the controller is tested with two different reference trajectories of square wave and sine wave and each one with the same magnitude of 10 and 3 rad/sec frequency. The output responses are shown in Figures 5.12 and 5.13 respectively. The results show that the controlled output lateral displacement tracks the reference trajectory with a time lag of less than 0.1 seconds. The tracking error is due to the presence of a small modeling error which is caused by neglecting dynamics. It means that the pole placement controller is capable of providing system stability, suitable for the problem solution of the system control, allow tracking the desired trajectory and disturbance rejection.
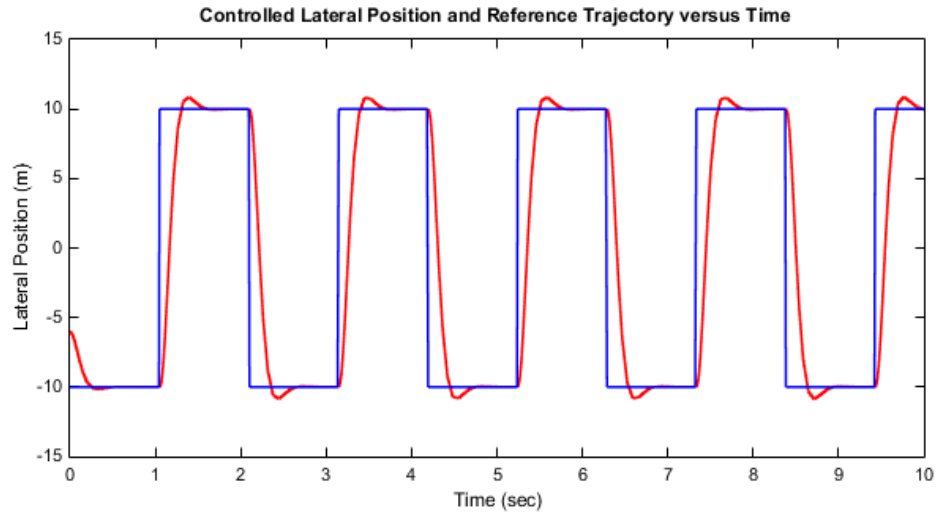
Figure 5.12 Tracking of square wave reference signal with output trajectory

(Plant output "red", reference signal "blue")
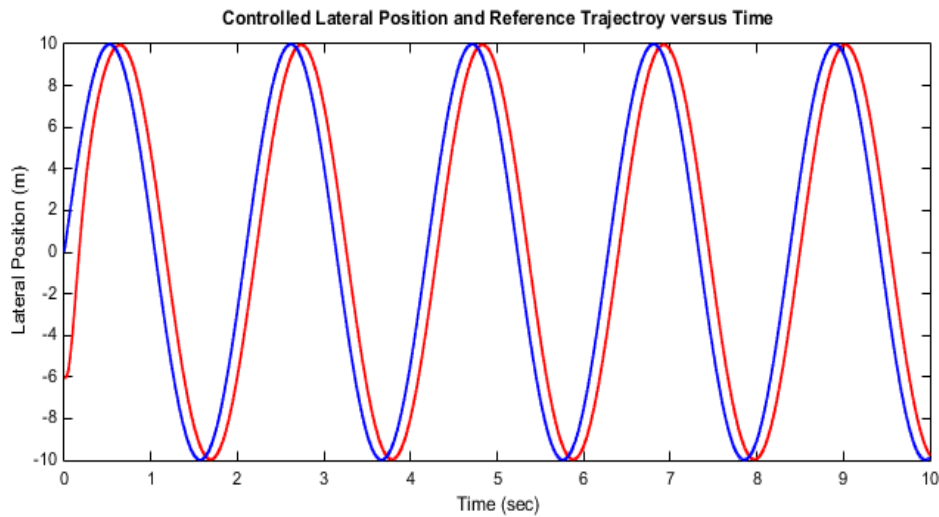
Figure 5.13 Tracking of sine wave reference signal with output trajectory

(Plant output "red", reference signal "blue")

Figure 5.14 shows the root locus of the controlled system, it can be seen that the system eigenvalues S_i are replaced with the desired closed eigenvalues μ_i by the designed controller.

$$K_1 = -402;$$

$$AA = A - B \cdot k;$$

$$AA = (1.0e + 04) \times \begin{bmatrix} 0 & 0.0001 & 0 \\ 0.1405 & 0 & -0.0004 \\ 2.7088 & 0.0651 & -0.0070 \end{bmatrix}$$

71

$$BB = B \cdot k_1;$$

$$BB = \begin{bmatrix} 0 \\ 0 \\ -2540.64 \end{bmatrix}$$

$$CC = [62 \quad 0 \quad 0]; \quad DD = [0];$$

$$sys = ss(AA, BB, CC, DD);$$

$$rlocus\ (sys)$$
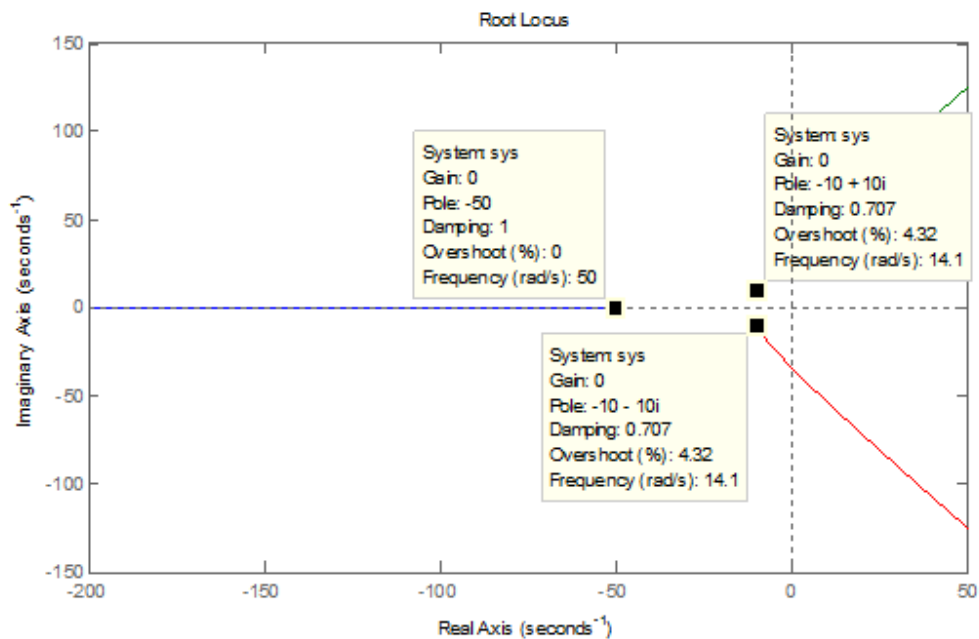
Figure 5.14 Root locus of the controlled system

From the results that obtained above, it can be noticed that the controller achieves the desired performance, but may be produce a large control signal in that may saturate and lead system be having a nonlinear system. This is the natural result of pole placement which achieves the desired performance without considering the control energy. These results prove that the system with the pole placement controller can work properly with linear and nonlinear system and give better results compared with the other classical controller.

5.7 PID Controller

PID is the main technique in the classical control category which is the most commonly used feedback controller widely used in industrial control systems [58]. PID controller consists of three control terms; the P term is dependent on the current

error, I term as the accumulation of previous error values and D term as a prediction of future errors based on current rate of change. The three actions are combined and used to adjust the system process via a control element. The PID controller calculates the error value and tries to reduce it by adjusting the controller parameters and thus adjusting the control inputs to the process. The general form of PID controller used in most of the studies is:

$$u(t) = K_p \left(e(t) + \frac{1}{T_i} \int_0^t e(\tau) d\tau + T_d \frac{de(t)}{dt} \right) \tag{5.20}$$

where, $u(t)$ denote the control signal, K_p is the proportional gain, T_i is integral time, T_d is derivative time. K_p, T_i and T_d are the control parameters for tuning and $e(t)$ is the difference between the reference point and the actual plant output.

$$e(t) = y_{desired}(t) - y(t) \tag{5.21}$$

The equation can also be represented in the frequency domain, with the mean of the Laplace transform such a structure can be represented as a transfer function.

$$U(s) = \left(P + \frac{I}{s} + D.s \right).E(s) \tag{5.22}$$

$$Gc(s) = \frac{U(s)}{E(s)}$$

$$G_c(s) = \frac{D \cdot S^2 + P \cdot s + I}{s}$$

$$Gc(s) = K_p + \frac{K_i}{s} + K_d s \tag{5.23}$$

The controller mainly consists of two zeros and one pole at origin corresponding to the three main parts as they improve the dynamic response and reduce the steady state error. The transient response is improved by a finite zero, which is created from the derivative part of the open loop system. The system type is also increased by one due to a pole added to the origin of the integral part which leads to eliminate and reduce the steady state error [59].

The proposed PID controller is designed to control the lateral position in the electromagnetic guidance system which is implemented using a MATLAB simulation model as depicted in Figure 5.15. The three parameters of PID controller can be determined tune able either manually or automatically to get the best

performance of the controlled system and to meet the desired process specifications of the step response.
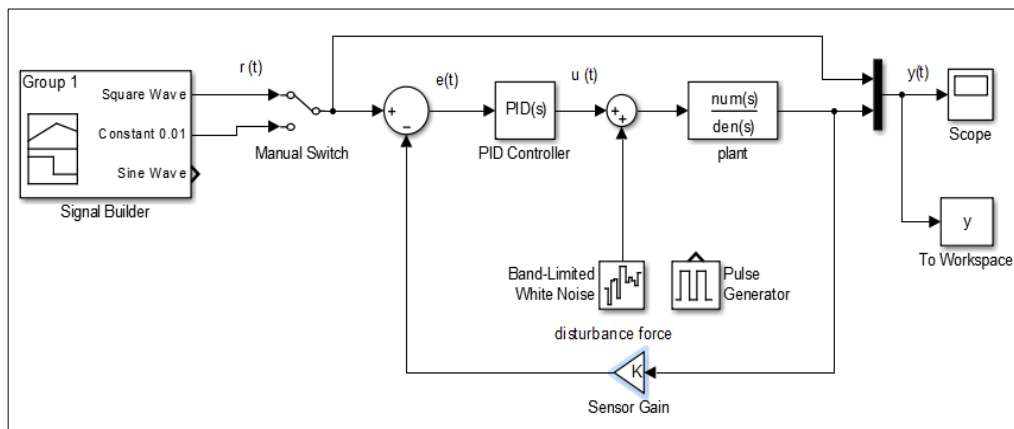
Figure 5.15 Simulation of closed loop PID controller system

Step input with different magnitude and square wave reference trajectory with amplitude of 0.01 and frequency of 10 rad/sec are applied and tested with the system respectively as shown in Figures 5.16 and 5.17. The results prove that the selected reference trajectory is followed by the controlled output position successfully and the controller can provide satisfactory performance for the variation in amplitude of step input.
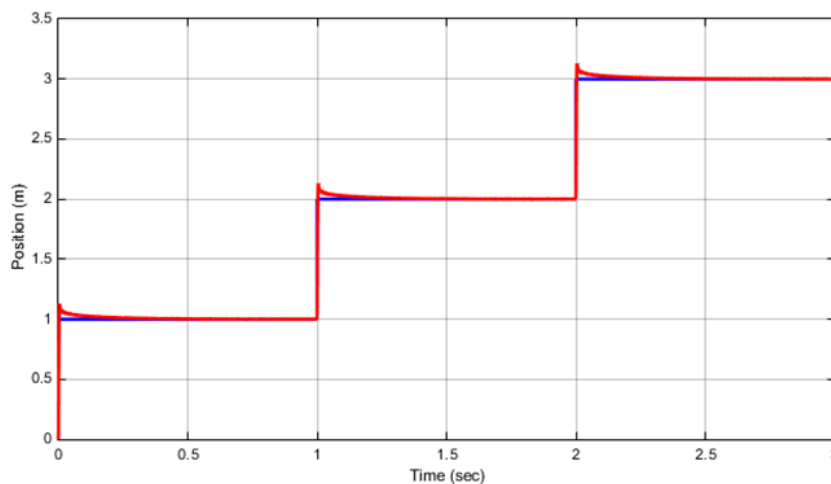
Figure 5.16 Step input tracking response for PID controller

(Plant output "red", reference signal "blue")
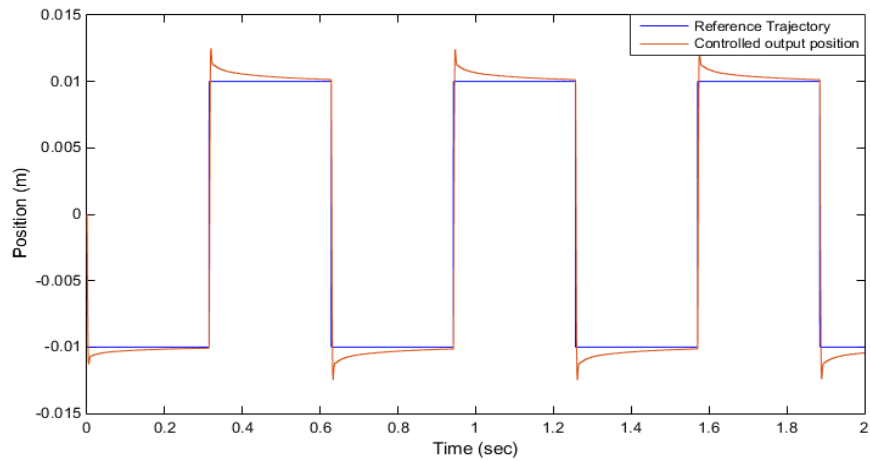
Figure 5.17 Square wave tracking response for PID controller without disturbance force

In addition, the performance of the system is tested by applying the block of band limited noise and pulse generator as a disturbance force with amplitude 1 between 0.05 and 0.1 seconds, The response of the external disturbance is zoomed in Figure 5.18 that the proposed controller has a good performance and desirable tracking response in terms of disturbance rejection and tracking the reference trajectory and being insensitive to parameter variations.
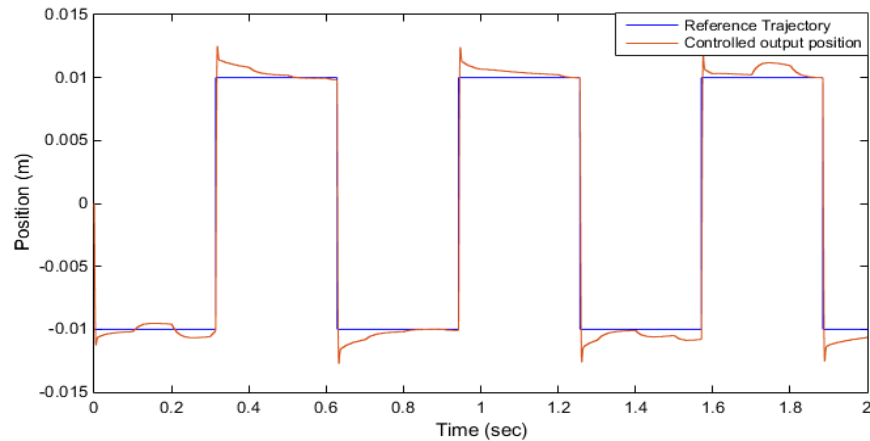
Figure 5.18 Square wave tracking response for PID with including disturbance force

Figure 5.19 presents a comparison of the step response for the planning model with the pole placement and PID controller. As seen, the proposed PID controller has less settling time and higher overshoot in comparison with pole placement controller. On the other hand, in terms of positioning accuracy, pole placement is the most accurate controller followed by PID controller.
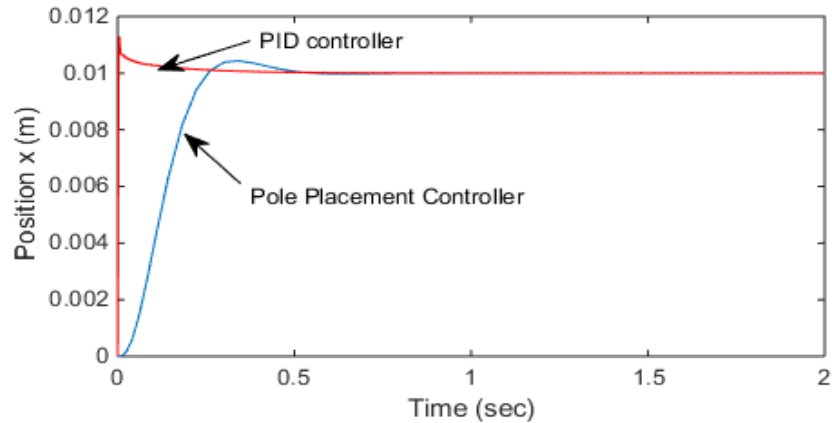
Figure 5.19 A comparison between the responses of Pole placement and PID controller

Summary

To control and stabilize the guidance system several different suitable controllers of classic and adaptive controller are introduced and proposed theoretically which are applied to the transfer function and state space models.

Phase- lead controller is designed utilizing root locus techniques through the design of GUI with MATLAB. The compensated system is stable with phase-lead controller is shown on the root locus plot in Figures above that the right half-plane pole is transferred to left-half plane.

After checking and calculating the controllability and observability matrix of the system and finding their ranks. Complete state feedback controller using pole-placement technique is tested based on the state space model to find the value of feedback gain matrix with respect to the equilibrium points. The prototype has been successfully tested and stabilized using pole placement technique and the guidance system is demonstrated with the desired operating gap. The output of the system tracks step change of the reference trajectory as shown in the resulting graph. So this technique is more suitable and robust than the other classic controller for controlling the system and solution of control problem.

So the efficiency of the system is investigated with the PID controller through conducting simulations in MATLAB/Simulink and an external pulsed disturbance force is applied to the system, the results illustrate that the proposed controller is a robust controller with a suitable transient. PID is better than Phase-Lead controller in terms of trajectory tracking and rejecting disturbance.

CHAPTER 6

EXPERIMENTAL SETUP AND SYSTEM COMPONENTS

6.1. Introduction

In this chapter, the simulation and hardware implementation of experimental setup and required components are presented in details. Figure 6.1 shows a schematic of the physical setup of the electromagnetic guidance system, which consists of dual electromagnets actuators with ferromagnetic platform, photoelectric laser sensor, two isolation and MOSFET driver circuits, 2 power MOSFET with RCD snubber circuits and the controller circuit which is used as a digital controller to process the control algorithm and to generate 2 control signals of PWM to the system. The description of each component will be explained in the following section.
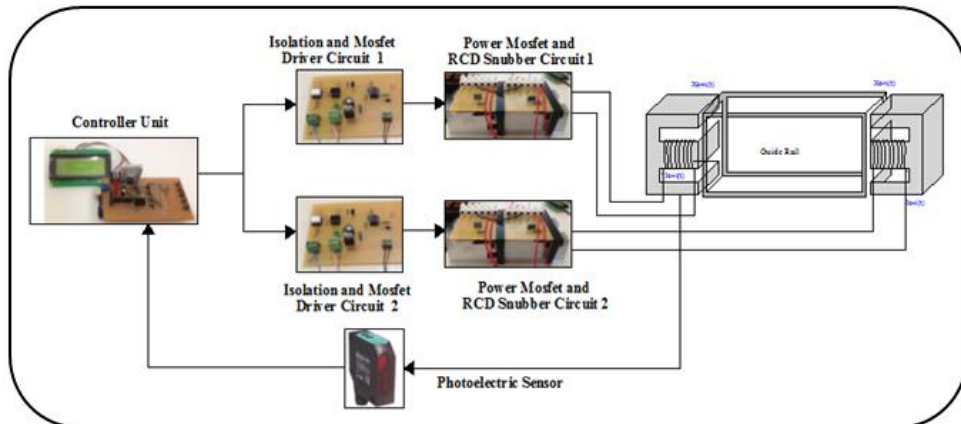
Figure 6.1 Schematic diagram of physical hardware of the guidance system

6.2 Principle of System Operation

In an attractive electromagnetic guidance system two electromagnets are used to produce the guidance force. To overcome the irregularities and dynamics coupled motion between two electromagnets, photoelectric laser displacement sensor is installed to detect the horizontal position between the electromagnets and the ferromagnetic platform and then report the measured position to the controller circuit via an Arduino board. The signal from the sensor is in the form of an analog

77

output current ranging from (4-20) mA, the signal is sent to Arduino platform through a multiplexed ADC channel and the Arduino displays them on the LCD.

The Arduino solves the control algorithm to produce the required pair of PWM control signals according to the difference between the set point and the present position and they send to the driver circuits to adjust the average current through the coil. Power MOSFET based on the driver circuit varies the voltage across it according to the PWM signal produced from the Arduino board. Thus the two positions are controlled through PWM technique which can be done by changing the duty cycle of the PWM signals.

To avoid magnetic interruption optical coupler is provided between the Arduino board and the MOSFET to isolate the power voltage level of Arduino and the MOSFET. The driver part is used to amplify the value of PWM coming from the output of the optocoupler which is not capable for driving the MOSFET. Snubbers circuits are required to protect the power MOSFET and to improve the performance which are placed across semiconductor devices, snubbers circuit can limit di/dt or dv/dt, overvoltage and overcurrent when the switching device change state from off state to on state and vice versa and protects the switching element from harmful effects of electromagnetic inductor.

6.3 Electromagnetic Coil

Figure 6.2 shows the photograph of experimental mechanism arrangement of the electromagnetic guiding device, which is designed to simulate and represent the lateral motion in a MAGLEV transportation system. This device consists of two E-shaped electromagnets and each one is adopted at each side of the linear guide-way.

An electromagnet is a magnet that runs by an electric current to produce the magnetic field, the strength of an electromagnet force can easily be varied by changing the amount of electric current that flows through it. The currents flow of the left and right electromagnet windings alternately according to the air-gap position error [6]. The number of coil turns for the electromagnets are chosen as 553 turn, mass of the electromagnet is 12.5 kg. Values of inductance and resistance coils are 0.142 H, 2.05 Ω and 0.152 H, 2.04 Ω respectively. The rate of required currents to put two electromagnets in the center of the plate nearly are (1.25 and 1.1) A.
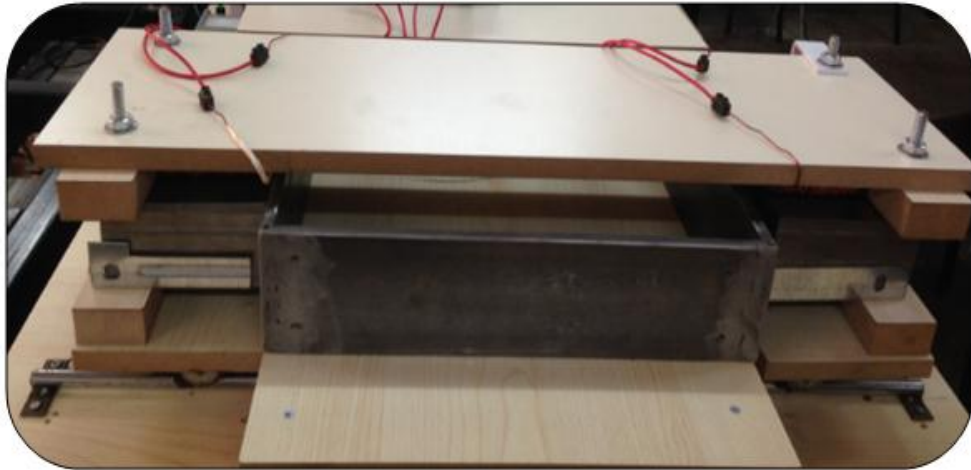
Figure 6.2 Photograph of experimental mechanism of the guiding system

In addition, in the guiding device two auxiliary wheels are adopted under two electromagnets along the X-axis direction to keep the motion and to reduce the friction as much as possible and to mimic the lateral motion of a system [22]. Mechanical limit movements of these two actuators are positioned to restrict the air-gap range to 0-20 mm.

6.4 Isolation and MOSFET Driver Circuit

The interface circuit of isolation and MOSFET driver circuit consists of two main parts as indicated in Figures 6.3 and 6.4. The former part is isolation part and the later part is MOSFET driver part.
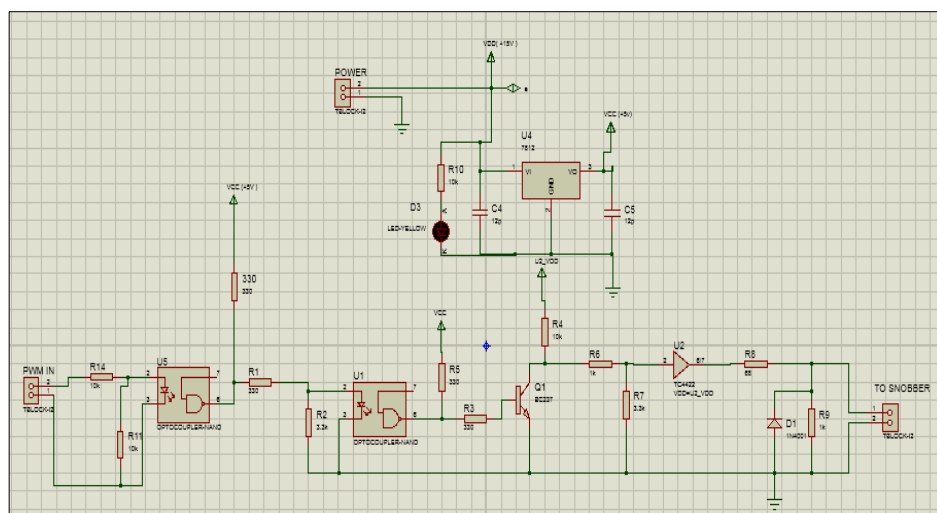
Figure 6.3 Proteus simulation of isolation and MOSFET driver circuit
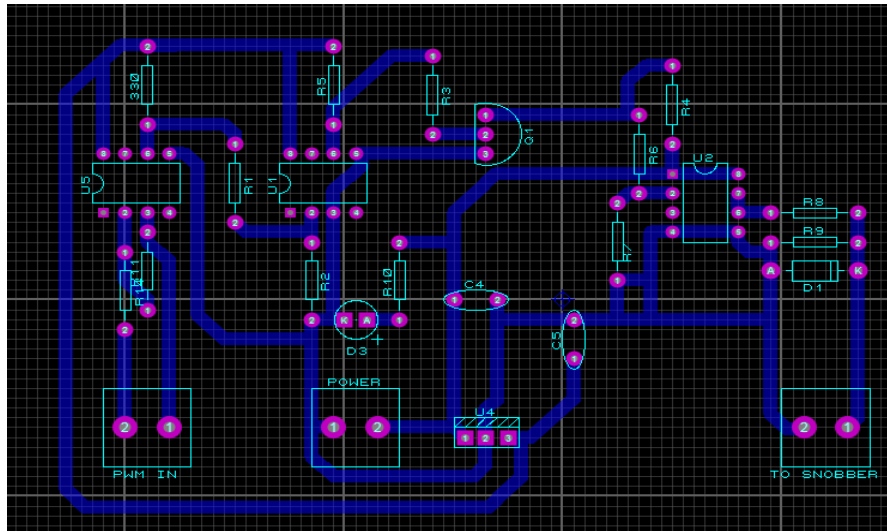
Figure 6.4 Design of PCB schematic of isolation and MOSFET driver circuit
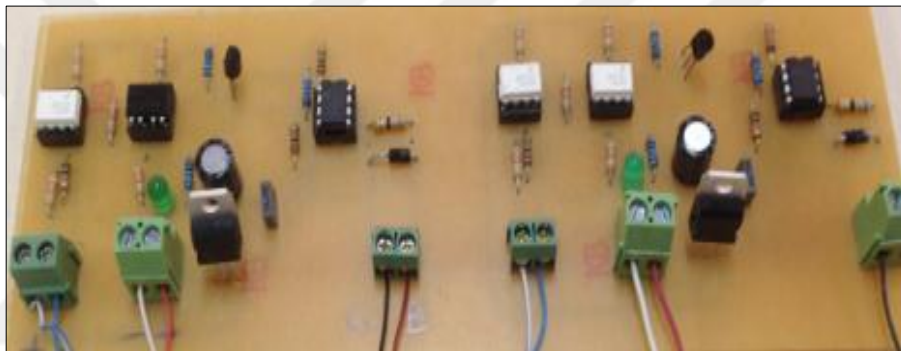
Figure 6.5 Isolation and MOSFET driver circuit photo

6.4.1 Optocoupler 6N137

Optocoupler (Vishay 6N137) is employed in the isolation part to avoid magnetic interruption and to isolate two different voltage levels between the low voltage of Arduino board (PWM control signals) and the high voltage and current in MOSFET.

The optocoupler 6N137 is a single channel consists of high efficient input LED coupled with an integrated optical photodiode IC detector as shown in Figure 6.6. The detector has an open drain NMOS-transistor output, providing less leakage compared to an open collector Schottky clamped transistor output. The speed of the 6N137 is very high 10 MBd typical, Low input current capability is 5 mA, performance operation for temperature range is -40°C to +100 °C temperature [60].

Optocoupler (Vishay 6N137) can be used in various application; computer peripheral interface, PLC, microprocessor system interface, digital fieldbus isolation: (CC-link,

80

SDS, device Net, profibus), AC plasma display panel level shifting, high speed DAC and ADC conversion, multiplexed data transmission, ATE input/output isolation, ground loop elimination and digital control power supply [60].

BC237 npn transistor is used to invert the output signal of the optocoupler and to supply enough current to drive the Mosfet driver (TC4422) [61]. A R3 resistor of 330 Ω is connected to the optocoupler's photo-transistor in order to minimize the delay of the optocoupler. On the other hand R5 (10KΩ) is the pull-up resistor that determines the rise time of the output waveform of 6N137 [62].
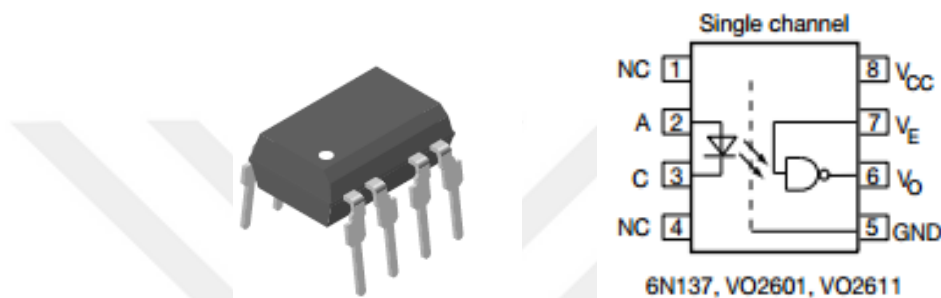
Figure 6.6 Internal schematics and pin configuration of 6N137 [60]

6.4.2 MOSFET Driver

MOSFET driver TC4422 is used as a gate driver in the second part of the interface circuit to drive the power MOSFET in order to turn on and off the power MOSFET quickly and minimize the rise time. Pin configuration and functional diagram are given in Figures 6.7 a, b.

The TC4422 is high current buffer/drivers capable of driving large MOSFETs and IGBTs. It is essentially immune to any form of upset except direct overvoltage or over-dissipation. The TC4422 input may be driven directly from either TTL or CMOS (4.5V to 18V). Fast rise and fall times is (30) n sec with 4,700 pF load and (180) nsec with 47,000 pF load, high peak output current is 9A, high continuous output current is 2A, short internal delay is 30 nsec typically and low output impedance is 1.4 Ω typically. Additionally, for the input 300 mV of hysteresis is built, providing noise immunity and allowing the device to be driven from slowly rising or falling waveforms. Microchip TC4422 can be used in wide range of application for Pulse Generators, Local Power ON/OFF Switch, Line Drivers for

Extra-Heavily-Loaded Lines, Motor and Solenoid Driver and Driving the Largest MOSFETs and IGBTs [63].

Diode D1 (IN4001) is connected across the gate-source of the power MOSFET to avoid any potential negative current flow from gate to source if the gate voltage is negative and is lower than the source voltage [62].

(a)   (b)
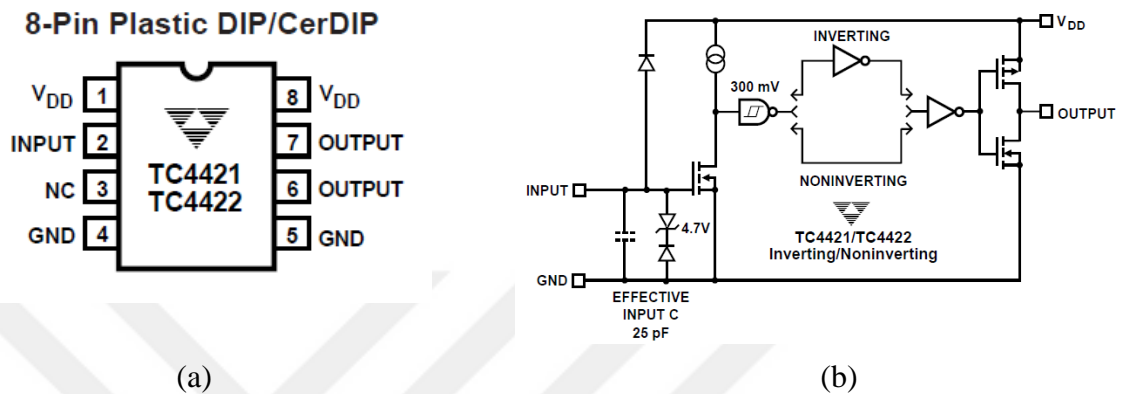
Figure 6.7 a) Pin configuration of the TC4422 b) Functional block diagram of TC4422 [63]

6.5 Power MOSFET and RCD Snubber Circuit

6.5.1 High Power Switching Device (Power MOSFET)

The high power switching device will be used to power the electromagnet coil. It is needed for the current control to allow all the current available to pass through it or either blocks the current. Three devices can be used to do high power DC switching are Gate Turn- Off (GTO's) thyristors, (MOSFET's) high Power Metal Oxide Semiconductors and Insulated-Gate Bipolar Transistors (IGBT's) [64].

For such a system power MOSFET (STP75NF75) is used as a high speed switching device in the part of switching circuit as indicate in Figure 6.8. MOSFET is a voltage controlled device, the main terminals are the drain, source and the gate, the current flow from drain to source being controlled by the gate to source voltage, therefore power MOSFET utilize a gate voltage to allow current to pass, or not pass through. MOSFET is capable of working at high frequencies (~10's of kHz.). It has the following electrical characteristics, drain source voltage VDSS is 75V, continuous drain current ID is 80A, typical and maximum on resistance RDS (ON) are 9.5 mΩ, 11 mΩ respectively, transistor polarity is N channel, minimum and

maximum operating range of temperature is -55°C to 175°C and the power MOSFET needs a positive gate voltage between +3v to 30 v to turn ON [65].

STP75NF75 can be used as a primary switch in advanced high efficiency, high-frequency isolated DC-DC converters for computer applications and telecom. It is also intended for any applications with a low gate drive requirement [65].

Pin1–Gate
Pin2–Drain
Pin3–Source
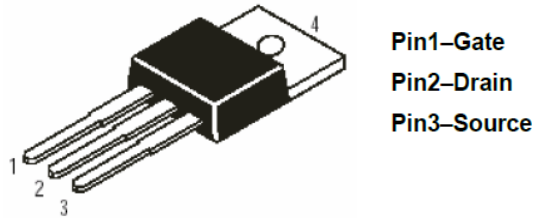
Figure 6.8 Power MOSFET [65]

The average of voltage that supply to the electromagnets coil through the power MOSFET is given by (6.1), power MOSFET can turn the amount of currents on and off under the control of a low signal level voltage [66].

$$V_{(average\ of\ coil)} = \left({t_{on}}/{T} \right) \cdot V_{input} \tag{6.1}$$

where,

$V_{(average\ of\ coil\ )}$ = average voltage supply to the coil,

$V_{(input\ )}$ = input voltage, t_{on} = time on of switches,

T = period of PWM, (t_{on}/T) = duty cycle of PWM
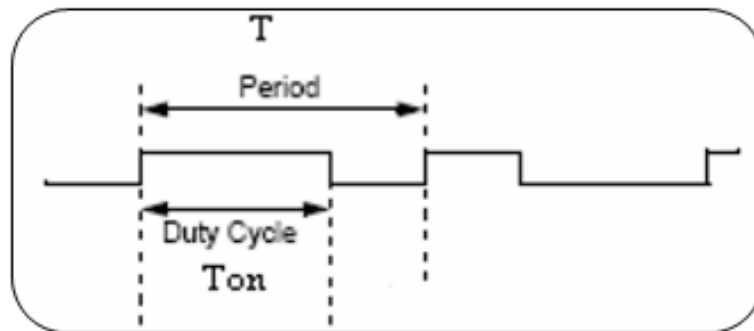
Figure 6.9 PWM signal [66]

The average output voltage V_{ave} can be changed between 0 and Vin by controlling the duty cycle, thus, the current flow can be controlled which across the electromagnets through the switching device.

6.5.2 RCD Snubber Circuit

Snubbers are an essential part of power switching circuits whose function is to control the effects of circuit reactance to enhance and improve the performance of the switching circuits and result in higher reliability, higher efficiency, higher switching frequency, smaller size and lower weight. Snubbers may be either passive or active circuit. The elements of the passive snubber circuit are limited to resistors, capacitors, inductors and diodes while active snubbers elements include of transistors or other active switches [67].

Snubbers can do many things; reduce or eliminate voltage or current spikes during turn-off and turn on transients respectively, limiting the rate of rise (di/dt) of currents through the device at turn- on, limiting the rate of rise (dv/dt) of voltage across the device at turn- off , Shaping the switching trajectory of the device as it turns on/off, transfer power dissipation from the switch to a resistor or a useful load, Shape the load line to keep it within the safe operating area (SOA) and reduce total losses due to switching [68,69]. Passive Resistor-Capacitor-Diode (RCD) turn-off Snubber is used in such system as shown in Figure 6.10. At turn-off in the presence of this snubber, with a constant of di/dt the current decreases in the transistor ic and (Io-ic) flows into the capacitor through the snubber diode.

Snubber diode (Ds) is required to discharge the magnetic energy safely when the MOSFET goes into the off-mode. It shorts out the snubber resistance (Rs) and some of the supply voltage across the snubber capacitance (Cs), switching device is saved and protected from the over voltage. When the switch is turn-on, the voltage on the C_s is discharged across R_s. C_s is determined in (6.2).

$$C_S = \frac{I_0 \cdot t_S}{2 \cdot E_0} \qquad F \tag{6.2}$$

where, I_0 is the reference current, t_s is the switch fall time and E_0 is supply voltage of the electromagnet. Capacitance of the snubber circuit can be found from the reference current, fall time is 10^{-5}s and supply voltage is 12 V.

Snubber resistance could be found using the following equation:

$$R_S = \frac{t_{on\,min}}{5C_S} \qquad \Omega \tag{6.3}$$

where, a minimum turn-on time of the switching device ($t_{on\,min}$) is about 5/1023 for 3900 Hz PWM.
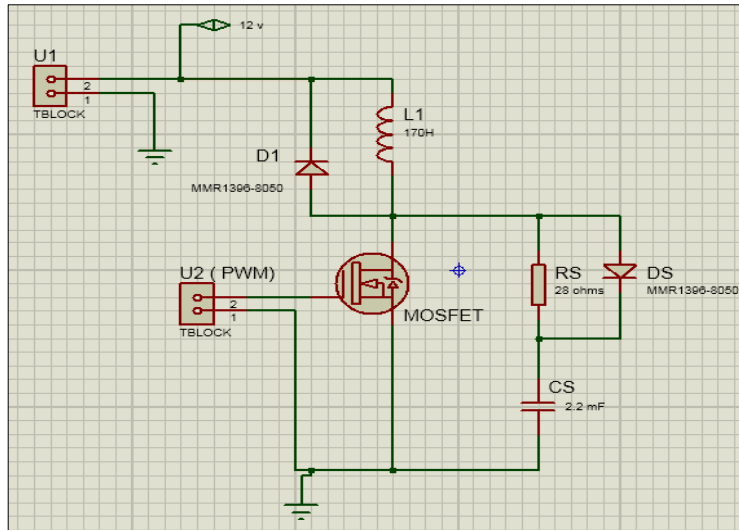
Figure 6.10 Layout schematic of RCD snubber circuit
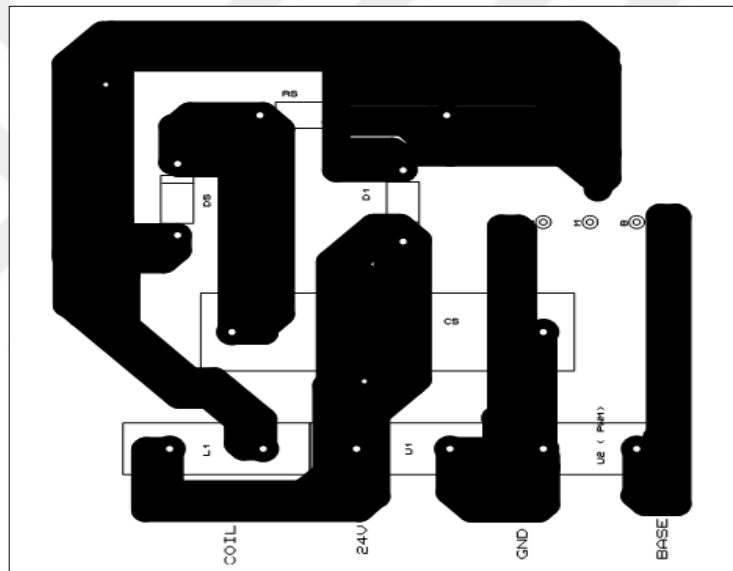
Figure 6.11 Design of PCB schematic of snubber RCD circuit
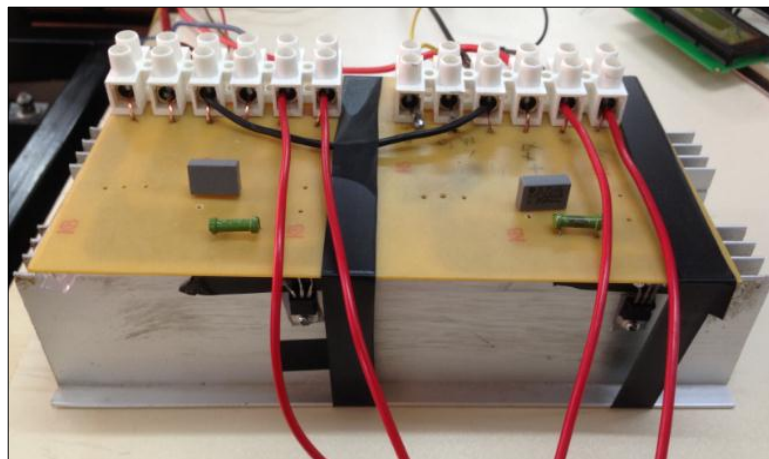
Figure 6.12 Photo of snubber RCD circuit

6.6 Photoelectric Laser Displacement Sensor

In industrial sensors there are many types of sensors to get air-gap distance, the most common technologies are photoelectric, inductive, magnetic, capacitive and ultrasonic [70]. In this study photoelectric laser sensor (PLS) (VDM18-100/32/105/122) is used to provide the feedback position signal in the horizontal direction to the controller circuit as shown in Figure 6.13, which is manufactured by Pepperl + Fuchs.

Figure 6.13 VDM18-100/32/105/122 photoelectric laser sensor [71]

Generally for target detection photoelectric sensor provides three primary methods; diffused, thru-beam and retro-reflective. The VDM18-100/32/105/122 sensor is working on the method of diffused mode. Sensing in diffused mode sometimes called proximity mode, the transmitter and receiver are in the same housing. Light from the transmitter strikes the target and the light is reflected at arbitrary angles, some of the reflected light returns to the receiver and the target is detected [70].

Due to the targets angle and ability to reflect light some of the transmitted energy is lost, the results of sensing range in diffused mode are shorter than the other two modes thru-beam and retro-reflective modes [70].

Photoelectric sensor is made up of a light source (LED) as a transmitter, a phototransistor as a receiver, a signal converter and an amplifier. The phototransistor receives the incoming light and analyzing it, verifies that it is from the LED and appropriately triggers an output as shown in Figure 6.14 [70].
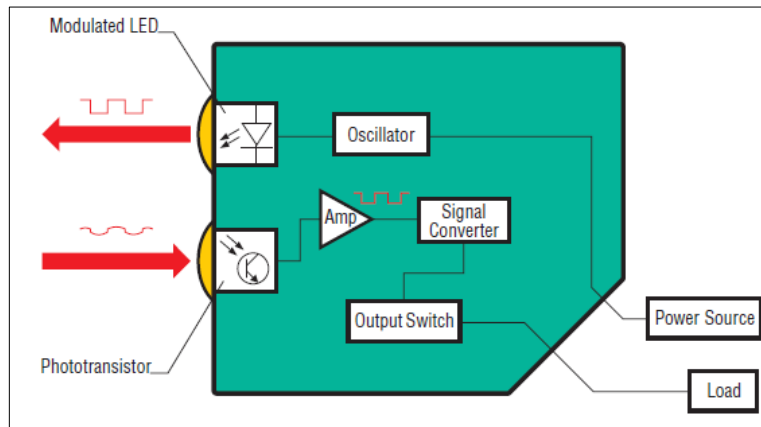
Figure 6.14 Internal configuration of the VDM18-100/32/105/122 [70]

(VDM18-100/32/105/122) has 5 pins-cable connection; supply, ground, analog output current which is (4-20 mA) between the end and beginning of operating range, one switch output function is PNP and the last pin is controlling input. Sensor supply voltage is 18-30 volt DC, the sensor runs with 19 V DC. Method of measurement is laser triangulation, the wavelength is 650 nm, switching frequency is <= 1 kHz and measuring range is about 30 ... 100 mm. The laser displacement sensor was unable to sense the distance between the ranges from zero to 30mm as shown in Figure 6.15. Due to very fast response characteristic (0.4 ms response time) and high resolution this type of sensor is suitable for rapid scanning process [71].
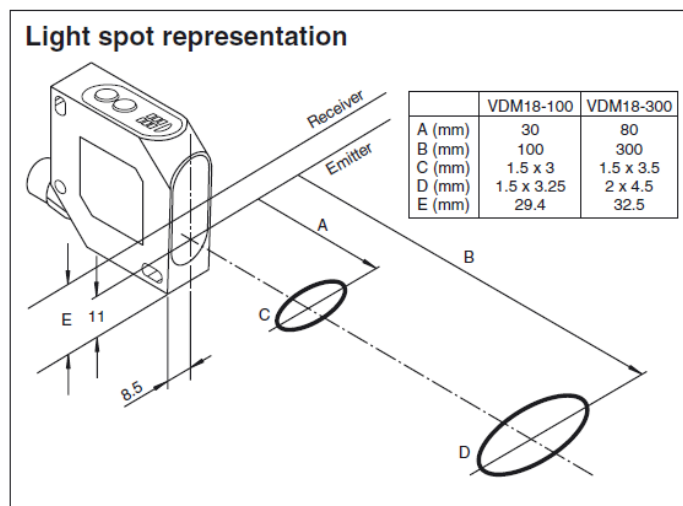
Figure 6.15 Light spot representation of VDM18-100/32/105/122 [71]

In such type of photoelectric sensor the distance is sensing based on the Pulse Ranging Technology (PRT) method. The sensor accurately measures the distance to an object or reflector. The sensor emitter sends short, intense bursts of light that are

reflected back to the sensor's single receiver as shown in Figure 6.16. Offering continuous distance data, it measures the actual distance to an object or reflector with repeatability and precision [72].
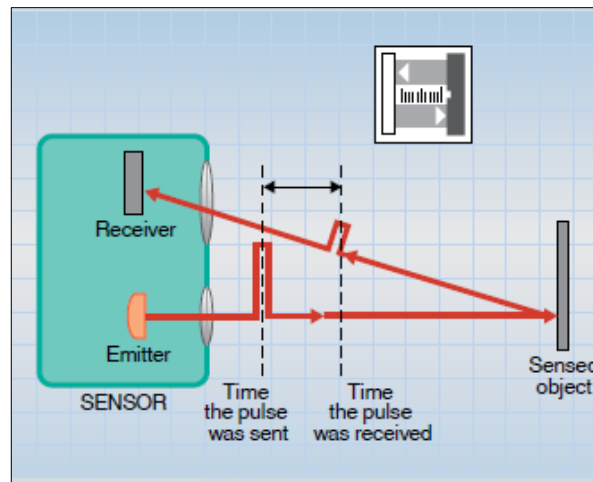
Figure 6.16 Sensing the distance based on the pulse ranging technology method [72]

The distance from the sensor to the object (S) can be calculated, using the speed of light in air as a constant (c) and the time duration between the pulses was sent and the time was received. See Figure 6.17 [73].
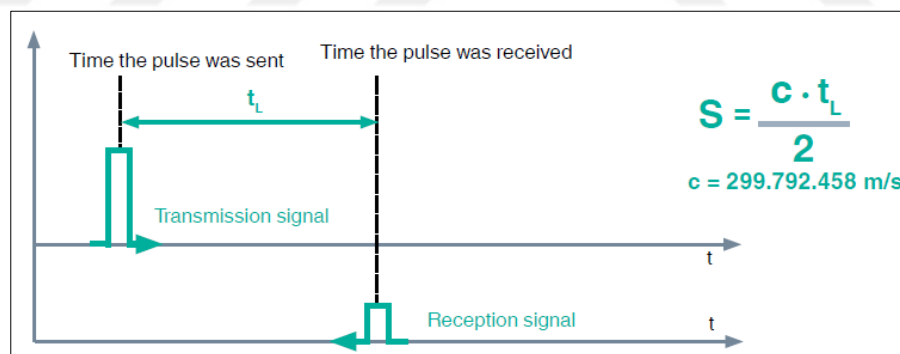
Figure 6.17 Principle of operation of a PRT distance measurement sensor [73]

Typical applications of Pulse Ranging Technology sensor are; collision avoidance on overhead conveyors, measurement of distance to stacker crane, container dimensions measurement, elevator positioning, precise level and measurement [72].

The current output of the sensor flows through the 254 Ω resistors to produce a voltage, the voltage on the resistor is measured for distance information. Experimentally, the output voltage of the resistor is collected with changing target's distance as determined in Table 6.1.

Table 6.1 Photoelectric sensor voltage-distance data

Distance (x) (cm)	Voltage (Vs) (volt)	Slope (β) (V/m)
3	5.07 (20 mA)	169
3.5	4.83	138
4	4.53	113.25
4.5	4.24	94.22
5	3.95	79
5.5	3.67	66.72
6	3.41	56.83
6.5	3.13	48.15
7	2.85	40.7
7.5	2.55	34
8	2.21	27.65
8.5	1.88	22.11
9	1.64	18.22
9.5	1.35	14.21
10	1.07 (4 mA)	10.7
	Gain (Average Slope)	**β = 62**

Output voltage- distance curve can be obtained using Microsoft Excel, the relationship between the output voltage of the sensor and the distance is supposed as a linear equation. The curve and equation are given in Figure 6.18. The average slope of the curve is the gain of the sensor which can be determined using differentiation at all sensing region. The gain of the sensor is found as β =62 and the sensor output voltage is beta multiplied by air-gap distance.
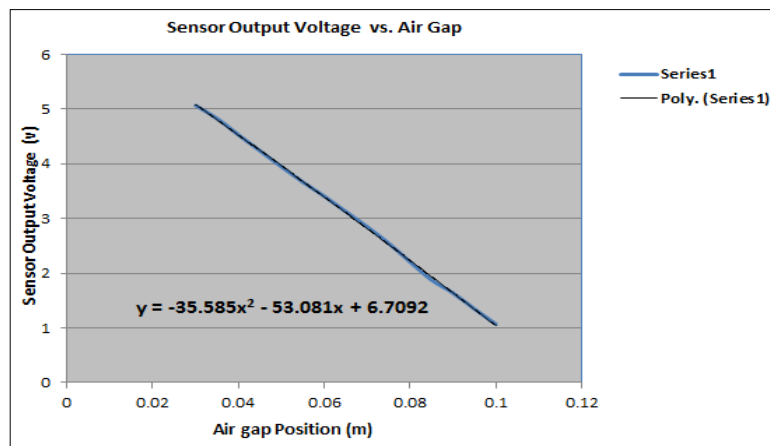
Figure 6.18 Output voltage of the sensor with distance

6.7 Microcontroller Board (Arduino / Genuino MEGA 2560)

Arduino is an open-source electronics prototyping platform based on flexible easy to use hardware and software. The Arduino Genuino MEGA 2560 has been selected for the purpose of controlling the position in such system and for processing multi-functions. The first channel (A0) of analog to digital converter is multiplexed to read the incoming feedback signal, which is coming from the photoelectric laser sensor. Eight channels of digital pins are used to set the value of set point (desired position) and the value of controller parameters (KP, KI, KD) using push buttons.

Mega 2560 is used for processing control algorithm and generating pair of control PWM signals, according to the error signal which is the difference between the actual position and the desired position. The fuzzy PID control algorithm is applied and 8-bit, 3900Hz of 2 PWM control signals are produced by duty cycle generators of the Arduino board, then the duty cycles will send to the coil drivers. Control parameters and duty are sent to the (4*20) LCD and can be read on the screen of the LCD.

Arduino/ Genuino Mega 2560 is a microcontroller board based on the ATmega2560. It has 16 analog pins of inputs each of which provide 10 bits of resolution, the data acquired for each analog pin are set to a value between 0 and 1024, which corresponds to 0 to 5 V, respectively. 54 digital pins of input/output, 15 of these pins can be utilized as PWM function, a 16 MHz crystal oscillator, 4 UARTs (hardware serial ports), an ICSP header, a power jack, with a reset button and USB connection.

The Arduino mega has five internal timers; timer 0 to timer 4, the internal timer 0 is used for PWM channel on pins (13, 4) and also is used for the milli ( ) and other timing functions are; Timer1 used for PWM channel on pins (12, 11). Timer 2 is used for PWM channel on pins (10, 9). Timer 3 is used for PWM channel on pins (5, 3, 2) otherwise timer 4 is used for PWM channel on pins (8, 7, 6). The pin configuration of the Arduino / Genuino MEGA 2560 is given in Figure 6.19 [74].

Technical specification of Arduino / Genuino MEGA 2560 Model [75]

Arduino offers several models with different characteristics. The main differences between the modules are the number of input and output pins, the type of

microcontroller and the capacity of the flash memory. The main features of the MEGA 2560 module are shown in the Table 6.2 [75].
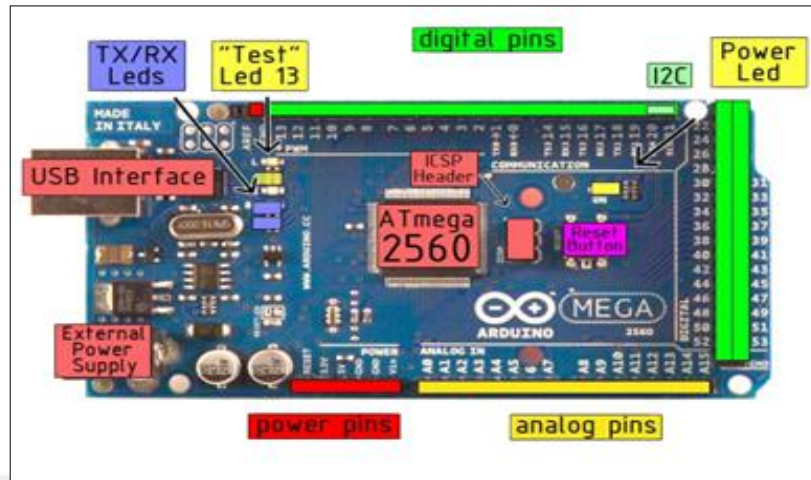
Figure 6.19 Pin configuration of the Arduino / Genuino MEGA 2560 [74]

Table 6.2 Core features of the Arduino / Genuino MEGA 2560 [74]

Parameter Name	Value
Operating voltage	5V
Input voltage (recommended)	7-12 Volt
Input voltage (limit)	6-20 Volt
Digital I/O Pins	54 pins (15pins of them provide PWM output)
Analog input pins	16
DC current per I/O Pin	20 mA
DC current for 3.3V Pin	50 mA
Flash memory	256 KB of which 8 KB used by boot loader
SRAM	8 KB
EEPROM	4 KB
Clock speed	16 MHz
Length	101.52 mm
Width	53.3 mm
Weight	37 g

6.7.1 Controller Circuit

The configuration of the controller circuit for controlling the displacements is shown in Figure 6.20. The simulation of the circuit was done with Proteus ISIS software to verify the program developed in order to debug any error occurs from the program. This circuit is used as a master circuit where all the command or instructions are applied to the Arduino MEGA 2560 that are needed to the project, design of PCB schematic and appearance of circuit photo are shown in Figures 6.21 and 6.22.
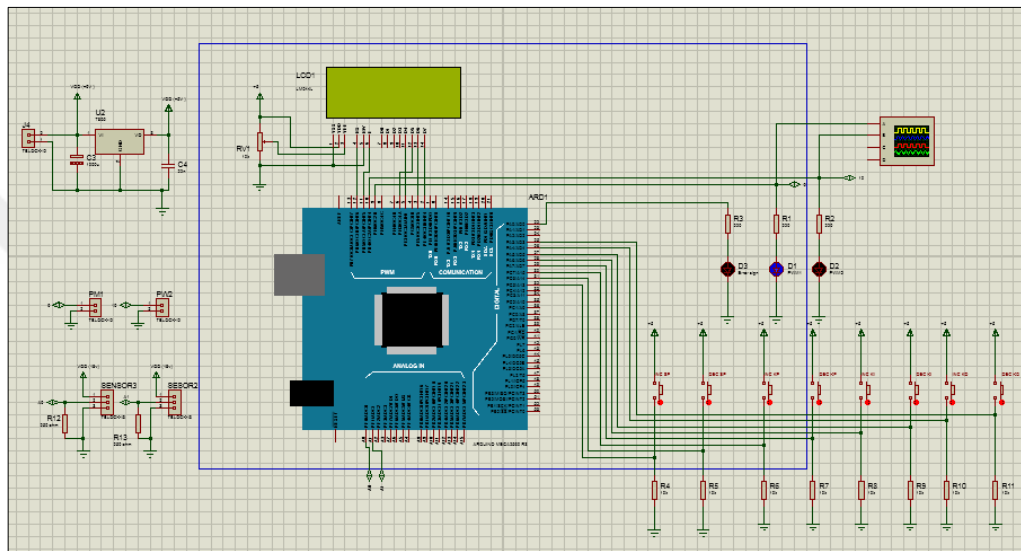
Figure 6.20 Schematic circuit diagram for position control
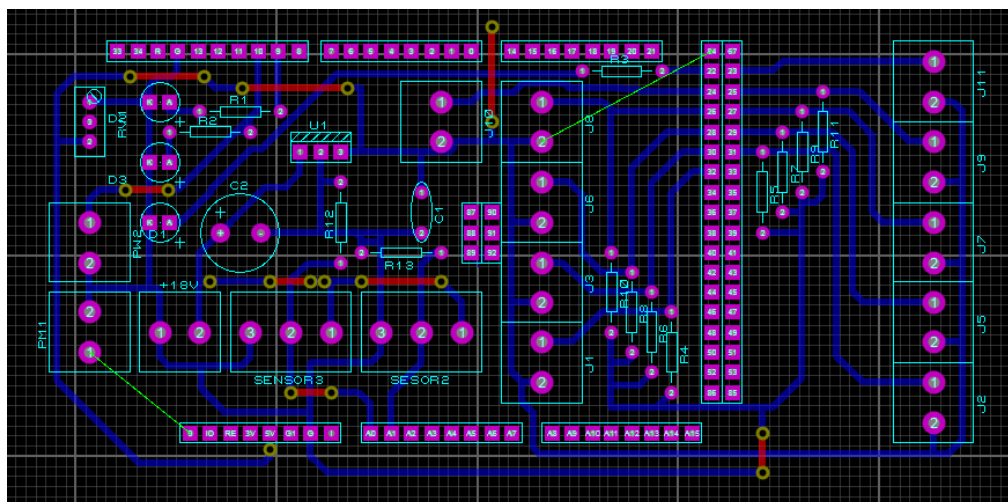
Figure 6.21 PCB schematic of controller circuit diagram

Two of the push buttons are assigned in the circuit to set the value of set point, which are used for decreasing and increasing the value. In addition, six of the push buttons

are assigned and set in the circuit for decreasing and increasing the value of the controller parameters (KP, KI and KD) respectively.
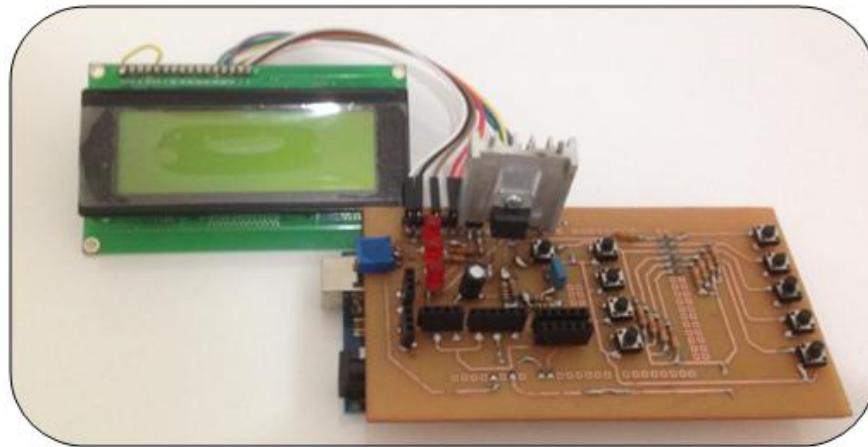
Figure 6.22 A photo of Arduino / Genuino MEGA 2560 control circuit with LCD

Figure 6.23 shows the illustration of LCD display of the Proteus software on the simulation for testing the program. The set time for the timer interrupt function is 5 cycles, meaning that, for every 5 cycles the LCD will display the current value of the position. The first line showing the position feedback and set point value, in the second line there are two values corresponding to the value of error and proportional gain, the third line showing the value of change of voltages in the duty cycle of PWM while the fourth line is used for setting the values of integral and derivative gains of PID controller. Figure 6.24 shows two output signals of the system using digital oscilloscope.
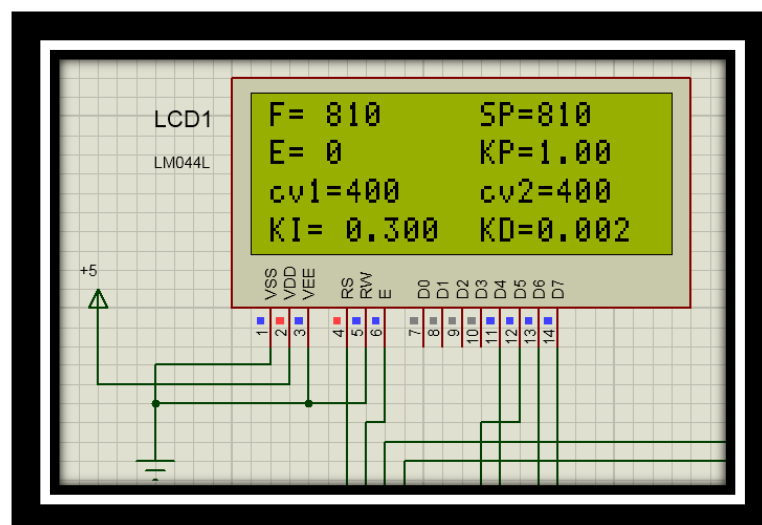
Figure 6.23 LCD display on the Proteus software for the simulation
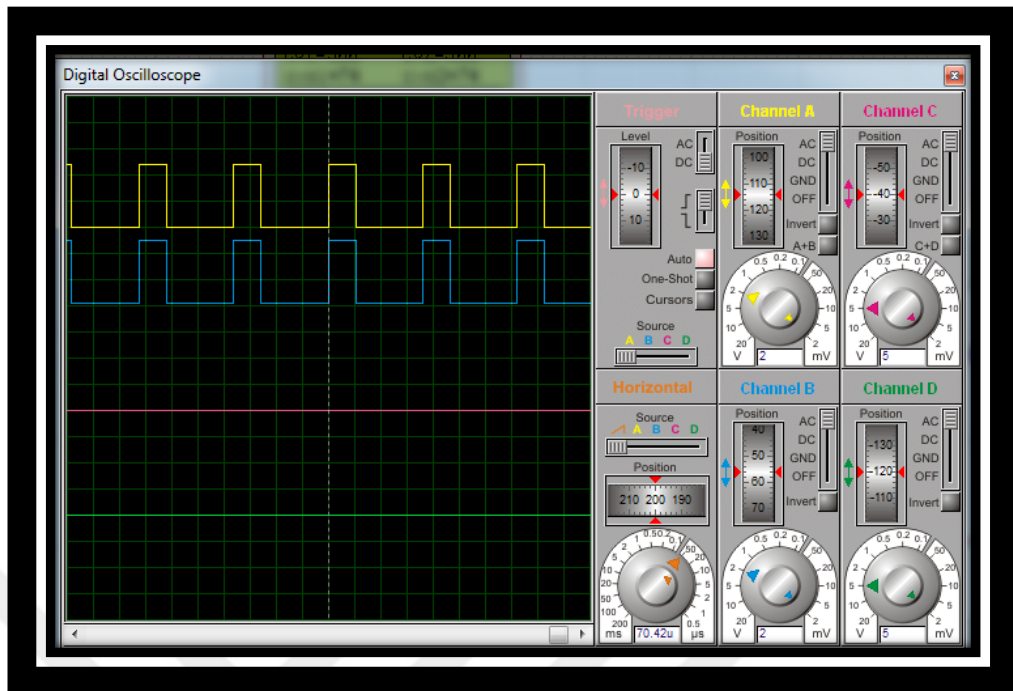
Figure 6.24 Output signals of the system using digital oscilloscope

Summary

In this chapter, the experimental setup and its components are described. Two electromagnets are designed and their electrical values are measured using LCR meter. Photoelectric laser sensor is installed with the system to provide the feedback position signal to the controller circuit. The Mega2560 is used to implement control algorithm and generating two controls PWM signals to control the plant and to get analog distance information from the sensor and converting this to 10-bit digital one.

Generated control signals are sent to a power switching device (Power MOSFET) through isolation and driver circuit. Optocoupler is used in isolation section to separates microcontroller board and power voltage levels. Driver section of the card is used as a gate driver to produce enough current to drive the Power MOSFET.

Snubbers circuit protects the power MOSFET from overvoltage and overcurrent when the switching device change state from on state to off state and vice versa and protects the switching element from harmful effects of electromagnetic inductor.

CHAPTER 7

SOFTWARE IMPLEMENTATION AND EXPERIMENTAL RESULT

7.1 Introduction

This chapter discusses the results obtained during the experiment and proposed a control algorithm for software implementation. The microcontroller on the board is programmed using the Arduino Integrated Development Environment (IDE) based on the processing project, which is used as a compiler for writing the control algorithm and implementing the software. The proposed control algorithm of the controller is illustrated and detail that corresponds to the calculated error between the reference position and the actual data. The results of the controller are discussed and the performance is studied.

7.2 Software Implementation

The software is very important to realize the desired control algorithm. For software implementation of this project, Arduino IDE is the software environment used to create the program, which is called "sketch," that is executed by the Arduino hardware. After writing the program the IDE uses a modified C language compiler to build, translate, and downloaded the code to the microcontroller board to run the control algorithm and to achieve a real time control [76].

7.2.1 Developed Algorithm for Electromagnetic Guidance System

Arduino acts as a brain of the whole control system. At the start of the program, the main file is uploaded to the board via IDE in a computer using USB cable. Establishing the serial communication at 9600 bits of data per second. The Arduino board measures the output voltage (position) from the sensor in an analog fashion, the signal read from the analog pin is converted to a digital signal using a 10- bit analog to digital converter. As such the analog pins read 0V to 5V in integer values between 0 and 1023 units, which takes around 100 microseconds (0.0001 s) to read an analog input, thus the rate of maximum reading in a second is approximately

10,000 times. The laser sensor provides an accurate linear representation of position between the minimum range of 230 and maximum range 1023. The reference value for the system is set to about 0.01 m (i.e.810 counts), so the air-gap distance between two electromagnets and guide-way has to be maintained at 0.01 m, in other words the control algorithm strives to achieve this desired position. The pins that communicate with the LCD are defined. In the next step, the algorithm interpolates the values obtained according to determined values established for each position in the range of measurement.

The program consists of two parts of the main and interrupt program, the Arduino will always run the main program until an interrupt is occurring. Interrupt service routine is defined on ADC through the function of (ISR (ADC_vect)), if analog to digital conversion is finished, ADC Interrupt flag bit is set high. When Arduino receives an interrupt flag, it will jump to interrupt processing.

In the subroutine, the value of actual position is compared with the desired position and the correction will be done by Arduino to always maintain the two electromagnets at the desired position. If both values are the same, the output of the controller will be 0 and the two output will became equal. Otherwise, if the value is smaller or bigger than the set point, Fuzzy PID controller is activated and the output will be determined between 0 and 600. In both cases the output will be sent to Arduino to establish an action and to generate appropriate 2 duty cycles of PWM for two actuators. The output value determines how much time should be on the power control to adjust the average current in the coil.

Hence the control algorithm is applied according to the error signal, then two signals of duty cycle are sent for driving the power MOSFET for controlling the electromagnets in order to guide and maintaining the system at desired position. Updated information (PWM duty cycles, measured distances) are sent to LCD then exit the interrupt routine. Finally, in the last step, the system returns to the first step without any delay, and the system acquires new values to start the process. Figure 7.1 shows the flowchart of the developed control algorithm and program operation steps for the electromagnetic guidance system.

```
                    ┌─────────────────┐
                    │      Start       │
                    └─────────────────┘
                              │
                              ▼
┌───────────────────────────────────────────────────────────────┐
│                        Initialization                           │
│  • Define the type of Pin Modes (setting the input and output pins) │
│  • Initialize and selecting 2 digital pins (9, 10) as PWM output │
│  • Initialize Timer2 in timer mode for PWM pins                  │
│  • Define LCD connection port and establishing serial communication at 9600 bits │
│  • Define (ADC) pin as 10 bit                                   │
└───────────────────────────────────────────────────────────────┘
                              │
                              ▼
              ┌──────────────────────────────────┐
              │            Initialize:            │
              │  Set point,  u(0)=0   KP, KI, KD =0 │
              │  e(0)=0,    e(k-1)=0,   e(k-2)=0   │
              └──────────────────────────────────┘
                              │
                              ▼
                     ┌─────────────────┐
            ┌───────▶│    While (1)    │◀───────┐
            │        └─────────────────┘        │
            │                 │                 │
            │                 ▼                 │
            │          ◇─────────────◇       0  │
            │         ╱   While (interrupt ╲────┘
            │         ╲      -ADC)        ╱
            │          ◇─────────────◇
            │                 │ 1
            │                 ▼
            │     ┌──────────────────────────────┐
            │     │ Read analog sensor data from  │
            │     │        ADC channel            │
            │     └──────────────────────────────┘
            │                 │
            │                 ▼
            │     ┌──────────────────────────────┐
            │     │ Calculate error = Set point - Sensor Data │
            │     │ Calculate change of error (ce) =e (k) - e (k-1) │
            │     └──────────────────────────────┘
            │                 │
            │                 ▼
            │     ┌──────────────────────────────┐
            │     │ Check the sign and amplitude of error │
            │     └──────────────────────────────┘
            │                 │
       Yes  │                 ▼                No
            │          ◇─────────────◇
            │  ┌──────╱   Error = 0   ╲──────┐
            │  │      ╲               ╱      │
            │  ▼       ◇─────────────◇       ▼
            │ ┌───────────────┐   ┌──────────────────────────────┐
            │ │ cv1=cv2 = 400 │   │ Calculate PID output = OUT1+TP+ TI+ TD │
            │ └───────────────┘   │        TP =KP*e(k)            │
            │         │           │   TI = KI* (TI1 +e(k)* dt)    │
            │         ▼           │ TD=KD*(e(k) -2*e(k-1) + e(k-2)) │
            │ ┌───────────────┐   │   Calculate Fuzzy Logic output: │
            │ │ Send data to Arduino to │ └──────────────────────────────┘
            │ │ Generate 2 equal PWM signals │         │
            │ │ for two switching MOSFET │             ▼
            │ └───────────────┘                       A
            │         │
            │         ▼
            │ ┌───────────────┐
            │ │ Send information to the LCD │
            │ └───────────────┘
            │         │
            └─────────┘
```

97

A

Fuzzification step:
(Change the numerical value to fuzzy set)
Finding triangular membership value using:
x-a/b-a where (a<=x<=b)
c-x/c-b where (b<=x<=c)

Fire the fuzzy rule:
Using rule, if and then rule
if case1=value and case2 =value then
(The output is the min value between two cases)

Defuzzification step:
(Change the fuzzy set to numerical value)
Using center of area method to find two outputs
The outputs will be used as PWM duty cycles

Output1 (D1) =Fuzzy output (cv1) + PID output
Output2 (D2) =Fuzzy output (cv2) + PID output

No   Check (D1, D2) range >1023   Yes

D1, D2 =1023

Check D1, D2 range <- 1023   Yes

D1, D2 =-1023

No

Changing the controller outputs form 10 bit to 8 bit:
cvo1 =map (D1, -1023, 1023, -255, 255)
cvo2 =map (D2, -1023, 1023, -255, 255)

Transform the results to the corresponding PWM form:
Calculated Duty1 =cvo1
Calculated Duty2 = cvo2

Send information to the LCD   →   **Return**

Figure 7.1 Flowchart of the control algorithm

7.2.2 Processing Explanation of Main Program

a- Generating PWM in Arduino

Pulse-Width Modulation is a technique that controls the width of the pulse based on modulator signal information. PWM can be used to encode information for supplying electrical power to a load [77]. Arduino 2560 provides 12 pins supporting PWM on digital I/O pins which are from 2 to 13 included, analogWrite function is utilized to set the duty cycle of a PWM pulse train. PWM is represented in binary signals, which has two signals high and low periods and the width of the pulse varies between 0 and the period T (2 ms).

PWM has two different modes; fast PWM and phase correct PWM. Pins 13, 4 configured to the fast PWM mode that the timer 0 counts from 0 to 256, otherwise the other timers of PWM pins configured to the phase correct PWM mode that the timer counts from zero to 510 different states. The frequencies of the pin can be determined from the formula: Clock / Prescaler / PWM mode number of states. [78]

- Timer 0 controlled the frequency of pins 4 and 13:

  16 MHz / 64 / 256 = 976.56 Hz

- Timer (1-4) controlled the frequency of other PWM pins:

  16 MHz / 64 / 510 = 490.20 Hz

Pins 9 and 10 are selected to generate 2 PWM signals, which operate at a frequency approximately 3900 Hz. In the Arduino compiler the PWM frequency cannot be readily changed from the default value of 490 Hz, the internal register (TCCRnB = (TCCRnB & 0xF8) | i) must be modified to change the PWM frequency. The "n" refers to the particular internal timer (2) and (i) is chosen depending on which timer is associated with the PWM pin whose frequency you want to change.

PWM Pins of (9, 10) can be controlled only by an 8 bit digital number (that is needed to write a value between 0 and 255 to the PWM pin). In our current experiment the reading of analog pins between 0 and 1023, it means that the output value of the controller is a 10 bit fashion, so it need to make a corresponding conversion in the controller output form 10 bit to 8 bit, which can be done by using one alternative command called map ( ) which handles the analog-input-range to the PWM-output-range conversion. Its syntax is, map (value to scale, from Low, from High, to Low, to High) [79].

7.3 Control Algorithm Process and Experimental Results

Due to the nonlinearity of the guidance system and changing in the dynamic response of the system with the variation of operational condition, it is impossible to get better results with linear controller design as PID and this lead to combine and use nonlinear controller to design the controller.

The fuzzy PID controller is proposed to control such system by combining a Fuzzy Logic in intelligent controller and Proportional, Integral and Derivative (PID) type of classical controller. Then the designed controller is coded in C language and implemented in real-time on Arduino mega2560 (Microcontroller board) as a control platform.

The part of PID controller will be digitally designed from the discrete-time PID controller formula which should be represented in the z-domain, equation (5.23) needs to be transferred into Z domain to make it suitable for implementation on a microcontroller board. This is done using the forward difference rule which is given in (7.2) for replacing the derivative and the integral terms.

$$u(z) = \left[K_p + \frac{K_i \cdot T_s}{(1 - z^{-1})} + \frac{K_d}{T_s}(1 - z^{-1})\right] \cdot e(z) \tag{7.1}$$

where, $$S = \frac{1 - z^{-1}}{T_s} \tag{7.2}$$

and T_s is sampling time or sampling periods. Equation (7.1) can be written as:

$$u(z) - z^{-1}u(z) = K_p(1 - z^{-1})\,e(z) + K_i T_s e(z) + \frac{K_d}{T_s}(1 - 2z^{-1} + z^{-2})e(z) \tag{7.3}$$

The mathematical relationship between the control error and the control value is called the control algorithm. For a PID controller, this is a differential equation. The final formula of difference equation will be:

$$u_k = u_{k-1} + K_p[e_k - e_{k-1}] + K_i T_s e_k + \frac{K_d}{T_s}[e_k - 2e_{k-1} + e_{k-2}] \tag{7.4}$$

where, u_k is the variable of controller output which means the current across the electromagnet coil, u_{k-1} is the control signal of the previous sampling, e_k is current error, then e_{k-1} is error of previous sampling and e_{k-2} is previous to previous error. Equation (7.4) is programmed and implemented to apply the proposed PID controller.

Fuzzy Logic Controller (FLC) is one of the most used applications of fuzzy set theory which can be used instead of digital control systems. In the fuzzy controller, computation is made by using words rather than numbers. To describe the fuzzy set membership functions are used as the main tools for the fuzzy operations [80]. The most well-known model of fuzzy inference system (FIS) in FLC is the Mamdani model, which consists of four sections namely; fuzzifier, rule base, fuzzy inference process and defuzzifier. Figure 7.2 shows the architecture of a fuzzy logic control system [81].
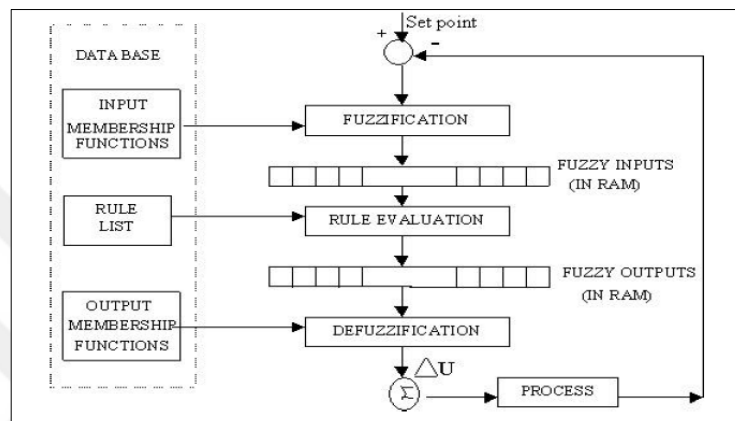
Figure 7.2 Fuzzy logic control system architecture [82]

Fuzzification: - It converts a numerical input variables into linguistic variables based on a membership function in order to make it suitable with the fuzzy set [81]. In practice, there are different types of membership functions such as the triangular, Gaussian, trapezoidal, S-curve, bell-shaped and sigmoidal waveform [80]. Triangular type is more adapted for membership functions than other types of fuzzy sets. Each membership function is defined by a name called a label.

In designing the fuzzy controller for such system, two input variables must be defined in terms of linguistics. Five symmetrical triangular type functions are defined for each of the two input fuzzy variables and the same number for two output variables [80]. Properties of a fuzzy inference system is shown in Figure 7.3.

Error (e) is the first input variable which is the difference between desired (set point) and measured position from the sensor, as well as the other input is the change of error (ce) which are given in the following equations and these two equations will be used in C programs for Arduino.

$$e\,(k) = dref - dnew \tag{7.5}$$

$$ce\,(k) = e\,(k) - e\,(k-1) \tag{7.6}$$

The limit of error (e) in position is expressed by a number in the interval from -120 to 120 with five linguistic terms, these regions are: {NL, NS, ZE, PS, and PL} corresponding to Negative Large, Negative Small, Zero, Positive Small and Positive Large respectively. Similarly, for the change of error (velocity) (ce) the fuzzy sets are presented as {NL, N, Z, P, PL} over the interval from -60 to 60. The graphical representation of the membership functions for two input variables are shown in Figure 7.4 a and b [81].
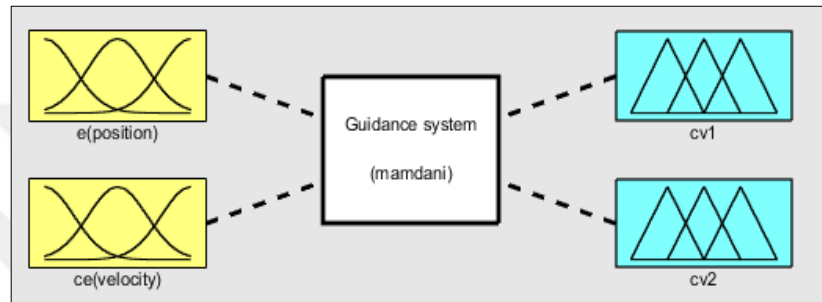
Figure 7.3 Properties of fuzzy inference system (FIS)

(a)   (b)
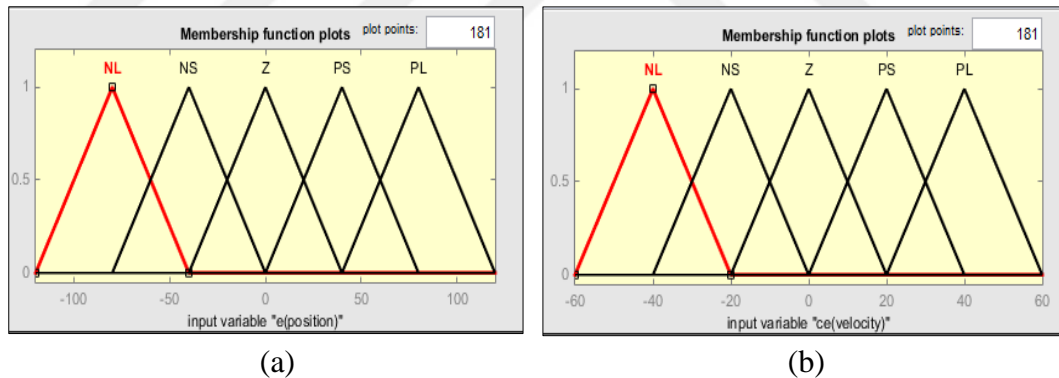
Figure 7.4 Triangular membership functions of a) error b) change of error

The membership functions for two output variables are presented in five fuzzy memberships as {Z, L, M, H, VH}, The fuzzy sets used for firing angle are as follows: Z = zero, L = large, M = medium, H = high, VH = very high. Then they changed to numerical number using defuzzification step, two output variables were normalized to be fit the range of (0 to 600). Output voltages (cv1, cv2) are used to calculate the needed change of voltages for two coils which will be used to control the positions in both sides [81]. These voltages enable the system position to follow a desired reference track. The membership functions for two output variables are shown in Figure 7.5

(a)   **(b)**
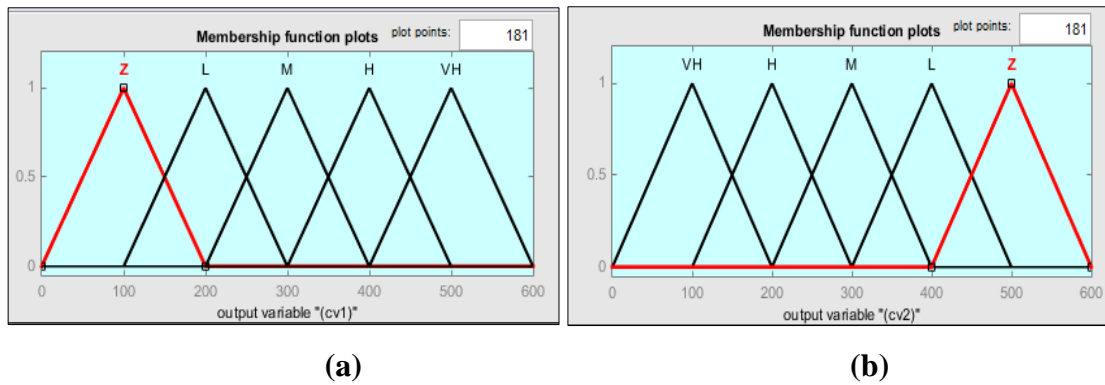
Figure 7.5 Triangular membership functions of a) first output of change of voltage (cv1) b) second output of change of voltage (cv2)

Rule Base: - It consists of two parts IF (antecedent) THEN (consequent) where antecedent part defines the condition and consequent part gives the corresponding control action, in rule set theory the set junction is usually used AND statement identify a familiar between two sets and for set unions OR statement is used to identify the entire membership of two sets, many approaches taken in determining the relation of the fuzzy rule [83].

After designing the membership function the rules for fuzzy controller were written for designing the two inputs of error and change of error. FLC uses the Mamdani fuzzy inference system to relate two input variables to output variables. The memberships are regulated by relationship (If error (e) is ----- and change of error (ce) is ---Then control output (cv) is----) as a rule by Rule Editor and five membership functions with 25 rules should be written ($5^2=25$ rules) in rule base matrix. All fuzzy rules (5x5) of fuzzy logic controller used in the proposed system are summarized in Table 7.1 [81].

Fuzzy inference process: - it combines membership functions with the control rules to derive the fuzzy output [81].

Table 7.1 Rule base of fuzzy logic controller of an electromagnetic guidance system

ce \ e	NL	NS	Z	PS	PL
NL	NL	NL	NL	NS	Z
NS	NL	NL	NS	Z	PS
Z	NL	NS	Z	PS	PL
PS	NS	Z	PS	PL	PL
PL	Z	PS	PL	PL	PL

103

Defuzzification: - Defuzzification operation is opposite the fuzzification operation. In this stage, the output of fuzzy logic controller is converted from a linguistic variable (fuzzy output values) to a numerical variable (crisp values) [83]. There are several types of defuzzification methods: Center of Area (CoA), average of maxima or Mean of Maximum method (MoM) and Center of Maximum (CoM). The centroid method (also called center of area or center of gravity) is the most commonly used type in the defuzzification method rather than the other types, which is defined in (7.7) [83].

$$COA = \frac{\sum_{i=1}^{n} \mu(x(i)) \cdot x(i)}{\sum_{i=1}^{n} \mu(x(i))} \tag{7.7}$$

where, COA is the controller output, n is the number of rules, $\mu x(i)$ is the membership value of fuzzy set calculated for the input variables, $x(i)$ is the center of area of fuzzy set of i-th of the rule. To calculate the output of CoA the following steps are required:

- Initially, a centroid point for each output membership function is determined on the X-axis and the areas of the membership functions are computed.
- The membership functions are limited in height by the applied rule strength.
- The defuzzified output is derived from a weighted average of centroid points on the X-axis.

After optimization, it was found that the crisp outputs that are needed to stabilize the system for cv1 between range (0 to 600) and for cv2 between (600-0).

After checking the sing of error whether it is plus or minus, the controller output u is calculated with respect to the updated error and its value is checked whether it is greater than its maximum value; let equal to its maximum value, if it is less than the minimum value; let equal to its minimum value. The controller output will indicate the actual duty cycles for the PWM control signals which are used to drive the power MOSFETs and they are required to put two electromagnets from their initial position to the desired set-point distance.

Initially, PD -FLC controller is implemented to improve the dynamic response of the system and achieve stable response quickly by tuning PD parameters in real time. However, the steady-state error of the system remains large, for eliminating a steady-

state error the conventional integral (PI) term is activated. The gain values of KP, KI are manually adjusted by trial and error method until the system responds quickly enough and is up to the required standards. At tunning the PI controller is essential to understand the effect of these terms on the system.

At the beginning a simple empirical approach is to start just using the proportional term and by zeroing the integral gain. The integral part (I) is responsible for reducing a steady-state error if an actual value is close to a reference signal as well as the proportional part is responsible for reducing the rise time and reduce a steady-state error. The coefficients of KP, KI are determined by experimentation to control the system, the values are KP = 1 and KI = 0.2.

7.4 Experimental Result

To consider the actual operating condition the two following conditions are considered in the experimental test to see that the guidance system works properly with the effect of the controller to keep two electromagnets at a central position (10 mm).

Condition 1: The magnet is kept to the left side initially, i.e., $x(0) = 0.0$ mm and the maximum gap is set at 20mm (x_{max} =20mm).

Condition 2: The magnet is kept to the right side initially, i.e., $x(0) = 0.015$ mm and the maximum gap is set at 15 (x_{max} =15mm).

Figure 7.6 shows the state of the system at equilibrium position that the two electromagnets draw the currents about (1.2 and 1.1) A to maintain the two magnets in the center of the ferromagnetic platform, although the controller performance is not very optimal.
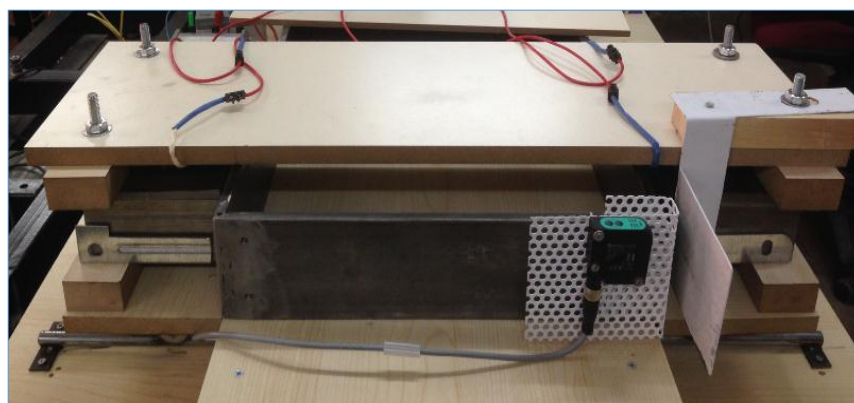
Figure 7.6 Photograph of the controlled system at equilibrium position x_0=10 mm

Figure 7.7 (a, b) depict the generated output waveforms of the voltage PWM control signals from the Arduino board and from the outputs of the isolation and MOSFET driver circuits at the desired position, which are captured on an oscilloscope to trigger the two MOSFET's with a switching frequency of 3900Hz. Sometimes there were small oscillations in the position due to quantization, truncation and computation errors of the 8-bit microcontroller board. ADC and DAC quantization errors are the primary reason for these oscillations rather than the computational errors. Figure 7.8 shows the mentioned parameters and gains of the controller on the LCD when the system is getting to the reference air-gap distance. The sensor output waveform is shown in Figure 7.9 for the controlled two electromagnets.
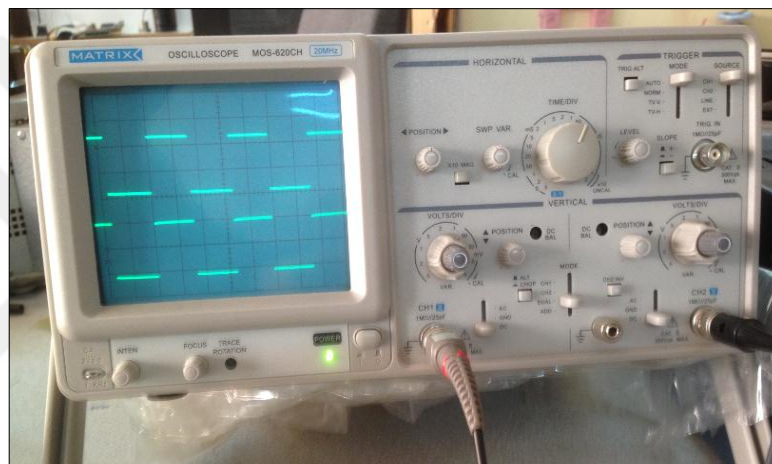
(a)
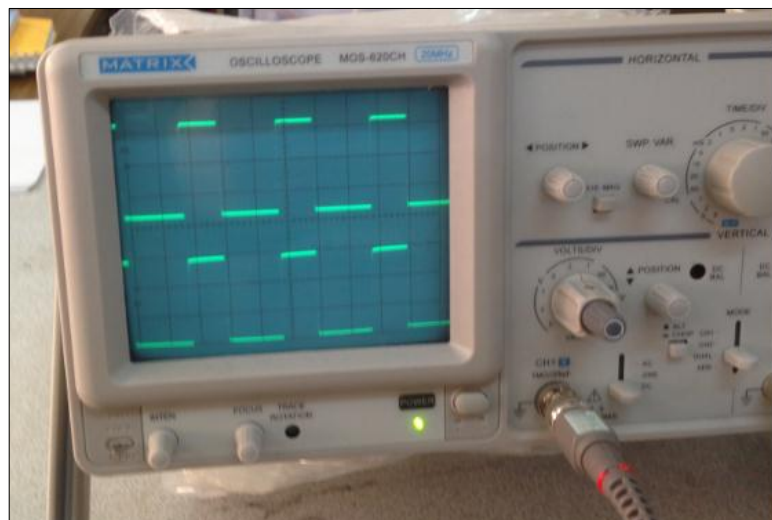
(b)

Figure 7.7 Practical controlled outputs of PWM signals in OSC (a) on the Arduino outputs (b) on the isolation and MOSFET driver circuit outputs.
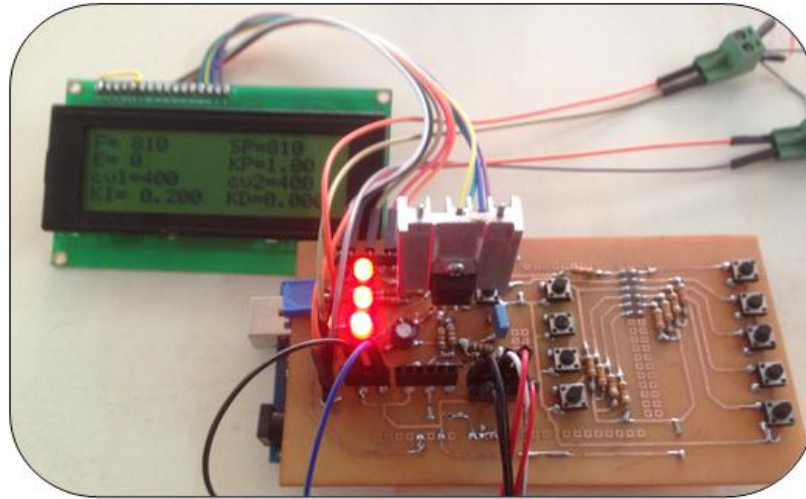
Figure 7.8 Practically actual & reference position on LCD
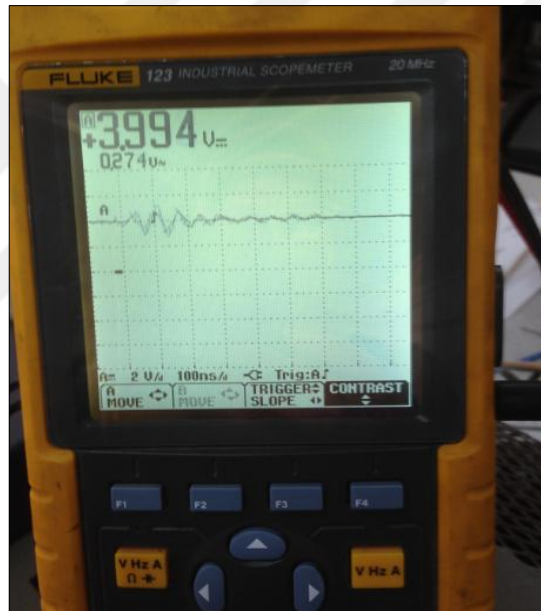
Figure 7.9 Sensor output waveform

To check the performance and robustness of the proposed control system, there are some cases that need to be taken into consideration such as external disturbance which is entered by the user, Internal disturbances (generated by the system like changing the value of resistance and inductance and fluctuation in the power supply) and parameter variation (changing the weight of the magnets). According to Newtonian laws, the actual dynamic equation of the system can be represented with parameter variation (changing the weight of the magnets) and external disturbance, the actual dynamic model realistically becomes:

$$(m + \Delta m)x''(t) = F_{gR}(i_R, x_R) - F_{gL}(i_L, x_L) + Fd \tag{7.8}$$

In such system the effect of external and internal disturbance force are considered. It can be noticed that with including the disturbance force to the system by the user the electromagnets returns to the central position, but the performance becomes poor because of the external disturbance force occurring. Additionally, the performance of the controller is tested by changing the value of set point and changing the value of resistance and inductance of the coils during working, it can be noticed that does not affect the performance of the controller.

So, the Hybrid Fuzzy PID controller is applied successfully is an effective way to a non-linear guidance system based on nonlinear structural characteristics to minimize error in a system at a desired state. The performance of the controller was tested where some experiments were done in variations of PID parameter. The PID gain parameter such as KP is chosen to decrease the rise time, KD is chosen to reduce the overshoot and settling time and finally KI is chosen to eliminate the steady state error. The FLC -PID has faster transient responses and is better than other several control method, when compared to the pure classical PID or the pure fuzzy controller applications. The Arduino hardware platform is also able to implement the control algorithm fast enough to keep the magnets in a stable position.

Summary

The Fuzzy logic PID controller is programmed into the microcontroller board to control the air-gap lengths of an electromagnetic guidance system. The Arduino IDE is used to both program and communicates with the Arduino board. Domain of fuzzy sets of error (e), change of error (ce) and control amount of voltages (cv1 and cv2) are defined and quantized into 5 membership functions with establishing the fuzzy control rule. In the defuzzification step these linguistic values are transformed into the numerical value of the control variable by using the center of area method then the outputs of fuzzy controller are denoted as duty cycle. After implementing the three steps in an iterative way the controller is fine tuned to perform the required task in the neighborhood of the equilibrium point. According to the system response the parameters of (KP, KI and KD) are tuned and changed manually with the fuzzy controller by observing system behavior until the desired system response is obtained. So the controller performance is tested with fuzzy PID which is able to meet the set point at 0.01m and to attenuate the disturbance.

CHAPTER 8

CONCLUSION AND FUTURE WORK

8.1 Conclusion

The guidance system is a key system in high- speed maglev train to keep the vehicle centrally on the guide-way during travel. A comprehensive model of an electromagnetic guidance system was constructed to investigate the dynamic behavior of the guidance system in high- speed maglev train and controlling it.

The following is a summary of the system model:

- A design procedure for DC electromagnet coil has been presented utilizing analytic solutions between the variables of system design. Two-dimensional FEA has been used as a concurrent with the analytical approach to fine-tune the final design process.

- The dynamic model of proposed guidance system was derived from an assumed configuration of two electromagnets and ferromagnetic plate to control the lateral system motion. To overcome the guide-way irregularities and coupled motion dynamics between the two electromagnets, photoelectric distance sensor in laser type was installed to detect the actual position, the magnets work together with a sensor to keep two electromagnets at the desired position.

- Mathematical modeling of an electromagnetic guidance system was systematically presented to represent the transfer function and state space models. The system was hardly nonlinear and open loop unstable, which becomes a difficulty for control designer. System linearization was employed using the Taylor Series expansion method.

- For stable operation of an electromagnetic guidance system phase lead was optimized using root locus design GUI written by Prof. Saadat. PID controller was designed using MATLAB Simulink to control the air-gap displacement on both sides around the equilibrium position. In addition, complete state feedback controller based on pole-placement technique was designed and applied to

control the system. In terms of disturbance and trajectory tracking, pole placement controller is better than the other types.

- The practical progress of the project has been divided mainly into two parts, the software part includes the programming of the microcontroller board to determine the system operation and the hardware part includes the physical parts of the system which include a sensor, two electromagnets, interface circuits to drive and protect the electromagnets and Arduino mega2560.

- In the experimental setup, Fuzzy PID controller was designed, programmed and implemented as the control algorithm to control the system. Arduino mega2560 was used as a microcontroller board to implement the control algorithm and to generate appropriate 8-bit of PWM control signals to drive the switching devices that supplying the guiding system. The analog air-gap distance was measured through the channel of ADC converter and parameters of PID controller were adjusted using digital input pins.

- Reasonable PWM duty cycles were obtained corresponding to the current error to maintain the two electromagnets at desired position. The system was controlled experimentally and the performance of the controller was tested that Fuzzy PID was able to attenuate the disturbance that able to meet the set point.

8.2 Recommendations for Future Work

For possible investigation of an electromagnetic guidance system in the next studies the following avenues of research are recommended:

- Considering three-dimensional (3D) of finite element analysis instead of two dimensional for analyzing the design procedure.

- Using digital signal processor instead of Microcontroller board (Arduino mega 2560) due to high speed processing, more accuracy in computation, 12-bit analog input and 16-bit PWM output, 32-bit fixed or floating point operation.

- Analysis and design of a guided actuation system based on a multi-variable controller.

- Increasing the number of the actuators from two electromagnets to four electromagnets and controlling the system completely.

- Implement pole placement control on the system digitally to study the performance and the robustness of this technique.

REFERENCES

[1]   Bohn, G., & Steinmetz, G. (1984). The electromagnetic levitation and guidance technology of the transrapid test facility Emsland. Magnetics, *IEEE Transactions on*, **20(5)**, 1666-1671.

[2]   Mohd Firdaus, B. (2012). Modeling of magnetic levitation (maglev) train. Master of Science in Electrical and Electronics Engineering, University Malaysia Pahang.

[3]   Biswas, P. K., & Bannerjee, S. (2012). Analysis of UI and UU type rail and actuator used in electromagnetic levitation system using FEM software. *International Journal of Emerging Technology and Advanced Engineering*, **2(5)**, 32-39.

[4]   Eastham, A. R., & Hayes, W. F. (1988). Maglev systems development status. *Aerospace and Electronic Systems Magazine*, IEEE, **3(1),** 21-30.

[5]   Lee, H. W., Kim, K. C., & Lee, J. (2006). Review of maglev train technologies. *Magnetics, IEEE Transactions on*, **42(7)**, 1917-1925.

[6]   Lee, B. S. (2000). Linear switched reluctance machine drives with electromagnetic levitation and guidance systems (Doctoral dissertation, Virginia Polytechnic Institute and State University).

[7]   Rekha Punnami, P., Sahithi R. (2013). Design of Frictionless Train System using Magnetic Levitation. Department of Mechanical Engineering Gokaraju Rangaraju Institute of Engineering and Technology, Bachupally, Hyderabad – 500 090, A.P, India.

[8]   Paudel, N. (2012). Dynamic suspension modeling of an eddy-current device: An application to MAGLEV (Doctoral dissertation, The University of North Carolina at Charlotte).

[9]   He, J. L., Rote, D. M., & Coffey, H. T. (1994). Study of Japanese electrodynamic-suspension maglev systems (No. ANL/ESD--20). Argonne National Lab., IL (United States). Energy Systems Div.

[10]   Ando, M., Nakamichi, Y., Ajiki, K., Shigeeda, H., & Suzuki, M. (2002). Surge Characteristics of Propulsion Coils Including Mutual Coupling for Maglev. *Quarterly Report of RTRI*, **43(1)**, 13-19.

[11]   Sakamoto, T., & Nakayama, M. (2006). Levitation–guidance stabilization of superconducting maglev through LSM currents. *Mathematics and Computers in Simulation*, **71(4),** 404-414.

[12]   He, J. L., Coffey, H. T., & Rote, D. M. (1995). Analysis of the combined maglev levitation, propulsion, and guidance system. *IEEE transactions on magnetics*, **2(31),** 981-987.

[13]   Murai, T., Yoshioka, H., Iwamatsu, M., & Sawada, K. (2002). Optimized Design of 8-Figure Null-Flux Coils in EDS. MAGLEV. Railway Technical Research Institute, JAPAN.

[14]   Trumper, D. L. (1990). Magnetic suspension techniques for precision motion control (Doctoral dissertation, Massachusetts Institute of Technology).

[15]   Trumper, D. L., Olson, S. M., & Subrahmanyan, P. K. (1997). Linearizing control of magnetic suspension systems. *Control Systems Technology, IEEE Transactions on*, **5(4),** 427-438.

[16]   Chen, M. Y., Wang, M. J., & Fu, L. C. (1999). Modeling and controller design of a maglev guiding system for application in precision positioning. In *American Control Conference* IEEE. **5** pp. 3072-3076.

[17]   D'Arrigo, A., & Rufer, A. (2000). Integrated electromagnetic levitation and guidance system for the swissmetro project. *In Proceedings of International Conference on Magnetically Levitated Systems and Linear Drives (MAGLEV'2000)* (pp. 263-268).

[18]   Cassat, A., Espanet, C., Bouquin, V., & Jufer, M. (2006). Passive guidance forces of polarized linear motors combined with levitation actuators working in partial vacuum–application to Swissmetro. In *Proceedings of MAGLEV 2006* (Vol. **1**, No. LAI-CONF-2007-003, pp. 351-362).

[19]   Aming, H., Longhua, S., Hengkun, L., & Wensen, C. (2007). Research of Force Feedback Controlling on High Speed Maglev Train Guidance System. In *Control and Automation, 2007. ICCA 2007. IEEE International Conference on* (pp. 1381-1384). IEEE.

[20]   Hu, Q., Liu, H., & Ou, L. (2010). Fuzzy PID nonlinear control of maglev guiding system for linear elevator based in feedback linearization. In *Fuzzy Systems and Knowledge Discovery (FSKD), 2010 Seventh International Conference on* (Vol. **3**, pp. 1277-1280). IEEE.

[21]   Narita, T., Oshinoya, Y., & Hasegawa, S. (2010). Control of electromagnetic levitation transport of flexible steel plate (fundamental considerations on elastic vibration control under transport). In *Power Electronics Conference (IPEC), 2010 International* (pp. 284-288). IEEE.

[22]   Lee, J. D., Wang, Z. B., Lu, J. Q., Chen, X. R., & Duan, R. Y. (2011). Cascade control strategy design for electromagnetic guidance system. In *Industrial Electronics and Applications (ICIEA), 2011 6th IEEE Conference on* (pp. 2803-2808). IEEE.

[23]   Hu, Q., Mingliang H., and Hao L. (2011). Adaptive sliding mode control of maglev guiding system for ropeless elevator based on feedback linearization. *Control and Decision Conference (CCDC),* 2011 Chinese. IEEE.

[24]   Hu, Q., Wang, H., & Yu, D. (2012). H∝ robust control for electromagnetic guiding system suspension altitude of linear elevator. In *Control and Decision Conference (CCDC), 2012 24th Chinese* (pp. 2305-2308). IEEE.

[25]   Hasan, A., Mohammad Bagher, B. S., & Hadi, A. (2012). A PID sliding mode control for ropeless elevator maglev guiding system. *Energy and Power Engineering*, 2012.

[26]   Hu, Q., Hao, M., & Yu, D. (2012). Neural sliding mode control on suspension gap for single electromagnetic guiding actuator of linear elevator. In *Control and Decision Conference (CCDC), 2012 24th Chinese* (pp. 2728-2732). IEEE.

[27]   Kim, C. H., Kim, K. J., Yu, J. S., & Cho, H. W. (2013). Dynamic performance evaluation of 5-dof magnetic levitation and guidance device by using equivalent magnetic circuit model. *Magnetics, IEEE Transactions on*, **49(7),** 4156-4159.

[28]   Kim, C. H., Ahn, C., Park, J. W., & Park, D. Y. (2013). Levitation and guidance control of passive magnetic levitation tray system. In *Robotics (ISR), 2013 44th International Symposium on* (pp. 1-2). IEEE.

[29]   Deshpande, M., & Mathur, B. L. (2011). Magnetic Levitation: Choice of Core Shape, Elimination of Position Sensors and Implementation of Robust Controller. *International Journal of Science and Advanced Technology* (ISSN 2221-8386)

[30]   McLyman, C. W. T. (2011). Transformer and inductor design handbook. CRC press.

[31]   Biswas, P. K., & Banerjee, S. (2012). ANSYS Simulation Based Comparative Study between Different Actuators and Guide-ways used in DC Electromagnetic Suspension Systems. *International Journal on Electrical Engineering and Informatics*, **4(2)**, 217.

[32]   AVSAR, Y. (2015). Design and analysis of EI core structured transverse flux linear reluctance actuator. *Turkish Journal of Electrical Engineering & Computer Sciences*, **23**(4), 945-955.

[33]   Olson, S. M. (1994). Nonlinear compensation of a single degree of freedom magnetic suspension system (Doctoral dissertation, Massachusetts Institute of Technology).

[34]   Carpenter Technology Corporation. Technical Datasheet, 1989. Available at: http://cartech.ides.com/datasheet.aspx?i=103&e=189&c=TechArt

[35]   Wai, R. J., & Lee, J. D. (2005). Performance comparisons of model-free control strategies for hybrid magnetic levitation system. *IEE Proceedings-Electric Power Applications*, **152(6)**, 1556-1564.

[36]   Rajeshkanna G. (2012).   Design, development and testing of an electro magnet for industrial waste metal scraps cleaning. *International Journal of Electrical Engineering & Technology (IJEET).*

[37]   Tiwari, S., Sarasvat, V., & Pal, A. K. (2010). Tyre Safety by Electromagnetic Field. *Journal S-JPSET*.

[38]   Dixon, L. H. (2000). Section 5 Inductor and Flyback Transformer Design.

[39]   Cho, H. W., Han, H. S., Lee, J. M., Kim, B. S., & Sung, S. Y. (2009). Design considerations of EM-PM hybrid levitation and propulsion device for magnetically levitated vehicle. *Magnetics, IEEE Transactions on*, **45(10),** 4632-4635.

[40]   Meeker, D. (2006). Finite Element Method Magnetics--Version 4.0 User's Manual.

[41]   Baltzis, K. B. (2010). The finite element method magnetics (FEMM) freeware package: May it serve as an educational tool in teaching electromagnetics? *Education and Information Technologies*, **15(1),** 19-36.

[42]   Zakaria, Z., Mansor, M. S. B., Jahidin, A. H., Azlan, M. S. Z., & Rahim, R. A. (2010). Simulation of magnetic flux leakage (MFL) analysis using FEMM software. In *Industrial Electronics & Applications (ISIEA), 2010 IEEE Symposium on* (pp. 481-486). IEEE.

[43]   Baltzis, K. B. (2008). The FEMM Package: A Simple, Fast, and Accurate Open Source Electromagnetic Tool in Science and Engineering. *Journal of Engineering Science & Technology Review*, **1(1)**.

[44]   Available at http://femm.software.informer.com

[45]   Ali. O. A. (2012). Control of Single Axis Electromagnetic Levitation System, Master thesis, Electrical-Electronics Engineering, University of Gaziantep, Gaziantep.

[46]   Shu'aibu, D., & Adamu, S. (2009). Design and implementation of a phase-lead compensator for magnetic levitation. *Global J. of Engineering Technelogy*, **2(1)**, 35-49.

[47]   Banerjee, S., Pal, J., & Prasad, D. (2010). Performance study of the controller of an attraction type levitation system under parametric change. *J. Electrical Systems*, **6(3)**, 377-394.

[48]   Banerjee, S., Sarkar, M. K., & Chakraborty, C. (2013). Analysis, design, fabrication and testing of three actuators based electromagnetic levitation system for vehicle applications. In *Industrial Electronics Society, IECON 2013-39th Annual Conference of the IEEE* (pp. 7250-7255). IEEE.

[49]   Sarkar, M. K., Banerjee, S., Saha, T. K., & Ghoshal, S. P. (2013). Implementation of GSA based optimal lead-lead controller for stabilization and performance enhancement of a DC electromagnetic levitation system. *Journal of Control Engineering and Applied Informatics*, **15(3),** 11-20.

[50]   Suebsomran, A. (2014). Optimal Control of Electromagnetic Suspension EMS System. *Open Automation and Control Systems Journal*, **6**, 1-8.

[51]   Awelewa, A. A., Samuel, I. A., Ademola, A., & Iyiola, S. O. (2013). An Undergraduate Control Tutorial on Root Locus-Based Magnetic Levitation System Stabilization. *International Journal of Electrical & Computer Sciences IJECS-IJENS*, **13(1).**

[52]   Banerjee, S., Prasad, D., & Pal, J. (2007). Design, implementation, and testing of a single axis levitation system for the suspension of a platform. *ISA transactions*, **46(2)**, 239-246.

[53]   Katsuhiko Ogata, (2002) Modern control Engineering, Fourth Edition, University of Minnesota , Aeeizb.

[54]   Ma, J., Fan, W., & He, F. (2008). Parameters self-adjusting fuzzy PID control in magnetic levitation system. In *Systems and Control in Aerospace and Astronautics, 2008. ISSCAA 2008. 2nd International Symposium on* (pp. 1-5). IEEE.

[55] Jeong, H. H., Yang, J. H., & Yun, S. N. (2012). Control of Magnetic Bearing System. INTECH Open Access Publisher, (http://dx.doi.org/10.5772/51185).

[56] Challa, S. (2007). Magnetic levitation on a steel ball. Degree of Master of Science in Electrical and Computer Engineering. Addis Ababa University, School of Graduate Studies.

[57] Shu'aibu, D. S., Syed-yusof, S. K., Fisal, N., & Adamu, S. S. (2010). Low Complex System for Levitating Ferromagnetic Materials. *International Journal of Engineering Science and Technology*, Vol. **2(6),** 2010, 1844-1859.

[58] Sailan, K., & Kuhnert, K. D. (2013). DC Motor Angular Position Control Using PID Controller for the Purpose of Controlling the Hydraulic Pump. In *International Conference on Control, Engineering & Information Technology (CEIT'13), Proceedings Engineering & Technology* (Vol. **1**, pp. 22-26).

[59] Yadav, S., Tiwari, J. P., & Nagar, S. K. (2012). Digital control of magnetic levitation system using fuzzy logic controller. *International Journal of Computer Applications*, **41(21),** 22-26.

[60] 6N137 datasheet, Vishay, Available via URL: http://www.alldatasheet.com/datasheet-df/pdf/154057/VISHAY/6N137.html

[61] BC237, npn transistor, Fairchild Available via URL: http://www.datasheetcatalog.org/datasheet/fairchild/BC237.pdf

[62] Chai Pei K. (2010). Magnetic Levitation - Driver and Controller. Bachelor of Electrical Engineering, University Teknologi Malaysia

[63] TC4422, 9A High-Speed Mosfet Drivers Datasheet Available via URL: http://ww1.microchip.com/downloads/en/DeviceDoc/20001420F.pdf

[64] Friend, P. (2004). Magnetic Levitation train technology. Progress report, Bradley University.

[65] STB75NF75, Power MOSFET, Available via URL: http://www.st.com/web/en/resource/technical/document/datasheet/CD0000277 71.pdf

[66] Dawood, S. M., & Thejeel, D. R. H. PIC 16F877A Microcontroller Based Multiple DC Motors Controller. *Asian Transactions on Engineering (ATE ISSN: 2221-4267)* Volume, **3**.

[67] Snubber Circuits: Theory , Design and Application Philip C. Todd

[68] William P. Robbins . Snubber Circuits Lecture Notes . Dept. of Electrical and Computer Engineering

[69] Severns, R., & Reduce, E. M. I. (2006). Design of snubbers for power circuits. International Rectifier Corporation.

[70] http://files.pepperl fuchs.com/ The Fundamentals of Photoelectric Sensors

[71] VDM18-100/32/105/122 datasheet. pepperl fuchs , Available via URL: http://www.pepperlfuchs.com/global/en/2274_entfernungsmessger_te_distan zsensoren.htm.

[72]http://canada.newark.com/wcsstore/ExtendedSitesCatalogAssetStore/cms/asset/p df/americas/common/storefront/pepperl-fuchs/distance-based-photoelectric-sensors.pdf

[73] http://www.sensing.net/exhibit/panels/assets Technical considerations for selecting distance-based photoelectric sensors.pdf

[74] Arduino Products. Available at: https://www.arduino.cc/en/Main/ArduinoBoardMega2560

[75] Granado Navarro, M. Á. (2012). Arduino based acquisition system for control applications. Master in Science in Telecommunication Engineering & Management. Universttat Politecnics De Catalunya.

[76] Zeno, M. J. (2011). Design of an Autonomous Self Correcting Platform Using Open Source Hardware (Doctoral dissertation, Rensselaer Polytechnic Institute).

[77] Benripley. Software development and diy audio. 2014. Available at: http://www.benripley.com/diy/arduino/three-ways-to-read-a-pwm-signal-with-arduino.

[78] Arduino playground. 2014. Available at: http://arduino.stackexchange.com/questions/3182/what-is-the-frequency-of-pwm-output-on-arduino.

[79] Bret C., Dan L. and Andres R. Introduction to Micro-Controllers. Portland State University.

[80] Sahin, M. E., & Okumus, H. I. (2012). A fuzzy-logic controlled PV powered buck-boost DC-DC converter for Battery-Load system. *In Innovations in Intelligent Systems and Applications (INISTA), 2012 International Symposium* on (pp. 1-5). IEEE.

[81] Badran, M. A., Hamood, M. A., & Faris, W. F. (2013). Fuzzy Logic Based Speed Control System for Three-Phase Induction Motor.". Eftimie Murgu" Resita, Anul XX, NR, 1.

[82] Bandara, G. E. M. D. C., Ivanov, R., & Gishin, S. (1999). Intelligent fuzzy controller for a lead-acid battery charger. In *Systems, Man, and Cybernetics, 1999. IEEE SMC'99 Conference Proceedings. 1999 IEEE International Conference on* (Vol. **6**, pp. 185-189). IEEE.

[83] Elreesh, H. A. (2011). Design of GA-Fuzzy Controller for Magnetic Levitation Using FPGA (Doctoral dissertation, The Islamic University of Gaza).

APPENDIX

Code

```
*********************************************************************
Project title: Design, Construction and Control of Electromagnetic Guidance System
Author: Sulaf Ibrahim Ezzat
Software: Arduino Integrated Development Environment (IDE)
Hardware: Arduino Mega 2560 board
Date: 12th of September 2015
*********************************************************************
```

```cpp
#include <LiquidCrystal.h>
#include <stdlib.h>
#include <avr/io.h>
#include <avr/interrupt.h>
#include <math.h>

const int numRows = 4;
const int numCols = 20;

//LiquidCrystal  lcd(RS Pin,  Enable Pin,  D4 Pin,  D5 Pin,  D6 Pin,
D7_Pin) // These  pins are used on LCD
LiquidCrystal lcd(12, 11, 5, 6, 3, 2);

// Define push button for setting setpoint, KP, KI and KD gain
const int  buttonPin1 = 23;  // Up pushbutton to increase SetPoint
const int  buttonPin2 = 25;  // Down pushbutton to decrease SetPoint
int buttonState1=0;          // current state of the button 1
int buttonState2=0;          // current state of the button 2
int lastButtonStateSP=0;     // previous state of the button

const int  buttonPin3 = 27;  // Up pushbutton to increase KP
const int  buttonPin4 = 29;  // Down pushbutton to decrease KP
int buttonState3=0;          // current state of the button 3
int buttonState4=0;          // current state of the button 4
int lastButtonStateKP=0;     // previous state of the button

const int  buttonPin5 = 26;  // Up pushbutton to increase KI
const int  buttonPin6 = 28;  // Down pushbutton to decrease KI
int buttonState5=0;          // current state of the button 5
int buttonState6=0;          // current state of the button 6
int lastButtonStateKI=0;     // previous state of the button

const int  buttonPin7 = 30;  // Up pushbutton to increase KD
const int  buttonPin8 = 32;  // Down pushbutton to decrease KD
int buttonState7=0;          // current state of the button 7
int buttonState8=0;          // current state of the button 8
int lastButtonStateKD=0;     // previous state of the button
```

```cpp
//*** Define parameters of PID controller
double KP;      // initial  value of proportional gain
double KI;      // initial value of integral gain
double KD;      // initial value of differential gain
int setPoint;   // set input pin for defining the value of set point
int SP1;        // set input pin  for setting the value of set point

int Error=0;     // error signal by (set point - actual position)
int Error1=0;    //previous error of the system e(k_1)
int Error2=0;    //previous to previous error of the system e(k_2)

//***PID terms
double TP=0;     // proportional term
double TI=0;     // integral term
double TD=0;     // differential term
double integral=0;      // accumulative error
double derivative=0;
double desired_power;    //desired power on 10 bit ( change 0-1023)
double desired_power1;   //desired power on 8 bit ( change 0-255)
double OUT1 = 0;         //  previous PID result (uk-1)
double OUT = 0;          // current output PID controller u(k)
int D1,D2;               // output of Fuzzy PID controller

volatile byte readFlag = 0;   //  interrupt values

int pwm1 = 9;      // select the pin for the pwm1 (to the right coil)
int pwm2 = 10;     // select the pin for the pwm2 (to the left coil)
int ErsignledPin = 22;  // LED pin for checking sign of error
int ledState = LOW;     // led State used to set the LED

//** Define parameters of Fuzzy logic controller
int distance;
int e,x,ce, a=0, b=0;      //  define error, change of error
int cv1, cv2;       //define change of voltage1, voltage 2 on 10 bit
int cvo1, cvo2;     //define change of voltage1, voltage 2 on 8 bit
float nl,ns,ze,ps,pl;  //define labels of membership functions
float x1=0, x2=0, x3=0, x4=0, x5=0;
float menl, mens,meze,meps,mepl, mcenl, mcens,mceze,mceps, mcepl;

float min_val_A, min_val_B, min_val_C, min_val_D, min_val_E;
float min_val_F, min_val_G, min_val_H, min_val_I, min_val_J;
float min_val_K, min_val_L, min_val_M, min_val_N, min_val_O;
float min_val_P, min_val_Q, min_val_R, min_val_S, min_val_T;
float min_val_U, min_val_V, min_val_W, min_val_X, min_val_Y;
float max_val_1, max_val_2, max_val_3, max_val_4, max_val_5;

void setup()
{
Serial.begin(9600); //  begin serial communications, at 9600 bits
(set the data rate per second (baud)

//***changing frequency of PWM from 500 HZ to 3900 HZ
int myEraser = 7;  // this is 111 in binary and is used as an eraser
TCCR2B &= ~myEraser;   // this operation (AND plus NOT), set the
three bits in TCCR2B to 0
// clear the value of CS02, CS01, CS00, write a new value:
int myPrescaler = 2;   // this could be a number in [1 , 6]. In this
case, 3 corresponds in binary to 011.
TCCR2B |= myPrescaler;  //this operation (OR), replaces the last
three bits in TCCR2B with our new value 011
```

```cpp
// ***Configure the ADC  converter
//Use prescale factor 128,ADC conversion clock frequency divider to
128 ADC Clock 16MHz/128 = 125kHz

ADCSRA = ((1 << ADPS2)| (1 << ADPS1) | (1 << ADPS0));
ADMUX = 0xA2;         //Initial channel selection
DIDR0 = 0xFF;         //Disable digital input on analogue inputs A0-7
DIDR2 = 0xFF;         //Disable digital input on analogue inputs A8-15
//Set Voltage reference to Avcc (5v), Left adjust converted value
ADMUX = (1 << REFS0) |(0 << REFS1)| (1<< ADLAR);
//Select free running 13 ADC clock cycles per conversion ADC sample
rate 250kHz/13 = 19.23kS/s
ADCSRB &= ~((0 << ADTS2) | (0 << ADTS1) | (0 << ADTS0));
ADCSRA |= (1 << ADIE);    // Enable interrupts
ADCSRA |= (1 << ADEN);    //Turn on ADC
interrupts();             //sei(); Enable the Global Interrupts
readFlag = 0;             // Kick off the first ADC
ADCSRA |= (1 << ADSC);    //start the first conversion


// set up the LCD's number of columns and rows:
lcd.begin(20, 4);
lcd.setCursor(6,1);
lcd.print("Welcome To");
lcd.setCursor(2,2);
lcd.print("EM Guidance System"); // Print a message on the LCD.
delay(1000);
lcd.clear();


 // declare the Pins as an INPUT:
pinMode(distance, INPUT);    //declares pin A2 as feedback 1
pinMode(buttonPin1, INPUT);  //pin button as a input to increase SP
pinMode(buttonPin2, INPUT);  //pin button as a input to decrease SP
pinMode(buttonPin3, INPUT);  //pin button as a input to increase KP
pinMode(buttonPin4, INPUT);  //pin button as a input to decrease KP
pinMode(buttonPin5, INPUT);  //pin button as a input to increase KI
pinMode(buttonPin6, INPUT);  //pin button as a input to decrease KI
pinMode(buttonPin7, INPUT);  //pin button as a input to increase KD
pinMode(buttonPin8, INPUT);  //pin button as a input to decrease KD

// declare the PWM Pin as an OUTPUT:
pinMode(pwm1, OUTPUT);
pinMode(pwm2, OUTPUT);
pinMode(ErsignledPin, OUTPUT);
}

void data_read()
{
    distance=analogRead(A2);  //read the value from A2
    lcd.setCursor(0,0);
    lcd.print("F=");
    lcd.setCursor(3,0);
    lcd.print(distance);
    lcd.print(" ");

    setPoint=810+SP1;       //  setting the value of setpoint
    lcd.setCursor(11,0);
    lcd.print("SP=");
    lcd.setCursor(14,0);
    lcd.print(setPoint);
    lcd.print("  ");
```

```
        e=setPoint-distance;        // calculating the error
        lcd.setCursor(0,1);
        lcd.print("E=");
        lcd.setCursor(3,1);
        lcd.print(e);
        lcd.print(" ");

        //checking sign of error
        if(e<0)  digitalWrite(22,HIGH);
        if (e>0) digitalWrite(22,LOW);

        lcd.setCursor(11,1);
        lcd.print("KP=");
        lcd.setCursor(14,1);
        lcd.print(KP);
        lcd.print("  ");

        lcd.setCursor(0,2);
        lcd.print("cv1=");
        lcd.setCursor(4,2);
        lcd.print(D1);
        lcd.print(" ");

        lcd.setCursor(11,2);
        lcd.print("cv2=");
        lcd.setCursor(15,2);
        lcd.print(D2);
        lcd.print("  ");

        lcd.setCursor(0,3);
        lcd.print("KI=");
        lcd.setCursor(4,3);
        lcd.print(KI,3);
        lcd.print("  ");

        lcd.setCursor(11,3);
        lcd.print("KD=");
        lcd.setCursor(14,3);
        lcd.print(KD,3);
        lcd.print("  ");
    }

  //*** SETTING THE SETPOINT ***
  void sp_read()
{
buttonState1 = digitalRead(buttonPin1); // read the pushbutton up
if (buttonState1 != lastButtonStateSP) {
    if (buttonState1 ==HIGH)  // increment the counter
    {
        SP1+=1;
        lcd.setCursor(14,0);
        lcd.print(setPoint);
        lcd.print("  ");
     }
     delay(100);
     }
lastButtonStateSP = buttonState1;  // save the current state
buttonState2 = digitalRead(buttonPin2);  // read the pushbutton down
    if (buttonState2 != lastButtonStateSP) {
        if (buttonState2 == HIGH)    // decrement the counter
     {
```

```arduino
      SP1-=1;
      lcd.setCursor(14,0);
      lcd.print(setPoint);
      lcd.print("  ");
      }
      delay(100);
      }
lastButtonStateSP = buttonState2;    // save the current state
}

/// *** KP SETTING ***
void kp_read()
{
buttonState3 = digitalRead(buttonPin3);   // read the pushbutton up
if (buttonState3 != lastButtonStateKP) {
if (buttonState3 ==HIGH)   // increment the counter
    {
      if (KP>=1) {
         KP+=0.1;
         lcd.setCursor(14,1);
         lcd.print(KP,2);
         lcd.print("  ");
                  }
      else {
      KP+=1;
      lcd.setCursor(14,1);
      lcd.print(KP);
      lcd.print(" ");
            }
    }
      delay(100);
      }
lastButtonStateKP = buttonState3;    // save the current state
buttonState4 = digitalRead(buttonPin4);  // read the pushbutton down
if (buttonState4 != lastButtonStateKP) {
if (buttonState4 == HIGH)  // decrement the counter
    {
      KP-=0.1;
      if (KP<0) KP=0;
      lcd.setCursor(14,1);
      lcd.print(KP);
      lcd.print(" ");
    }
      delay(100);
   }
lastButtonStateKP = buttonState4;  // save the current state
}

//*** KI SETTING ***
void ki_read()
{
buttonState5 = digitalRead(buttonPin5);   // read the pushbutton up
if (buttonState5 != lastButtonStateKI) {
if (buttonState5 == HIGH)  // increment the counter
    {
    if (KI>=1) {
        KI+=0.01;
        lcd.setCursor(4,3);
        lcd.print(KI,3);
        lcd.print("  ");
                }
```

```
        else {
          KI+=0.1;
          lcd.setCursor(4,3);
          lcd.print(KI,3);
          lcd.print(" ");
             }
     }
       delay(100);
     }
  lastButtonStateKI = buttonState5;       // save the current state
  buttonState6 = digitalRead(buttonPin6);  // read the pushbutton down
  if (buttonState6 != lastButtonStateKI) {
  if (buttonState6 == HIGH)              // decrement the counter
     {
        KI-=0.1;
         if (KI<0) KI=0;
         lcd.setCursor(4,3);
         lcd.print(KI,3);
         lcd.print(" ");
     }
       delay(100);
     }
  lastButtonStateKI = buttonState6;    // save the current state
  }

//*** KD SETTING ***
void kd_read()
{
  buttonState7 = digitalRead(buttonPin7);   // read the pushbutton up
  if (buttonState7 != lastButtonStateKD) {
  if (buttonState7 == HIGH)  // increment the counter
     {
        KD+=0.001;
        lcd.setCursor(14,3);
        lcd.print(KD,3);   // displaying 3 digit after floating point
        lcd.print(" ");
        }
        delay(100);
     }
  lastButtonStateKD = buttonState7;  // save the current state
  buttonState8 = digitalRead(buttonPin8);  // read the pushbutton down
  if (buttonState8 != lastButtonStateKD) {
  if (buttonState8 == HIGH)  // decrement the counter
     {
        KD-=0.001;
        if (KD<0) KD=0;
        lcd.setCursor(14,3);
        lcd.print(KD,3);    // displaying 3 digit after floating point
        lcd.print(" ");
        }
          delay(100);
     }
  lastButtonStateKD = buttonState8;  // save the current state
  }

//*** PID Algorithm ***
void PID_calculate()
{
  noInterrupts();        //cli(); Disable the Global Interrupts

  if ((Error<0) &&(Error> 0)) Error=0;     //reset Error signal
```

```cpp
if ((Error1<0) &&(Error1> 0)) Error1=0;  //reset Error1 signal
if ((Error2<0) &&(Error2> 0)) Error2=0;  //reset Error2 signal
if ((OUT1<0) &&(OUT1> 0)) OUT1=0;   // reset previous PID result
if ((OUT<0) &&(OUT> 0)) OUT=0;    // reset OUT variable, current PID

Error = abs(setPoint-distance);
TP = KP*Error;
TI=KI*( TI+(Error*0.001));       // dt is sample time
TD= KD*(Error-2*(Error1)+ Error2);

//checking the range of previous TI
if (TI>200) OUT = 200;    // TI greater than 200, reset TI to 200
if(TI<-200) OUT = -200;   // TI less than -200, reset TI to -200
OUT = OUT1 + TP+ TI+ TD;

// checking the saturation range of current PID result
if (OUT >1023) OUT = 1023;
if (OUT <-1023) OUT = -1023;
OUT1<=OUT;
Error1<=Error;
Error2<= Error1;
desired_power=OUT;

// checking the range of setting desired power from the OUT
if (desired_power >1023) desired_power =1023;
if (desired_power <-1023) desired_power =-1023;

interrupts();   //  sei(); // Enable the Global Interrupts
}

//***********Fuzzy  Algorithm**********
void FUZZY_calculate()
{
noInterrupts();

if ((e<=5) && (e>=-5))   // inserting PD Controller to the fuzzy
{
e=(setPoint-distance)*0.05;  // Proportional part (KP*e)
ce=((e-x)/0.5)*0.04; // (present distance -past distance /delay)
x=e;
}
else
{
  e=setPoint-distance;
  ce=(e-x)/0.5; // (present distance -past distance /delay)
  x=e;
}

//float error (negative large) (float nl)
nl=e;
if(nl>=-120&& nl<=-80)
menl=(nl+120)/(-80+120);
else if(nl>=-80&& nl<=-40)
menl=(-40-nl)/(-40+80);
else
menl=0;

//float error negative small (float ns)
ns=e;
if(ns>=-80&& ns<=-40)
mens =(ns+80)/(-40+80);
```

123

```c
else if(ns>=-40&& ns<=0)
mens=(0-ns)/(0+40);
else
mens=0;

//float error zero (float z)
ze=e;
if(ze>=-40 && ze<=0)
meze = (ze+40)/(0+40);
else if(ze>=0&& ze<=40)
meze =(40-ze)/(40-0);
else
meze = 0;

//float error positive small (float ps)
ps=e;
if(ps>=0 && ps<=40)
meps = (ps-0)/(40-0);
else if(ps>=40 && ps<=80)
meps = (80-ps)/(80-40);
else
meps = 0;

//float error positive large (float pl)
pl=e;
if(pl>=40 && pl<=80)
mepl=(pl-40)/(80-40);
else if(pl>=80 && pl<=120)
mepl=(120-pl)/(120-80);
else
mepl=0;

//float change of error negative large (float nl)
nl=ce;
if(nl>=-60&& nl<=-40)
mcenl=(nl+60)/(-40+60);
else if(nl>=-40&& nl<=-20)
mcenl=(-20-nl)/(-20+40);
else
mcenl=0;

//float change of error negative small (float ns)
ns=ce;
if(ns>=-40&& ns<=-20)
mcens =(ns+40)/(-20+40);
else if(ns>=-20&& ns<=0)
mcens=(0-ns)/(0+20);
else
mcens=0;

//float change of error zero (float ze)
ze=ce;
if(ze>=-20 && ze<=0)
mceze = (ze+20)/(0+20);
else if(ze>=0&& ze<=20)
mceze =(20-ze)/(20-0);
else
mceze = 0;

//float change of error positive small (float ps)
ps=ce;
```

```
if(ps>=0 && ps<=20)
mceps = (ps-0)/(20-0);
else if(ps>=20 && ps<=40)
mceps = (40-ps)/(40-20);
else
mceps = 0;

//float change of error positive large (float pl)
pl=ce;
if(pl>=20 && pl<=40)
mcepl=(pl-20)/(40-20);
else if(pl>=40 && pl<=60)
mcepl=(60-pl)/(60-40);
else
mcepl=0;

//*** Define 25 RULE BASE from (A,B,C,....Y)for 5 memberships
//Rule #1
// taking the minimum value between the two inputs
//if((e==menl)&& (ce==mcenl)) //float min_val_A;
if(menl!=0 && mcenl!=0){
min_val_A=min(menl, mcenl);
}else{
min_val_A=0;
}

//Rule #2
//if((e==mens)&& (ce==mcenl))  //float min_val_B;
if(mens!=0 && mcenl!=0){
min_val_B=min(mens, mcenl);
}else{
min_val_B=0;
}

//Rule #3
//if((e==meze)&& (ce==mcenl))  //float min_val_C;
if(meze!=0 && mcenl!=0){
min_val_C=min(meze, mcenl);
}else{
min_val_C=0;
}

//Rule #4
//if((e==meps)&& (ce==mcenl))  //float min_val_D;
if(meps!=0 && mcenl!=0){
min_val_D=min(meps, mcenl);
}else{
min_val_D=0;
}

//Rule #5
//if((e==mepl)&& (ce==mcenl)) //float min_val_E;
if(mepl!=0 && mcenl!=0){
min_val_E=min(mepl, mcenl);
}else{
min_val_E=0;
}

//Rule #6
//if((e==menl)&& (ce==mcens))   //float min_val_F;
if(menl!=0 && mcens!=0){
```

```
min_val_F=min(menl, mcens);
}else{
min_val_F=0;
}

//Rule #7
//if((e==mens)&& (ce==mcens))  //float min_val_G;
if(mens!=0 && mcens!=0){
min_val_G=min(mens, mcens);
}else{
min_val_G=0;
}

//Rule #8
//if((e==meze)&& (ce==mcens))  //float min_val_H;
if(meze!=0 && mcens!=0){
min_val_H=min(meze, mcens);
}else{
min_val_H=0;
}

//Rule #9
//if((e==meps)&& (ce==mcens))  //float min_val_I;
if(meps!=0 && mcens!=0){
min_val_I=min(meps, mcens);
}else{
min_val_I=0;
}

//Rule #10
//if((e==mepl)&& (ce==mcens))  //float min_val_J;
if(mepl!=0 && mcens!=0){
min_val_J=min(mepl, mcens);
}else{
min_val_J=0;
}
//Rule #11
//if((e==menl)&& (ce==mceze))  //float min_val_K;
if(menl!=0 && mceze!=0){
min_val_K=min(menl, mceze);
}else{
min_val_K=0;
}

//Rule #12
//if((e==mens)&& (ce==mceze))  //float min_val_L;
if(mens!=0 && mceze!=0){
min_val_L=min(mens, mceze);
}else{
min_val_L=0;
}

//Rule #13
//if((e==meze)&& (ce==mceze)) //float min_val_M;
if(meze!=0 && mceze!=0){
min_val_M=min(meze, mceze);
}else{
min_val_M=0;
}
//Rule #14
//if((e==meps)&& (ce==mceze)) //float min_val_N;
```

```
if(meps!=0 && mceze!=0){
min_val_N=min(meps, mceze);
}else{
min_val_N=0;
}

//Rule #15
//if((e==mepl)&& (ce==mceze))  //float min val O;
if(mepl!=0 && mceze!=0){
min_val_O=min(mepl, mceze);
}else{
min_val_O=0;
}

//Rule #16
//if((e==menl)&& (ce==mceps))  //float min_val_P;
if(menl!=0 && mceps!=0){
min_val_P=min(menl, mceps);
}else{
min_val_P=0;
}

//Rule #17
//if((e==mens)&& (ce==mceps))  //float min_val_Q;
if(mens!=0 && mceps!=0){
min_val_Q=min(mens, mceps);
}else{
min_val_Q=0;
}

//Rule #18
//if((e==meze)&& (ce==mceps))  //float min_val_R;
if(meze!=0 && mceps!=0){
min_val_R=min(meze, mceps);
}else{
min_val_R=0;
}

//Rule #19
//if((e==meps)&& (ce==mceps))  //float min_val_S;
if(meps!=0 && mceps!=0){
min_val_S=min(meps, mceps);
}else{
min_val_S=0;
}

//Rule #20
//if((e==mepl)&& (ce==mceps))  //float min val T;
if(mepl!=0 && mceps!=0){
min_val_T=min(mepl, mceps);
}else{
min_val_T=0;
}

//Rule #21
//if((e==menl)&& (ce==mcepl))  //float min_val_U;
if(menl!=0 && mcepl!=0){
min_val_U=min(menl, mcepl);
}else{
min_val_U=0;
}
```

```
//Rule #22
//if((e==mens)&& (ce==mcepl)) //float min_val_V;
if(mens!=0 && mcepl!=0){
min_val_V=min(mens, mcepl);
}else{
min_val_V=0;
}

//Rule #23
//if((e==meze)&& (ce==mcepl))  //float min_val_W;
if(meze!=0 && mcepl!=0){
min_val_W=min(meze, mcepl);
}else{
min_val_W=0;
}

//Rule #24
//if((e==meps)&& (ce==mcepl)) //float min_val_X;
if(meps!=0 && mcepl!=0){
min_val_X=min(meps, mcepl);
}else{
min_val_X=0;
}

//Rule #25
//if((e==mepl)&& (ce==mcepl))  //float min_val_Y;
if(mepl!=0 && mcepl!=0){
min_val_Y=min(mepl, mcepl);
}else{
min_val_Y=0;
}

//maximum summation of the similar rule out put
//float max_val_1; calculate max value of negative large
max_val_1=sqrt(pow(min_val_A,2)+pow(min_val_B,2)+pow(min_val_C,2)+po
w(min_val_F,2)+pow(min_val_G,2)+pow(min_val_K,2));
a=0;
b=50;
x1= a-(max_val_1*(a-b));

//float max_val_2; calculate max value of negative small
max_val_2=sqrt(pow(min_val_D,2)+pow(min_val_H,2)+pow(min_val_L,2)+po
w(min_val_P,2));
a=25;
b=300;
x2= a-(max_val_2*(a-b));

//float max val 3; calculate max value of zero
max_val_3=sqrt(pow(min_val_E,2)+pow(min_val_I,2)+pow(min_val_M,2)+po
w(min_val_Q,2)+pow(min_val_U,2));
a=300;
b=400;
x3= a-(max_val_3*(a-b));

//float max_val_4; calculate max value of positive small
max_val_4=sqrt(pow(min_val_J,2)+pow(min_val_N,2)+pow(min_val_R,2)+po
w(min_val_V,2));
a=375;
b=450;
x4= a-(max_val_4*(a-b));
```

```cpp
//float max_val_5; calculate max value of positive large
max_val_5=sqrt(pow(min_val_O,2)+pow(min_val_S,2)+pow(min_val_T,2)+po
w(min_val_W,2)+pow(min_val_X,2)+pow(min_val_Y,2));
a=600;
b=370;
x5= a-(max_val_5*(a-b));

//DEFUZZITION  step: using Center of area method to discrete output

cv1=((max_val_1*x1)+(max_val_2*x2)+(max_val_3*x3)+(max_val_4*x4)+(ma
x_val_5*x5))/(max_val_1+max_val_2+max_val_3+max_val_4+max_val_5);

cv2=((max_val_1*x5)+(max_val_2*x4)+(max_val_3*x3)+(max_val_4*x2)+(ma
x_val_5*x1))/(max_val_1+max_val_2+max_val_3+max_val_4+max_val_5);

if ((e>=1)&&(e<=50))
{
D1=cv1-desired_power;
D2=cv2+desired_power;
}
else if ((e<=-1)&& (e>=-50))
{
D1=cv1+desired_power;
D2=cv2-desired_power;
}
else
{
D1=cv1;
D2=cv2;
}
if(D1>1023)  D1=1023;
if(D1<-1023) D1=-1023;

if(D2>1023)  D2=1023;
if(D2<-1023) D2=-1023;

cvo1=map (D1, -1023, 1023, -255, 255);
cvo2=map (D2, -1023, 1023, -255, 255);

analogWrite(pwm1,cvo1);      // send PWM1 to mosfet 1
analogWrite(pwm2,cvo2);      // send PWM2 to mosfet2
interrupts();   //  sei();   // Enable the Global Interrupts
}

void loop()
{
    data_read();
    sp_read();
    kp_read();
    ki_read();
    kd_read();
}

ISR(ADC_vect)          // ADC interrupt service routine
  {
    readFlag =1;   // Done reading
    FUZZY_calculate();
    PID_calculate();
    readFlag = 0;
  }
```